Laser-induced alignment

TOWARDS FIXED-IN-SPACE MOLECULES

PhD Dissertation

Christer Zoffmann Bisgaard
Department of Physics and Astronomy
University of Aarhus

August 2006

Preface

This Dissertation has been submitted to the Faculty of Science at the University of Århus, in order to fulfill the requirements for the PhD degree. The work presented has been carried out at the Department of Physics and Astronomy in the years 2002-2006 under the supervision of Henrik Stapelfeldt from the Department of Chemistry.

Acknowledgements

First of all, I am very grateful to Henrik Stapelfeldt for four excellent years under his always encouraging supervision. It has been an exciting journey with many stimulating discussions.

The people with whom I have shared many joyful (and sometimes very late!) hours in the lab are (in order of appearance): Emmanuel Péronne, Mikael D. Poulsen, Simon S. Viftrup, Tine Ejdrup, Lotte Holmegaard and Vinod Kummarappan. In their cheerful company time flies by with ease and suddenly you find that four yeas have passed. Many of the things I have learned in the meanwhile can be traced to my interaction with them. A special thanks goes to Vinod for careful proof-reading of the manuscript for this Dissertation. In the lab Jan Thøgersen has been an indispensable asset, always ready to get the laser in shape and assist on any question that may arise. Also thanks to Christian Petersen for good companionship during all of my eight years at the university.

During my time as a PhD student I have benefitted from our collaboration with

Edward Hamilton and Tamar Seideman at the Northwestern University in Evanston, IL, USA. Their calculations have brought my understanding of alignment further than any experiment alone would permit. All calculations on asymmetric tops presented in this Dissertation were carried out by Edward and Tamar.

Early on during my time in the group a very fruitful collaboration on strong-field ionization of molecules was initiated with Thomas K. Kjeldsen and Lars Bojer Madsen from the Department of Physics and Astronomy. Without the guidance of Lars with both rigorous theory and transparent physical arguments, my insight to strong-field physics would not have been the same. The calculations on strong-field ionization presented in this Dissertation were carried out by Thomas.

Over the years I have also benefitted greatly from the excellent support from the technical staff at the Department of Chemistry, especially the superb skills of Per Strand in the mechanical workshop must be mentioned, and the Vacuum and Electronics workshops at the Department of Physics and Astronomy have helped on many occasions.

In the summer of 2005 I also had the pleasure of spending two months in the group of Daniel M. Neumark at the University of California, Berkeley. I am thankful to Dan for allowing me to visit his lab and my best thoughts go to Jan R. R. Verlet, Aster Kammrath, Graham Griffin and the rest of the group for two unforgettable months there.

Last, but certainly not least, I am very thankful for the never ceasing love and support from my wife Kathrine.

Christer Zoffmann Bisgaard
August 2006

Outline

Chapter 1 This chapter provides a brief, historically inspired introduction to the idea of controlling the spatial orientation orientation of molecules.

Chapter 2 The theory of laser-induced alignment of molecules is described in detail and some illustrative numerical results are presented. This chapter forms the conceptual foundation for all the following chapters.

Chapter 3 An introduction to our detection technique, photo-fragment ion imaging, is given and the experimental setup is described.

Chapter 4 Our experimental results on nonadiabatic alignment of symmetric and asymmetric top molecules are presented. In particular the appearance of rotational revivals for both classes of molecules is demonstrated.

Chapter 5 The 'old' problem of adiabatic alignment is reconsidered in the light of some new experimental results which emphasize the crucial role of the rotational temperature.

Chapter 6 In this chapter it is demonstrated that for nonadiabatic alignment, two properly timed pulses can lead to a significant improvement of the degree of alignment over that obtainable in single-pulse experiments.

Chapter 7 Some applications of aligned molecules are discussed, in particular their use in photoelectron spectroscopy and in strong-field physics.

Chapter 8 In this final chapter some ideas for future experiments and directions are discussed.

List of Publications

The work presented in this dissertation has lead to the following publications:

I *Nonadiabatic Alignment of Asymmetric Top Molecules: Field-Free Alignment of Iodobenzene*
E. Péronne, M. D. Poulsen, C. Z. Bisgaard, H. Stapelfeldt and T. Seideman. Phys. Rev. Lett. **91**, 043003 (2003).

II *Role of symmetry in strong-field ionization of molecules*
T. K. Kjeldsen, C. Z. Bisgaard, L. B. Madsen and H. Stapelfeldt. Phys. Rev. A. **68**, 063407 (2003).

III *Nonadiabatic laser-induced alignment of iodobenzene molecules*
E. Péronne, M. D. Poulsen, H. Stapelfeldt, C. Z. Bisgaard, E. Hamilton and T. Seideman. Phys. Rev. A **70**, 063410 (2004).

IV *Nonadiabatic alignment of asymmetric top molecules: Rotational revivals*
M. D. Poulsen, E. Péronne, H. Stapelfeldt, C. Z. Bisgaard, S. S. Viftrup, E. Hamilton and T. Seideman. J. Chem. Phys. **121**, 783 (2004).

V *Observation of Enhanced Field-Free Molecular Alignment by Two Laser Pulses*
C. Z. Bisgaard, M. D. Poulsen, E. Péronne, S. S. Viftrup and H. Stapelfeldt. Phys. Rev. Lett. **92**, 173004 (2004).

VI *Tunneling ionization of atoms*
C. Z. Bisgaard and L. B. Madsen. Am. J. Phys. **72**, 249 (2004).

VII *Influence of molecular symmetry on strong-field ionization: Studies on ethylene, benzene, fluorobenzene, and chlorofluorobenzene*
T. K. Kjeldsen, C. Z. Bisgaard, L. B. Madsen and H. Stapelfeldt Phys. Rev. A **71**, 013418 (2005).

VIII *Alignment of symmetric top molecules by short laser pulses*
E. Hamilton, T. Seideman, T. Ejdrup, M. D. Poulsen, C. Z. Bisgaard, S. S. Viftrup and H. Stapelfeldt. Phys. Rev. A **72**, 043402 (2005).

IX *Alignment enhancement of a symmetric top molecule by two short laser pulses*
C. Z. Bisgaard, S. S. Viftrup and H. Stapelfeldt. Phys. Rev. A. **73**, 053410 (2006).

X *Three-dimensional alignment of molecules using a long and a short laser pulse*
S. S. Viftrup, C. Z. Bisgaard, V. Kumarappan, L. Holmegaard, H. Stapelfeldt, E. Hamilton and T. Seideman. In preparation (2006).

XI *Adiabatic alignment of very cold molecules*
V. Kumarappan, C. Z. Bisgaard, S. S. Viftrup, L. Holmegaard and H. Stapelfeldt.
In preparation (2006).

XII *Controlling the rotational revival structure of asymmetric tops*
L. Holmegaard, V. Kumarappan, S. S. Viftrup, C. Z. Bisgaard and H. Stapelfeldt.
In preparation (2006).

CONTENTS

CHAPTER 1

Introduction

The idea of using light induced forces to control and manipulate matter has lead to important progress in modern atomic, molecular and biological physics; it is at the very core of popular techniques such as laser cooling and optical tweezers. Both techniques can be used to control the translational degrees of freedom and optical tweezers can also be used to control the spatial orientation of cell-size objects. In this Dissertation the use of non-resonant infrared laser pulses to strongly confine the spatial orientation of small gas phase molecules will be described. Before doing so, a brief introduction to the topic shall be given; for a more detailed review of laser induced alignment the reader is referred to [1].

The initial drive for seeking control over the spatial orientation of molecules came from reactive scattering experiments with molecular beams. While steric effects have had a central role in chemistry for a long time, these experiments aim to quantify the effects in terms of reaction rates for different collision geometries. A standard example from introductory organic chemistry is S_N2 type reactions like the substitution of Cl with I in CH_3Cl

$$I^- + CH_3Cl \longrightarrow ICH_3 + Cl^-.$$

For this reaction the rate is significantly higher when the iodine ion attacks methylchloride along the C−Cl bond from the carbon end, as opposed to approaching the molecule from the chlorine end. To study bimolecular reactions in detail it is, there-

fore, highly desirable to be able to control the relative orientation of the two collision partners prior to the reaction. For symmetric tops this has been accomplished by using electrostatic hexapole focusing to select molecules in a specific rotational state followed by orientation in a static electric field [2]. This technique utilizes the stable precession of the angular momentum vector around the external electric field for symmetric tops, for asymmetric tops with the permanent dipole moment $\boldsymbol{\mu}$ along the A- or C-axis, and for linear molecules with either electronic or vibrational angular momentum, but is limited by the fact that, with a few exceptions, pure $|JKM\rangle$ states are only modestly confined. An alternative approach is the technique nicknamed 'brute-force orientation', where a strong static field alone is used to orient the molecules by creating directional hybrids of the field-free rotational states [3, 4]. If the molecules are very cold ($kT < \mu E$) they will be forced into confined librational motion around the electric field with the dipole moment preferentially pointing in the direction of the electric field. Early in the development of this technique it was realized that the very strong electric field in the focus of a pulsed laser would be able to confine the rotational motion much more efficiently [3] and this lead to the proposal of using infrared non-resonant lasers to align molecules [5]. The drawback of using the AC field of a laser to confine the rotational motion is that since the electric field of near-infrared laser pulses oscillates at a frequency much higher than molecular rotational frequencies, the head-vs-tail preference induced by a DC field is lost.

In parallel to this, the idea of laser-induced alignment was developed independently from studies of multi-electron dissociative ionization of molecules by strong laser fields. It was observed that the fragment ions from small, linear molecules were primarily ejected along the polarization axis. Two mechanisms, named geometrical and dynamical alignment, were proposed to explain these observations [6, 7]. In geometrical alignment the directionality of the fragments is caused by a strong angular dependence for the ionization probability which selects a subset of the sample of randomly oriented molecules. Contrasting this, dynamical alignment describes a situation where the laser field actually exerts a torque on the molecule and forces all of the molecules into alignment close to the polarization axis prior to ionization. In reality, both mechanisms may have played important roles for the observed fragment patterns; in particular, enhanced ionization provides a mechanism for a strong angular dependence of the production of molecules in high charge states [8, 9].

One concept that will be encountered many times throughout this Dissertation is that of rotational wave packets. A wave packet is a coherent superposition of eigenstates of different energies and is thus a non-stationary state. Since short laser pulses inherently come with large bandwidths, they provide a powerful way to create wave packets. An intense, non-resonant pulse with a duration much shorter than the rotational period will, for instance, create a superposition of rotational states in the electronic ground state via stimulated Raman transitions [10, 11]. If, instead, a short pulse, which is resonant with the transition to an electronically excited state, is used then a rotational wave packet is created in the excited state [12, 13]. Seideman [14] realized

that under conditions typical for many femtosecond pump-probe experiments, a broad rotational wave packet could (unintentionally) be created in both the ground and excited states via sequential Rabi cycling and that the phasing of the rotational states was such that the molecules would become aligned shortly after the pulse. Since a wave packet corresponds to a non-stationary state, the expectation value of a given observable is in general time-dependent. Rotational wave packets may, for instance, become angularly confined, but only during short intervals. On the positive side, the temporal evolution of the wave packet can lead to alignment under field-free conditions; Seideman [15] showed using an analytical approximation that the rotational kick by a near-resonant, short laser pulse in general leads to a higher degree of alignment after the pulse than during the pulse and Ortigoso *et al.* [16] showed numerically that a short, non-resonant pulse can induce similar behavior, even when thermal averaging is taken into account.

The field of laser-induced alignment has been characterized by fruitful interplay between theory and experiment. The initial inspiration for the pioneering theoretical papers [5, 14] came from experiments. The proposal of adiabatic alignment was quickly followed by a experimental confirmation by Kim and Felker [17] and later detailed studies followed from Stapelfeldt and co-workers [18, 19] culminated with the demonstration of three dimensional alignment [20]. Meanwhile, the idea of using short laser pulses to induce dynamical alignment, was proposed by theoreticians [14–16]. Once again, experiments followed soon after; the work by Rosca-Pruna and Vrakking [21], who made the first demonstration of dynamical alignment and showed the appearance of rotational revivals, marked the starting point for a vast amount of experimental studies on nonadiabatic alignment by many different groups. Many of these studies will be discussed together with the results presented below.

By now, laser induced alignment by both long and short pulses are well known phenomena and focus is moving towards applications of aligned molecules; indeed laser induced alignment is currently maturing as a valuable tool for fundamental research in several areas of physics and chemistry. Some of these application will be discussed in the end of this Dissertation.

CHAPTER 2

Theory of alignment

In this chapter the theory of molecular alignment by non-resonant laser fields is described. The chapter will serve as a reference for both a qualitative and a quantitative discussion of the experimental results.

2.1 Introduction

The interaction of a molecule with a nonresonant, nonionizing, near-infrared laser field is well described by the interaction between the polarizability of the molecule and the electric field of the laser. The interaction of the electric field with the permanent dipole moment (if the molecule happens to possess one) cycle-averages to zero since the direction of the electrical field reverses every half-cycle ($\sim$1.3 fs at 800 nm) [5, 22]. The interaction with the polarizability, on the contrary, corresponds to the laser inducing an electric dipole which then interacts with the external field. Since the direction of the induced dipole reverses with the direction of the electrical field this interaction does not average to zero. To put it simply, the induced dipole corresponds to the electrons being pulled away from their equilibrium position. As molecules often have structures extending into different directions in space, some directions are more favorable than others for the electrons. A consequence is that the interaction between the molecule and the laser field depends on the relative orientation between

the molecule and the polarization of laser and a torque is exerted on molecules which are not oriented in the most favorable geometry. If the laser pulse is short compared to the timescale for rotational dynamics of the molecule we can think of the laser pulse as giving the molecules a rotational kick that makes them spin. If, on the other hand, the duration of the laser pulse is long compared to rotational dynamics of the molecule, the electric field will slowly guide the molecules into the most favorable orientation.

From a quantum mechanical point of view, the confinement of the spatial orientation of a molecule requires a corresponding uncertainty in the conjugate coordinate. For the polar angle the conjugate coordinate is the angular momentum. What we need is thus a superposition of angular momentum states; more states leads to a higher limit on the angular confinement and thus makes feasible a higher degree of alignment. At optical frequencies this can be obtained via Raman transitions, either resonant or non-resonant.

To be more quantitative, the interaction of a molecule with a laser field $\boldsymbol{E}(t) = \boldsymbol{E_0}(t)\cos(\omega t)$ can be described by an induced potential

$$\hat{V}(t) = -\frac{1}{4}\sum_{i,j} E_{0,i}(t)\,\alpha_{ij}\,E^*_{0,j}(t), \tag{2.1}$$

where $i, j = X, Y, Z$ are the space-fixed coordinates and $\alpha_{i,j}$ is the polarizability tensor. Quantum mechanically the polarizability is determined by the probability for Raman transitions amongst the manifold of rotational states in the vibronic ground state [23]. The total Hamiltonian for the molecule-field system is the sum of the field-free Hamiltonian

$$\hat{H}_{\text{rot}} = \frac{\hat{J}_x^2}{2I_{xx}} + \frac{\hat{J}_y^2}{2I_{yy}} + \frac{\hat{J}_z^2}{2I_{zz}}, \tag{2.2}$$

and the induced potential. That is,

$$\hat{H} = \hat{H}_{\text{rot}} + \hat{V}(t). \tag{2.3}$$

In order to analyze the behavior of the system described by this Hamiltonian we need some more information. First of all we must know how rapidly the interaction potential changes with time; that is, the pulse duration must be specified. If, on the one hand, the pulse duration is long compared to rotational period of the molecule the molecule will undergo an adiabatic transition from a field-free state to a field-dressed state. Short pulses, on the other hand, lead to nonadiabatic interactions that create a coherent superposition of eigenstates, i.e., a wave packet. One thing is common for both regimes: perturbation theory cannot be used. Typical rotational constants for the molecules we have investigated are on the order of a few GHz (in frequency units). Typical intensities are on the order of 500 GW/cm^2 or more and polarizabilities[a] are a

[a] More precisely this is the polarizability volume. See Appendix A.3.

few Å^3. The interaction term is then on the order of several hundreds of GHz; obviously non-perturbative methods must be used for solving the equations.

This chapter will present an analysis of the two regimes of interaction exposing their advantages and disadvantages. The main focus will be on the interaction with a linearly polarized laser field which renders possible the control of one axis in the molecule. The final section deals with scenarios for full three-dimensional alignment.

2.2 Adiabatic alignment

Adiabatic alignment of linear molecules was first considered by Friedrich and Herschbach [5, 24], inspired by their earlier work on brute force orientation in molecular beam experiments [3]. The theoretical treatment of a symmetric top in an intense, non-resonant laser field was considered 20 years prior to Friedrich and Herschbach by Zon and Katsnel'son [25]. These authors, however, only consider the effect on the rotational spectrum, not the consequences for the spatial orientation of the molecules. If a molecule is exposed to a laser pulse with a slowly evolving envelope, the adiabatic theorem states that each state in the field-free system is transferred to the corresponding eigenstate in the presence of the field [26]. Explicit integration of the time-dependent Schrödinger equation by Ortigoso *et al.* [16] shows that for $\tau > 5 \cdot T_{\text{rot}}$ and for realistic intensities the evolution is purely adiabatic and recent work by Torres *et al.* [27] indicates that adiabatic behavior is found already when $\tau \gtrsim T_{\text{rot}}$. The eigenstates in the presence of the field are called pendular states since the bound states correspond to a molecule librating in the induced potential well, a motion much similar to the oscillations of a pendulum. In the case of a linear molecule interacting with a linearly polarized laser field the interaction potential is

$$\hat{V} = -\frac{E_0^2}{4}\left(\Delta\alpha \cos^2\theta + \alpha_\perp\right), \tag{2.4}$$

where the polarizability anisotropy, $\Delta\alpha = \alpha_\parallel - \alpha_\perp$, is the difference in polarizability along and perpendicular to the internuclear axis and θ is the angle between the polarization of the laser and the internuclear axis. With $\Delta\alpha > 0$ we see that the energy is minimized for $\theta = 0, \pi$, that is when the molecules are aligned with the internuclear axis parallel to the polarization of the laser field. Due to the cylindrical symmetry around the polarization of the laser the projection of the angular momentum vector onto the space fixed Z axis, M, is a conserved quantum number. In Fig. 2.1 the interaction potential has been plotted for the iodine molecule exposed to an intensity of $I = 100$ GW/cm^2. Also shown are the energy levels for the pendular states (only those with $M = 0$). The pendular states are labelled by $\tilde{J}$ which corresponds to the J quantum number of the field-free state that the given states correlates with when the field is adiabatically turned off. That is, the state $\tilde{J} = 1$ goes into the $J = 1$ state when the field is turned off slowly.

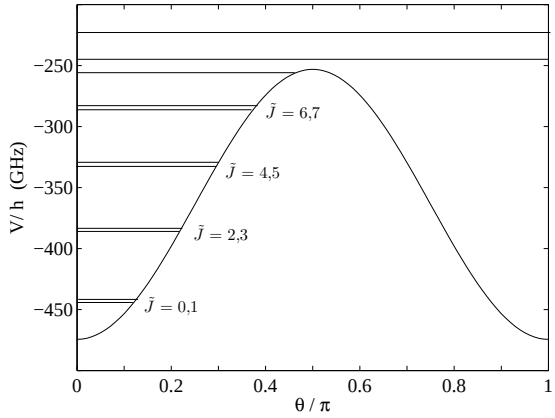

FIGURE 2.1: Interaction potential for I_2 at an intensity of 100 GW/cm^2. Also shown are the energy levels for the pendular states, $\tilde{J}$ ($M = 0$). The splitting of the nearly degenerate states ($\tilde{J} < 7$) has been exaggerated for illustrative purposes.

A striking feature of the energy level spacing is that the lower levels come in very closely spaced pairs. These pairs occur because the potential is a double well, their spacing correspond the tunnelling frequency between the two parts of the well. Although the energy levels are only shown in the upper ($\theta > \pi/2$) part of the potential each of the pendular states are delocalized in both ends of the potential since a trapping in one end would correspond to orientation which cannot be achieved by a single frequency near infrared laser in the adiabatic regime [5]. It is worth noting that for each pair, the two states have opposite parity. Secondly it is seen that the pairs up to $\tilde{J} = 4, 5$ have equidistant spacing. The reason is that the lowest states are confined to the region close the polar axis where the potential is well approximated by a harmonic potential and the molecules can be considered harmonic librators. From the figure it is clear that each of the pendular pairs experiences different confinement and therefore have different degrees of alignment. In a typical experiment a thermal sample of molecules is used and even for very cold molecules a range of field-free rotational states will be populated: a temperature of 1 K corresponds to an energy on the order of 20 GHz (compared to the rotational constants of a few GHz). Since each initial state is adiabatically transferred to the corresponding pendular state the same range of pendular states will be populated. To complicate things further, the degree of alignment also depends on the M quantum number (in a classical model M is just another measure for polar angle between the polarization of the laser and the angular momentum vector of the molecule). As shown by Friedrich and Herschbach the effective potential in the θ coordinate is strongly modified by a centrifugal term for $M \neq 0$ [24]. It is therefore clear that one must consider the ensemble average of the degree of alignment when

comparing with an experiment.

For symmetric tops the interaction potential is identical to the one for linear molecules; in the molecular frame the symmetry dictates that the two components of the polarizability tensor perpendicular to the top axis are identical. This class of molecules have an extra quantum number describing their field-free rotational motion: the projection, K, of the angular momentum vector onto the top axis (the z axis in the molecular frame). Since the interaction potential is invariant under rotations around the z axis (independent of the Euler χ angle), K is a conserved quantum number. Both the field-free energy and the energy of the pendular states do, however, depend on K.

Finally, we have asymmetric tops. This class of molecules is characterized by having three distinct moments of inertia in the molecular frame (or more precisely in the principal axes frame). Since there are no general restrictions from the symmetry of the molecules we must also expect them to have three distinct components of the polarizability tensor in the molecular frame[b]. The potential created by interacting with a linearly polarized laser field is then

$$\hat{V} = -\frac{E_0^2}{4}\left[\sin^2\theta\left(\alpha_{xx}\cos^2\chi + \alpha_{yy}\sin^2\chi\right) + \alpha_{zz}\cos^2\theta\right], \tag{2.5}$$

where α_{ii} are the components of the polarizability tensor in the molecular frame. The extra terms reflect the fact that for molecules who are not perfectly aligned ($\theta \neq 0, \pi$) it is advantageous to have the axis of second highest polarizability in the plane spanned by the polarization vector and the axis of highest polarizability. M is still a conserved quantum number due to the cylindrical symmetry (independence of ϕ). The projection of the angular momentum vector onto the z axis cannot be used to describe the field-free rotation of asymmetric tops, instead levels with the same value of J and M are given an index τ. States of different τ are mixed by the interaction with a non-resonant laser.

After these qualitative considerations it is now appropriate to consider how we can carry out a more detailed study of adiabatic alignment. As stated in the introduction the intensities applied in a typical experiment call for non-perturbative methods. In the following Section it will be outlined how to carry out such calculations and a few numerical results are presented to highlight the general properties of adiabatic alignment.

2.2.1 Numerical approach

To study adiabatic alignment is to study the properties of the pendular states. For linear molecules, the time-independent Schrödinger equation can be reduced to the

[b]The discussion is restricted to molecules were the principal axis frame is also the frame where the polarizability tensor is diagonal. This is ensured by the symmetry for molecules with point group symmetries D_2, C_{2v} and D_{2h} or higher.

well-studied spheroidal wave equation [5, 25]. The focus here will be on the pendular states of symmetric tops where this reduction cannot be carried out. Numerically, the results for linear molecules can trivially be obtained in the approach described below since linear molecules can be treated as symmetric tops with $K = 0$. The way to extend the methods presented here to asymmetric tops will be briefly outlined.

For a prolate symmetric top, the field-free Hamiltonian is

$$\hat{H}_{\text{rot}} = B\hat{J}^2 + (A - B)J_z^2, \tag{2.6}$$

and the total Hamiltonian is the sum of this term and Eq. (2.4). The time-independent Schrödinger equation can be written as a matrix equation by expanding the pendular state in the basis of symmetric top states

$$|\tilde{J}KM\rangle = \sum_{J'} d_{J'KM}|J'KM\rangle, \tag{2.7}$$

and projecting the Schrödinger equation

$$\left(\hat{H}_{\text{rot}} + \hat{V}\right)|\tilde{J}KM\rangle = E_{\tilde{J}KM}|\tilde{J}KM\rangle, \tag{2.8}$$

onto a specific eigenstate, $|JKM\rangle$

$$E_{JK}\, d_{JKM} + \sum_{J'} d_{J'KM}\, \langle JKM|\hat{V}|J'KM\rangle = E_{\tilde{J}KM}\, d_{JKM}. \tag{2.9}$$

The second equation is exactly the sought matrix equation, $\underline{\underline{H}} \cdot \underline{d} = E_{\tilde{J}KM}\underline{d}$. The elements of the Hamiltonian matrix can all be expressed analytically: the diagonal term $E_{JK} = BJ(J+1) + (A-B)K^2$ is just the field-free energy and the coupling terms $\langle JKM|\hat{V}|J'KM\rangle$ can be expressed in terms of Wigner 3-j symbols (see Appendix A.1). The pendular states can thus be found by diagonalizing this Hamiltonian, a trivial operation that can be carried out using standard routines, for instance those found in [28]. With the wave function at hand we have all the knowledge about the system we can ever obtain and one can for instance calculate the angular distribution, $P(\theta)$, of the symmetry axis (see Appendix A.2). To characterize the degree of alignment an often used measure is the expectation value of $\cos^2\theta$. It is straightforward to calculate the value of this observable using the angular distribution or using the expansion in the field-free states. There is, however, an easier way of calculating this observable without even finding the wave function! Using the Hellmann-Feynmann theorem [29], it is possible to extract this observable just from the energies of the pendular states as function of intensity since it follows from the theorem that

$$\langle \cos^2\theta \rangle_{\tilde{J}KM} = -\frac{\partial\left(E_{\tilde{J}KM} + \frac{1}{4}E_0^2\alpha_\perp\right)}{\partial\left(\frac{1}{4}E_0^2\Delta\alpha\right)}. \tag{2.10}$$

As stated at the beginning of this Section the degree of alignment depends strongly on which pendular state we consider. For comparison with experiments it is therefore essential that effects of thermal averaging are considered. In order to do so we must know the distribution of initial states. It is usually assumed that the populations follow the Boltzmann distribution. In this case the probability that a given initial state is populated is given by

$$w_i = \frac{e^{-E_i/k_B T}}{\sum_j e^{-E_j/k_B T}}, \tag{2.11}$$

with E_i the field-free energy of the i'th initial state. As will be discussed later, experiments show that the state distribution for cold molecular beams does not follow the Boltzmann distribution, for instance anisotropic distributions of M states have been observed. The deviations from the Boltzmann distribution are however small enough that we can safely neglect this effect for now. The thermally averaged value, $\langle \cos^2\theta \rangle_T$, can thus be obtained as

$$\langle \cos^2\theta \rangle_T = \sum_i w_i \langle cos^2\theta \rangle_i, \tag{2.12}$$

with $i = \{J, K, M\}$ being the initial state.

For calculations of the pendular states of an an asymmetric top the overall procedure is just as described above but the matrix elements of the Hamiltonian become slightly more involved. For asymmetric tops it is still an advantage to expand the pendular state wave function in the symmetric top basis since all matrix elements can then be expressed analytically. The basis of field-free rotational states for the asymmetric top is inconvenient since no analytical expressions exist for these states; they are most commonly found by diagonalizing the Hamiltonian matrix in the symmetric top basis. Once the total Hamiltonian has been expressed in the symmetric top basis, the procedure outlined above can readily be followed. The major challenge regarding asymmetric tops is a numerical one: since the interaction in Eq. (2.5) couples states of different indices τ, the blocks in the Hamiltonian are dramatically expanded compared to the symmetric top case (where the Hamiltonian is block diagonal in both K and M).

The black lines in Figure 2.2 shows the thermally-averaged expectation value $\langle \cos^2\theta \rangle_T$ for *tert*-butyliodide as a function of intensity for a range of rotational temperatures. In the figure several general features can be observed. First and foremost, the strong influence of rotational temperature on the degree of alignment is clearly seen. In an experiment at room temperature, for instance in a gas cell, only a weak degree of alignment can be obtained at non-ionizing intensities; for this molecule ionization by the aligning laser field will most likely set in at intensities of $2 \cdot 10^{12}$ W/cm^2 or so[c]. In pulsed, supersonic molecular beams temperatures below 10 K are commonly achieved and temperatures down to 0.1 K are feasible [30, 31]. In this cold

[c]This intensity was estimated from experiments on adiabatic alignment of iodobenzene which has a similar ionization potential.

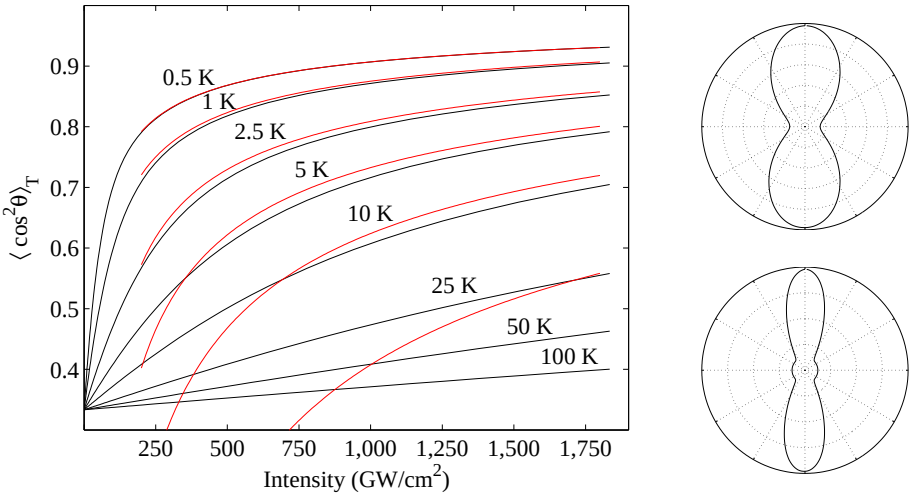

FIGURE 2.2: Left: The black curves show the degree of adiabatic alignment for *tert*-butyliodide as function of intensity calculated for a range of rotational temperatures by solving the time-independent Schrödinger equation. The red curves show the estimate given in Eq. (2.13). Right: Polar plots of the angular distribution, $P(\theta)$, at 1 K and an intensity of 100 GW/cm^2 (upper) and 1200 GW/cm^2 (lower) for a vertically polarized alignment laser. The radial scale is goes to 1.8 (6.8) in the upper (lower) graph.

regime, very high degrees of alignment can be obtained at quite modest intensities since only the lowest rotational states are populated. At low temperatures the alignment curves also reveal a saturation-like intensity dependence. Once all the pendular states are trapped in the harmonic region of the potential, increasing the intensity does not change the degree of alignment significantly. In a real experiment where molecules exposed to a range of intensities of the aligning laser are probed one can therefore obtain an almost uniform degree of alignment.

For linear molecules Seideman [32] gave an approximate expression for the degree of alignment in the high temperature limit

$$\langle \cos^2\theta \rangle \approx 1 - \sqrt{\frac{\pi kT}{\Delta\alpha E_0^2}} \left(\frac{3}{4}\frac{hB}{kT} + 1 \right). \tag{2.13}$$

The red curves in Fig. 2.2 shows the degree of alignment calculated from this equation for the temperatures from 0.5 K to 25 K. Surprisingly, the equation, which was derived for linear molecules, gives at very good estimate for the degree of alignment at low temperatures: at 0.5 K the numerically calculated curve and that obtained from the simple estimate are indistinguishable at intensities above 200 GW/cm^2. At the higher temperatures we observe significant deviations, especially at the lower intensities; the

domain of validity of this approximation is therefore $hB \ll kT \ll \Delta\alpha E_0^2$. A general property that can be derived from Eq. (2.13) is that for high temperatures ($kT \gg hB$, which is fulfilled even at very low temperatures for the iodine containing species considered in this work since $kT/h \approx 20$ GHz at 1 K) the degree of alignment only depends on the parameter $kT/\Delta\alpha E^2$. Friedrich and Herschbach [33] showed that in the high temperature, low intensity limit ($kT \gg \Delta\alpha E_0^2, hB$) adiabatic is well described by classical mechanics and that the degree of alignment in this limit only depends on this single parameter as well. If the degree of alignment only depends on this parameter we have a very powerful scaling law: by calculating the degree of alignment as function of intensity at one temperature we can find the degree of alignment at other temperatures simply by re-scaling the intensities. The scaling law was tested with the full numerical calculations for a symmetric top with temperatures in the range 1 K to 100 K and can be used with high precision.

Figure 2.2 also shows the angular distributions calculated at 1 K and an intensity of 100 GW/cm^2 and 1200 GW/cm^2 respectively. In both cases the distributions are strongly peaked along the laser polarization. Especially for high intensities and low temperatures it is reasonable to think of the molecule as being fixed-in-space. Investigations of orientational effects in molecules can thus be carried out systematically via fixation of the target by an alignment laser rather than having to worry about tedious deconvolutions. This qualitative picture is, of course, based on the assumption that the rotational degrees of freedom are decoupled from the process being investigated.

2.3 Nonadiabatic alignment

The term 'nonadiabatic alignment' covers a very broad range of scenarios since it basically deals with any pulse duration too short to be adiabatic. In this Dissertation only the short pulse limit, where pulse durations are on the order of 1/100th of the rotational period or less, is considered. This limit is particularly interesting since these pulse durations are in general capable of creating rotational wave packets that become highly localized when the external field is no longer present: the molecules can become aligned under field-free conditions. To show that this post-pulse alignment is a general feature of molecules exposed to the rotational kick from a short pulse interacting with the polarizability Seideman [32] and Averbukh and co-workers [34, 35] independently analyzed the rotational dynamics of a molecule exposed to a δ-kick and indeed found that the excited wave packet had relative phases encoded that inevitably lead to alignment. As shown by Averbukh and co-workers the short-time evolution of the rotational ground state can be fully understood by classical mechanics. Their model considers a classical ensemble of isotropically distributed linear, rigid rotors with negligible angular velocity. If these rotors interact with a very short laser pulse through the polarizability interaction (Eq. (2.4)) we can find their final angular velocity. The torque, $\tau = -\mathbf{r} \times \nabla V$ can be used to find the angular momentum,

$J = |\mathbf{J}|$, transferred to the rotors

$$J = \int \tau \, \mathrm{d}t = \tfrac{1}{4}\Delta\alpha \int E_0^2 \, \mathrm{d}t \sin(2\theta_0) \equiv IP \sin(2\theta_0), \tag{2.14}$$

where θ_0 is the initial angle, I is the moment of inertia and P is the interaction strength. Using $|J| = I|\dot{\theta}|$ we thus find

$$\dot{\theta} = -P \sin(2\theta_0). \tag{2.15}$$

It readily follows that rotors starting close the polarization of the laser ($\theta \sim 0, \pi$) obtain an angular velocity proportional to their angle with the polarization axis. At time $t = 1/(2P)$ all these rotors will be aligned along the polarization axis. Since the linear approximation of a sine function is a good approximation for quite large angles it will be a large fraction of the rotors that reach the polarization axis at nearly the same time; the ensemble becomes aligned albeit only for a short time. Two fundamental limitations of short pulse alignment are readily extracted from this simple model. First of all the molecules are only aligned for a short time. If the alignment is to be utilized in short pulse experiments this need not be a limitation at all. Secondly there is a limit to the degree of alignment. No matter how hard we kick the molecules starting at large angles (close to the equator) will always lag behind. In Chapter 6 it is experimentally and numerically shown that this limitation can be overcome by using more than one pulse.

The treatment of nonadiabatic alignment is organized as follows. First, details are given on the quantum mechanical theory of nonadiabatic alignment of symmetric tops. Second, the extension of this theory to asymmetric tops is sketched. Next, the effects of probing a finite volume in the focus is considered. This turns out to be important even for a qualitative comparison of numerical and experimental results. Finally, the consequences of an anisotropic distribution of M quantum numbers in the molecular beam are considered.

2.3.1 Symmetric tops

The fundamental difference between adiabatic and nonadiabatic alignment is that the time evolution must be considered explicitly in the latter case. Two time ranges are considered independently: the interaction with the laser pulse and the field-free evolution after the pulse. During the interaction between the molecules and the laser pulse we must resort to numerical methods to solve the time-dependent Schrödinger equation

$$i\hbar \, \partial_t |\psi(t)\rangle = \hat{H} |\psi(t)\rangle, \tag{2.16}$$

where the Hamiltonian, $\hat{H}$, is the sum of Eq. (2.6) and Eq. (2.4). Just as for the adiabatic case, we start by expanding the unknown wave function in the field-free

eigenstates of the symmetric top

$$|\psi_i(t)\rangle = \sum_{J'} C^i_{J'}(t)\,|J'KM\rangle, \tag{2.17}$$

where $i = \{J_i, K_i, M_i\}$ is a collective index denoting the initial state and K, M have been omitted in labelling the expansion coefficients, $C^i_{J'}(t)$, since these are conserved quantum numbers. Inserting this expansion into the time-dependent Schrödinger equation and projecting onto a specific eigenstate $|JKM\rangle$ we find

$$i\hbar\dot{C}^i_J(t) = E_{JK}C^i_J(t) + \sum_{J'} C^i_{J'}(t)\,\langle JKM|\hat{V}|J'KM\rangle. \tag{2.18}$$

This is a set of coupled, linear, first order differential equations. Details on the numerical approach taken to solve these equations are given in Appendix A.3. In brief, an adaptive step-size routine is used to propagate the differential equations during the interaction with the laser pulse. To minimize computational time the size of the basis set, that is the number of J states included, is dependent on the intensity of the alignment pulse. After the interaction with the laser pulse, the molecules rotate free of any external fields. The time evolution of the wave packet is then trivially found by considering the time evolution of each component in the wave packet

$$|\psi_i(t)\rangle = \sum_{J'} C^i_{J'}(t_0)\,|J'KM\rangle\, e^{iE_{J'K}(t-t_0)/\hbar}, \tag{2.19}$$

where t_0 is the time when the molecules become field-free.[d] Once the expansion coefficients are found the expectation value of $\cos^2\theta$ is readily calculated

$$\langle\cos^2\theta\rangle_i(t) = \sum_{J,J'} C^{i*}_{J'}(t)C^i_J(t)\,\langle J'KM|\cos^2\theta|JKM\rangle. \tag{2.20}$$

The thermal average is then obtained using Eq. (2.12).

To substantiate the theory outlined and to highlight some general features of nonadiabatic alignment a specific case will now be considered: *tert*-butyliodide interacting with a 1 ps laser pulse having a peak intensity of 6 TW/cm^2. According to the classical δ-kick model the molecules should align at about 0.5 ps after the laser pulse. Since this is shorter than the pulse duration we can immediately see that the molecules will start to align while they are still interacting with the laser pulse. This contradicts the assumptions in the δ-kick model, but the model can still be used to estimate and rationalize the effects of the pulse. We start by estimating the magnitude of the kick. The relevant quantity is the average angular momentum transferred to the ensemble. Using Eq. (2.14) we find

$$\langle J\rangle_{\delta\text{-kick}} = \sqrt{\langle J^2\rangle} = \tfrac{1}{\sqrt{2}}IP = 33, \tag{2.21}$$

[d] Chosen as the time where the intensity is below some fraction of the peak intensity.

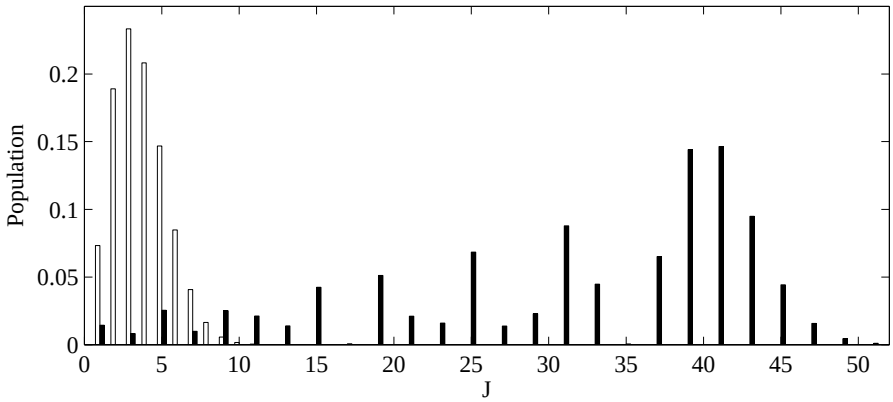

FIGURE 2.3: Open bars: relative population of the initial states at a temperature of 1 K. Shown is the relative populations (including M degeneracy) in the $K = 0$ subset of states. Full bars: relative population amongst the J states in the wave packet excited from the $|JKM\rangle = |000\rangle$ initial state by a laser pulse with $I = 6$ TW/cm^2 and $\tau = 1$ ps.

with J measured in units of $\hbar$. Solving the time-dependent Schrödinger equation we can extract the corresponding expectation value in the quantum mechanical treatment of the problem. The full bars in Fig. 2.3 show the populations in the J states, i.e. $|C_J|^2$, in the wave packet created from the $|JKM\rangle = |000\rangle$ initial state. Using these populations we can calculate the expectation value of the quantum mechanical $\hat{J}^2$ operator for the wave packet and thus find the average angular momentum in the wave packet

$$\langle J\rangle_{\text{wp}} = \sqrt{\langle \hat{J}^2\rangle} = \sum_{J'} |C_{J'}|^2 \, J'(J'+1) = 33. \tag{2.22}$$

Surprisingly, the classical model gives the correct value for the average angular momentum of the wave packet. However, the distribution of J states does show noticeable differences between the classical and quantum mechanical model.

In the quantum mechanical description, the wave packet is created by a sequence of rotational Raman transitions. The angular momentum of the wave packet therefore also reveals the large number of transitions used to create the wave packet. In Fig. 2.3 the open bars show the relative population amongst the $K = 0$ subset of initial states in an ensemble at a temperature of 1 K. Clearly at such low temperatures we can safely say that the rotation of the molecules is completely dominated by the kick from the laser pulse. If the initial ensemble was at room temperature, the peak in the Boltzmann distribution would be at $J = 44$ with a long tail extending to larger J values; in that case thermal motion cannot be neglected. Another property of the wave packet which is apparent from Fig. 2.3 is that it is very broad in J space. As discussed

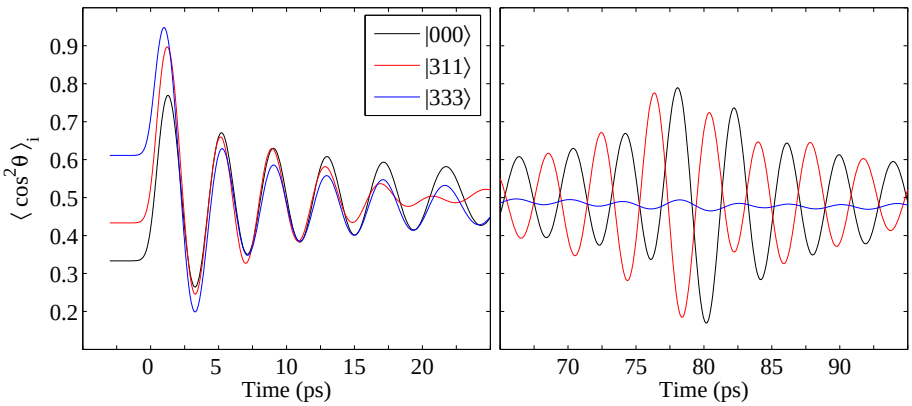

FIGURE 2.4: Initial state dependence in the dynamical evolution of the degree of alignment.The calculation is for *tert*-butyliodide exposed to a 1 ps pulse with a peak intensity of 6 TW/cm^2.

previously this renders possible a high degree of confinement in angular space that is, a high degree of alignment. In the left panel of Fig. 2.4, the black curve shows the degree of alignment for the wave packet evolving from the $|000\rangle$ initial state. At very short times, just over 1 ps after the peak of the alignment pulse, the molecules do indeed become strongly aligned. The high angular momentum of the wave packet is equivalent to the molecules rotating rapidly, so the degree of alignment drops rapidly after this peak. Due to the quantum mechanical nature of the molecules the degree of alignment does however exhibit damped oscillatory behavior. These fast oscillations are due to beatings between the rapidly oscillating phases of the highest J states in the wave packet (see below).

In spite of the fact that the J levels excited in the wave packet are much higher than the ones populated thermally, it turns out that thermal averaging is even more important for nonadiabatic alignment than for adiabatic alignment. For nonadiabatic alignment not only the degree of alignment but also the dynamical evolution is dependent on the initial state. Figure 2.4 shows the degree of alignment evolving from three different initial states of *tert*-butyliodide after interaction with the 1 ps laser pulse described above. The left panel shows the degree of alignment immediately after the laser pulse whereas the right panel shows the alignment in a time window at larger delays. At short delays, the degree of alignment is somewhat different for the different initial states but the frequencies and phases of the oscillations are almost identical. On a qualitative level they behave quite similarly. At the larger delays the behavior is dramatically different for each of the initial states. For the initial state $|JKM\rangle = |333\rangle$ the degree of alignment is hardly dependent on time in the window shown. This is in strong contrast to the evolution of the degree of alignment evolving from the $|000\rangle$ and

$|311\rangle$ states where large oscillations are observed. The oscillations are almost exactly out of phase.

Let us start by discussing the reason for the similarities at the early delays. As stated previously, the interaction term surpasses the field-free energy by orders of magnitude. It is therefore hardly surprising that three different initial states evolve into wave packets with very roughly the same content of J states — in all three cases the peak of the distribution is at $J \sim 40$. About two picoseconds after reaching its peak value the intensity of the laser field becomes negligible and the evolution of the wave packet fully determined by the field-free evolution of each component given in Eq. (2.19). From there we find that the Jth component of the wave packet acquires a phase of

$$\varphi_J = E_{JK}\Delta t/\hbar = 2\pi \left(BJ(J+1) + (A-B)K^2\right)\Delta t \tag{2.23}$$

upon propagating for a delay of Δt. In the case of linear alignment where K is a conserved quantum number, the second term contributes only to an overall phase shift of the wave function and need not be considered. From this equation we can directly extract the source of the ~ 4 ps period for the oscillations in the degree of alignment: they are due to beatings in the phase of the high J states in the wave packet (which are the ones with the highest population, see Fig. 2.3).

For a more detailed explanation we can write the temporal evolution of the observable $\langle\cos^2\theta\rangle_i(t)$ in Eq. (2.20) as

$$\begin{aligned}
\langle\cos^2\theta\rangle_i(t) &= \sum_{J',J''} C^{i*}_{J'}(t_0)\, C^i_{J''}(t_0) e^{-i(E_{J''}-E_{J'})\Delta t/\hbar} \langle J'KM|\cos^2\theta|J''KM\rangle \\
&= \sum_{J'} |C^i_{J'}|^2 \langle J'KM|\cos^2\theta|J'KM\rangle \\
&+ \sum_{J'} 2\,|C^i_{J'}|\,|C^i_{J'-1}| \langle J'-1KM|\cos^2\theta|J'KM\rangle \cos\left(\omega^{(1)}_{J'}\Delta t - \phi^{(1)}_{J'}\right) \\
&+ \sum_{J'} 2\,|C^i_{J'}|\,|C^i_{J'-2}| \langle J'-2KM|\cos^2\theta|J'KM\rangle \cos\left(\omega^{(2)}_{J'}\Delta t - \phi^{(2)}_{J'}\right),
\end{aligned} \tag{2.24}$$

with $\Delta t = t - t_0$ the delay from the time when the molecules became field-free, $\omega^{(n)}_{J'} = (E_{J'} - E_{J'-n})/\hbar$ and $\phi^{(n)}_{J'}$ is the phase difference at time t_0 between the components J' and $J'-n$ of the wave packet. The equation shows three contributions to the temporal evolution of $\langle\cos^2\theta\rangle$: a constant term, a term corresponding to beatings between levels with $\Delta J = \pm 1$ and a term with beatings between $\Delta J = \pm 2$ levels. Beatings between states with $\Delta J > 2$ cannot be observed in the time-evolution of $\langle\cos^2\theta\rangle$ due to the selection rules for the $\cos^2\theta$ operator. The strength of the oscillations is determined by two factors: the weight of the beating states in the wave packet, $|C^i_{J'}|\,|C^i_{J''}|$, and the matrix element of the observable, $\cos^2\theta$, connecting these states. The first factor turns out to show large differences for the three states considered here;

for the wave packet emerging from the $|000\rangle$ state parity is conserved and only even J states are populated whereas for the wave packet emerging from the $|333\rangle$ state there is an equal population in the even and odd J states. The similar appearance of the oscillations must therefore be due to the matrix elements, $\langle J'KM|\cos^2\theta|J''KM\rangle$. As shown in Appendix A.1 these can be expressed in terms of Wigner 3-j symbols. By examining the properties of the Wigner 3-j symbols (see Zare [36, Table 2.4]) it is found that the matrix element connecting states with $\Delta J = \pm 1$ scales as J^{-2} whereas for the element connecting $\Delta J = \pm 2$ the leading term in a series expansion is independent of J. With the distribution of J states peaking at high values of J the observable $\langle\cos^2\theta\rangle$ is not sensitive to the beatings between neighboring J states. The differences observed at the larger delays must be attributed to differences in the initially excited wave packet. Both the relative phases and the population in the individual J states are different for each of the initial states. The absence of alignment for the wave packet excited from the $|333\rangle$ state can be attributed to the fact that it contains an equal population in the even and odd J states — at $t = 1/(8B) = 80$ ps the $\Delta J = \pm 2$ beatings for even and odd J states are exactly out of phase by π.

The result of a calculation taking into account the thermal averaging at a temperature of 1 K is shown in Fig. 2.5. For comparison the degree of alignment for the wave packet excited from the $|000\rangle$ state is shown. About half the oscillations seen in the 0 K calculation are absent in the 1 K calculation whereas the rest persist. A closer inspection of the results reveal that the dynamics is perfectly periodic. At intervals spaced exactly by the rotational period of the molecule, $T_{\text{rot}} = 1/2B$ (B in frequency units) the initial wave packet is reconstructed [15, 21, 37–39]. This event is called a revival and is a purely quantum mechanical effect which can occur when the corresponding classical motion is stable. The reason for this peculiar behavior is found in the energy level structure of the molecule. If we consider the phase difference accumulated between two neighboring J states due to the field-free evolution

$$\varphi_J - \varphi_{J-1} = 2\pi\,(2B\,\Delta t)\,J, \tag{2.25}$$

we find that at time delays of $\Delta t = T_{\text{rev}} = 1/2B$ the phase difference between all neighboring states in the wave packet is exactly an integer multiple of 2π. The wave function is thus only changed by an unimportant overall phase. At the so-called half revival at time $t = T_{\text{rev}}/2$ we see that the relative sign between the components of the wave packet alternates. We note that the fractional revivals at times $T_{\text{rev}}p/q$ (with p, q mutual prime numbers) contain rich dynamics beyond that observed in the time-evolution of $\langle\cos^2\theta\rangle$ [34, 37, 40, 41]

Fig. 2.5 reveals another general feature of nonadiabatic alignment. The average value of $\langle\cos^2\theta\rangle_T$ away from the revivals is about 0.5, significantly higher than the value of $\frac{1}{3}$ for the initial isotropic distribution. This elevated basis level for the degree of alignment is sometimes referred to as the permanent alignment and is due to an anisotropic distribution of the angular momentum vectors after the interaction with

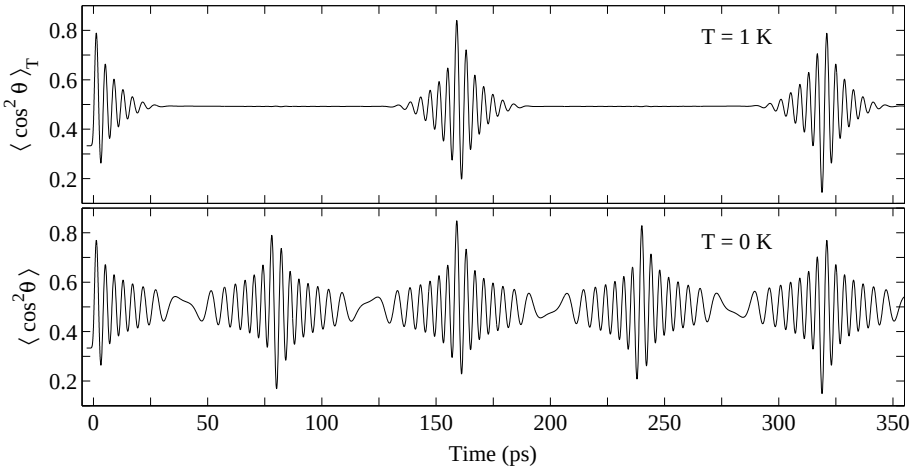

FIGURE 2.5: Alignment of *tert*-butyliodide exposed to a non-resonant laser pulse with an intensity of 6 TW/cm^2 and a pulse duration of 1 ps. The lower figure shows the dynamical evolution of the degree of alignment from the laser pulse until past the first full revival ($T_{\text{rev}} = 319.7$ ps) for a sample at zero Kelvin whereas the upper figure is for an rotational temperature of 1 K.

the laser pulse. In the wave packet very high J states become populated (Fig. 2.3) whereas M is conserved for the interaction with a linearly polarized laser pulse. The result is an ensemble with $\langle \hat{J}^2 \rangle_T \gg \langle J_Z^2 \rangle_T$ corresponding classically to the angular momentum being confined close to the plane perpendicular to the polarization axis. The absence of angular momenta close to the polar axis (molecules rotating in the plane perpendicular to polarization axis) is the reason for the higher value of $\langle \cos^2 \theta \rangle$ [38]. Quantum mechanically we can ascribe the permanent alignment to the constant term in Eq. (2.24).

2.3.2 Asymmetric tops

In the general case of asymmetric tops the numerical treatment becomes somewhat more involved. Part of the reason for this was outlined in the section on adiabatic alignment. The Hamiltonian representing an asymmetric top interacting with a linearly polarized non-resonant laser field is the sum of Eq. (2.2) and Eq. (2.5). As discussed previously the asymmetric top basis is inconvenient since the matrix elements of the interaction potential cannot be found analytically. Instead the wave function is expanded in the symmetric top basis, but now K is no longer a good quantum number

$$|\psi_i(t)\rangle = \sum_{J',K'} C^i_{J',K'}(t)\,|J'K'M\rangle. \tag{2.26}$$

Inserting into the time-dependent Schrödinger equation and projecting onto a specific state $|JKM\rangle$ the coupled differential equations for the expansion coefficients become

$$i\hbar\,\dot{C}^i_{JK}(t) = \sum_{J',K'} C^i_{J',K'}(t)\left\{\langle JKM|\hat{H}_{\rm rot}|J'K'M\rangle\,\delta_{J,J'} + \langle JKM|\hat{V}|J'K'M\rangle\right\}. \tag{2.27}$$

The first term corresponding to matrix elements of the field-free Hamiltonian is readily evaluated, see for instance Chapter 6 in Zare [36]. It is noted that the parity of K is conserved for this term. To evaluate the interaction term it is convenient to rewrite it in terms of Wigner rotation matrices since the matrix element is then reduced to an integral over a product of three rotation matrices which is readily evaluated using Eq (3.118) in Zare [36]. The interaction operator in Eq. (2.5) then becomes

$$\hat{V} = -\frac{E_0^2}{4}\left\{\tfrac{2}{3}\,\Delta\alpha_\parallel D^2_{00} - \tfrac{1}{\sqrt{6}}\,\Delta\alpha_\perp(D^2_{02} + D^2_{0-2})\right\}, \tag{2.28}$$

with $\Delta\alpha_\parallel = \alpha_{zz} - \frac{1}{2}(\alpha_{yy} + \alpha_{xx})$ and $\Delta\alpha_\perp = \alpha_{yy} - \alpha_{xx}$ the parallel and perpendicular polarizability anisotropy. An angle independent term corresponding to an overall energy shift has been omitted. From this expression we readily find the selection rules $K - K' = 0, \pm 2$ and $J - J' = 0, \pm 1, \pm 2$. The parity of K is thus conserved and a block diagonal representation of the Hamiltonian should be used in a numerical implementation.

After the interaction with the laser pulse the molecules rotate free of external fields and the evolution is determined solely by the Hamiltonian in Eq. (2.2). In this case it is advantageous to expand the wave packet in the eigenstates of this Hamiltonian rather than in the symmetric states. The transformation matrix is found by diagonalizing the asymmetric top Hamiltonian in the symmetric top basis. With the wave packet expressed in the field-free eigenstates the time evolution is merely a matter of phase evolution for each of the basis states

$$|\psi_i(t)\rangle = \sum_{J',\tau'} C^i_{J',\tau'}(t_0)\,|J'\tau'M\rangle\,e^{-iE_{J'\tau'}(t-t_0)/\hbar}. \tag{2.29}$$

With the wave packet expanded in the asymmetric top basis a transformation back to the symmetric top basis must be carried out to calculate the expectation value $\langle\cos^2\theta\rangle_i$. Numerically this is still advantageous over direct propagation of the wave packet in the symmetric top basis.

When observables like $\langle\cos^2\theta\rangle_T$ are considered at short delays after the alignment pulse, asymmetric tops behave much like symmetric tops. Under the right conditions an appreciable degree of alignment can be obtained in field-free conditions but the molecules only stay aligned for a brief period. The long term evolution of asymmetric tops is qualitatively different from the symmetric tops — it is not periodic on the time scale of the classical rotational period. The reason is that asymmetric tops do not

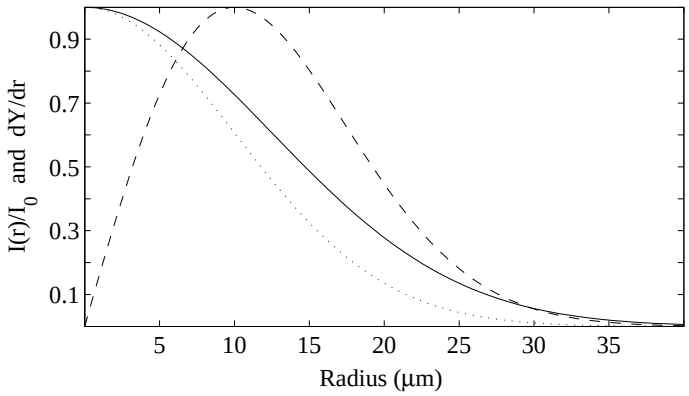

FIGURE 2.6: Radial intensity profile for the alignment (full line, $\omega_0 = 25\,\mu\mathrm{m}$) and probe (dotted, $\omega_0 = 20\,\mu\mathrm{m}$) laser pulses. Also shown is the relative detection probability pr radius (dashed). All three curves are normalized to their peak value.

have the regular energy level structure of symmetric tops, thus a complete rephasing of the wave packet is not obtained. Rather, for near symmetric tops partial rephasings are observed at times close to the revival time for the corresponding symmetric top. Partial rephasings are however also seen at other delays, more on this in Sec. 4.2. The main message is that the global maximum in the degree of alignment is always found during or immediately after the alignment pulse for asymmetric tops.

2.3.3 Focal volume averaging

To obtain even qualitative agreement between calculations and experiments on non-adiabatic alignment it turns out to be important to consider the consequences of the variation of the intensity of the aligning laser pulse within the volume being probed. This is particularly true for the experiments based on probing via single-photon resonant dissociation where the probe efficiency remains high in a large region of the pump focal volume. The main reason for the importance of these considerations is that the dynamical evolution of the degree of alignment is dependent on the intensity of the aligning laser field. More precisely, changing the intensity of the aligning laser changes the population distribution in the excited wave packet so the period and phase for the fast oscillations change.

Let us consider reconsider the example used above: *tert*-butyliodide at a rotational temperature of 1 K exposed to an alignment laser pulse with $\tau = 1$ ps and $I = 6$ TW/cm^2. Now, however, we will calculate the evolution of $\langle\cos^2\theta\rangle_T$ when the molecules are probed with an efficiency proportional to the intensity of the probe laser. The spot sizes are chosen as $\omega_0(\mathrm{align}) = 25\,\mu\mathrm{m}$ and $\omega_0(\mathrm{probe}) = 20\,\mu\mathrm{m}$. In Fig. 2.6

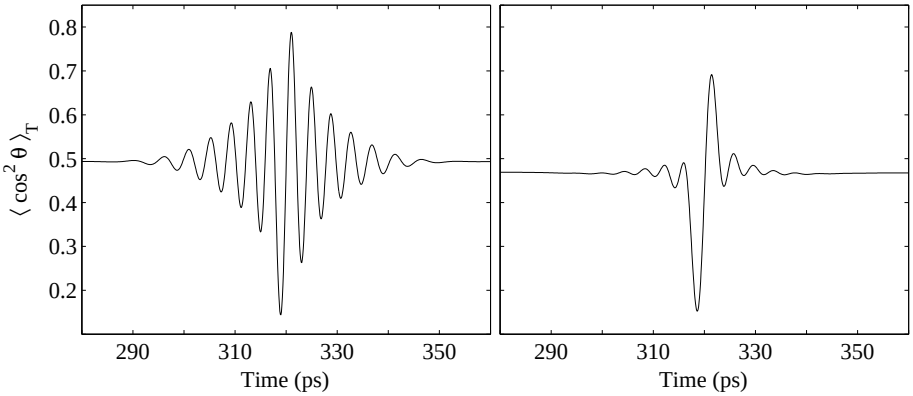

FIGURE 2.7: Focal volume averaging effects in the degree of alignment for *tert*-butyliodide at a temperature of 1 K exposed to a 6 TW/cm^2, 1 ps laser pulse. Left panel: peak intensity calculation, right panel: focal volume averaged result assuming a linear intensity dependence for probe efficiency.

the radial intensity distribution at the beam waist is shown for the alignment and probe laser beams assuming a Gaussian profile for both. Also shown is the relative detection probability as function of radius. For calculating this curve, it is assumed that the detection probability is independent of the position in the longitudinal direction such that the probed volume has cylindrical symmetry — this is a reasonable assumption for our molecular beam experiments. In this case the yield from a cylindrical shell of radius r and thickness dr is

$$\mathrm{d}Y \;=\; \sigma\, I(r)\, n\, \mathrm{d}V = A\, \exp\left(-\frac{2\,r^2}{\omega_{0,\mathrm{p}}^2}\right) r\, \mathrm{d}r, \tag{2.30}$$

with σ the photoabsorbtion cross section and n the number density of molecules. The relative detection probability plotted in Fig. 2.6 is $\frac{\mathrm{d}Y}{\mathrm{d}r}$ normalized to its peak value. In the numerical implementation the probe focal volume (cut off at $r = 1.7\,\omega_0(\mathrm{probe})$) is divided into 30 cylindrical isointensity shells. Calculations are then carried out at intensities corresponding to the value in the middle of each shell and the results, $\langle\cos^2\theta\rangle_T(I(r),t)$, are given a weight proportional to $\frac{\mathrm{d}Y}{\mathrm{d}r}$. The result of such averaging is shown in Fig. 2.5 together with the result from a calculation only at the peak intensity. Clearly a lot of information is lost due to focal volume averaging. Unless care is taken to avoid these effects it might be important to remember what may lie hidden under the observed results. This is especially true for experiments on strong-field ionization of molecules where intensity dependence and geometrical effects may be strongly coupled [8, 42].

Carrying out the focal volume averaging does of course imply longer computa-

tional times but the situation is not as bad as it may appear. First of all, in the numerical implementation for the symmetric tops an adaptive step size routine was chosen. This saves time during the slow evolution in the low intensity regions. Further one can make the size of the basis set dependent on the intensity, speeding up the calculations even further in the low intensity regions. See Appendix A.3 for further details.

2.3.4 Anisotropic M distributions

As noted previously, experiments show that in cold molecular beams the initial states are not populated according to the Boltzmann distribution [3, 43–45]. In the Boltzmann distribution the population is solely determined by the ratio of energy of the given initial state to the thermal energy kT. Degenerate M states are thus evenly populated for a given J. Experiments on seeded beams show that this is not the case. Choosing the molecular beam axis as the laboratory fixed X-axis, it is found that states of high $|M_X|$ are suppressed. The origin of this discrepancy lies in the geometrical cross section for collisions between the seeded molecules and the carrier gas. For a linear molecule the geometrical cross section is different for edge-on and broadside collisions with the latter collision geometry leading to the largest cross section. In the classical limit high $|M_X|$ states correspond to molecules rotating with their internuclear axes confined to the plane perpendicular to the the beam axis. These states will therefore primarily undergo broadside collision with the carrier gas atoms and since both elastic and inelastic collisions may change the M quantum number a non-thermal distribution is created. The anisotropic distribution of M states corresponds to an alignment of the angular momentum vector and thereby an anisotropic distribution of internuclear axis. The phenomenon is therefore often referred to as collisional alignment.

To quantify the degree of anisotropy, one can approximate the distribution of M states along the beam axis for a given J by

$$\rho_X(J, M_X) = P_J \, N_J \, [1 + a_2 P_2(\cos\vartheta)] \,, \tag{2.31}$$

with $P_2(x)$ the second Legendre polynomial, $\cos\vartheta = M_X/\sqrt{J(J+1)}$ and $P_J = \exp(-E_J/k_\mathrm{B}T)$ the Boltzmann probability for populating the given $|JM\rangle$ state. N_J is a normalization constant chosen such that

$$\sum_{M_X} \rho_X(J, M_X) = (2J+1) \exp\left(-\frac{E_J}{k_\mathrm{B}T}\right). \tag{2.32}$$

In most of our experiments the alignment laser is polarized perpendicular to the beam axis. The distribution in Eq. (2.31) must therefore be rotated by 90° when the direction of the laser polarization is used as the polar axis. The distribution of M states is this reference frame is

$$\rho_Z(J, M_Z) = \sum_{M_X} \left| d^J_{M_Z M_X}\left(\tfrac{\pi}{2}\right)\right|^2 \rho_X(J, M_X), \tag{2.33}$$

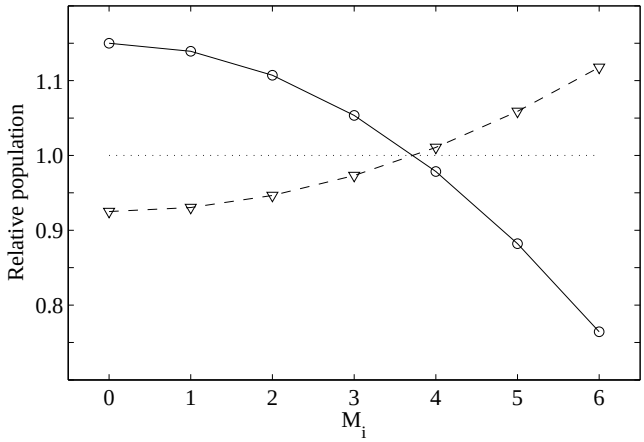

FIGURE 2.8: Relative population of $|J = 6, M\rangle$ states parallel to the beam axis (circles) and perpendicular to the beam axis (triangles) using $a_2 = -0.3$ in Eq. (2.31). Connecting lines serve to guide the eye; the dotted line marks the Boltzmann distribution where all M states are equally populated.

where $d^J_{M'M}(\theta)$ are the elements of the reduced Wigner rotation matrix. Figure 2.8 shows the relative distribution of M states within the $J = 6$ subset obtained from Eq. (2.31) and Eq. (2.33) using $a_2 = -0.3$. This value was chosen from the experiments by Friedrich *et al.* on I_2 seeded in He [3]. From the figure we readily see that the probability for populating a given M level can be changed by more than 20 % along the beam axis and by 10 % perpendicular to the beam axis.

Since the dynamical evolution of the degree of alignment shows a strong initial state dependence (see Fig. 2.4), one could be worried that these deviations from a Boltzmann distribution would affect observables like $\langle \cos^2\theta \rangle_T$. To test this concern calculations have been carried out using the initial state distribution represented in Eq. (2.33). The upper graph in Fig. 2.9 shows the result from a calculation of the thermally averaged degree of alignment resulting from a 100 fs, $2.5 \cdot 10^{13}$ W/cm^2 pulse interacting with I_2 assuming a Boltzmann distribution at a temperature of 5 K. The lower graph shows the difference between the calculation using the Boltzmann distribution and one using the anisotropic distribution of M states. The deviations are normalized to the permanent degree of alignment obtained for the Boltzmann distribution. In spite of changes in the M distribution of about 10%, the resulting degree of alignment deviates only by a few percent and there are no qualitative differences in the evolution. Calculations have also been carried out for CO_2 using the results from Weida and Nesbitt [43]. Instead of using a J dependent value of a_2, a constant value of -0.15 was chosen. From the results presented in their paper this represents a clear upper limit to the anisotropy under the conditions in our experimental setup (see

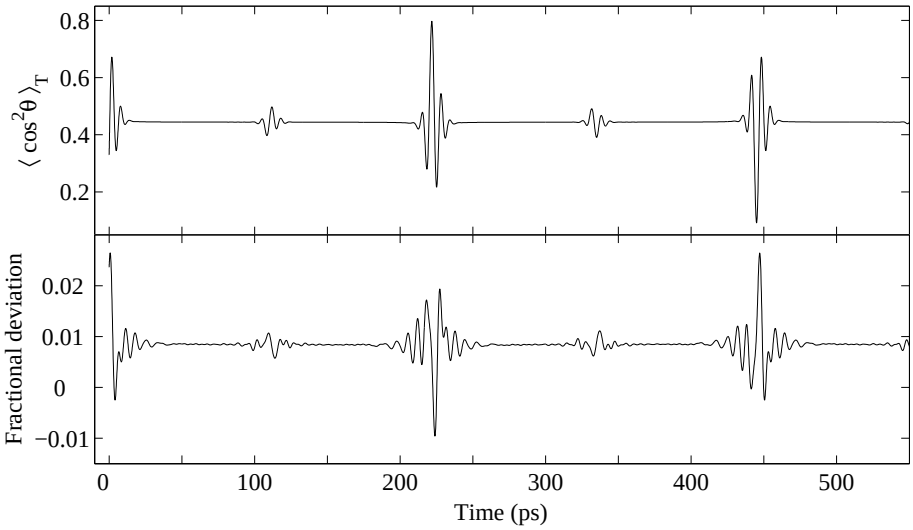

FIGURE 2.9: Upper graph: Degree of alignment for I_2 exposed to a 100 fs, $2.5 \cdot 10^{13}$ W/cm^2 laser pulse. Thermal averaging is carried out assuming a Boltzmann distribution of initial states at a temperature of 5 K. Lower graph: difference between the calculation using the Boltzmann distribution and one using Eq. (2.33) normalized to the permanent degree of alignment for the Boltzmann ensemble.

below). The reduced value compared to I_2 is at least partly due to the smaller velocity slip between CO_2 and He compared to I_2 and He. The resulting differences were once again on a few percent. A final concern comes from the experiments on O_2 by Aquilanti *et al.* [44]. Their experiments show that the degree of collisional alignment changes dramatically within the molecular pulse, with the fast molecules in the leading edge of the pulse exhibiting largest anisotropy. Since the anisotropies measured in Friedrich *et al.* [3] and Weida and Nesbitt [43] are averaged over the molecular pulse they may underestimate the effect in the leading edge of the pulse where the molecules are coldest and we therefore carry out our experiments.[e] As a worst case scenario we can assume an anisotropy $a_2 = -1.0$ and a very low temperature (at low temperatures the number of initial states that effectively contribute to the thermal averaging is low and the average becomes more sensitive to the actual states used). A calculation has been carried out for I_2 at a rotational temperature of 1 K with laser parameters as above. On a qualitative level the result are hardly different from the result of a calculation based on the Boltzmann distribution — nearly all deviations are within 5 % of the

[e] Molecular beam experiments using ns or shorter laser pulses are effectively using a velocity selected beam since the combination of a short interaction time and even a modestly tight focusing selects a small fraction of the molecular pulse.

permanent level with a single point showing an 8 % deviation. Considering the large uncertainties in the experimental determination of $\langle \cos^2 \theta \rangle$ it is reasonable to assume a Boltzmann distribution for the initial states.

One flaw in the above argument is the fact that the conditions in the experiments mentioned above do not match the conditions present in our experiments. In the experiments cited typical stagnation pressures were a few hundred Torr $\cdot$ mm whereas in our experiments they are typically at least an order of magnitude higher. This leads to a significantly higher number of collisions. From the detailed investigation in Weida and Nesbitt [43] it is still not clear what would happen at such high stagnation pressures. These authors do however speculate that the degree of collisional alignment will decrease at higher stagnation pressures. Our conditions may thus be even closer to the Boltzmann limit.

2.4 3D alignment

The theory outlined above applies to the case when the alignment laser is linearly polarized and it was shown that this can lead to control of the spatial orientation of one major axis in the molecule. Since most molecules are asymmetric tops with complex three dimensional structures it is interesting to identify schemes for controlling the complete three dimensional orientation (or alignment) of molecules. To obtain this kind of control the electrical field must have components in two orthogonal directions in space: once control is obtained over two axes in the molecule the third axis will automatically be fixed if the molecule is rigid.

The interaction potential created with electrical fields that are no longer linearly polarized can be obtained from Eq. (2.1) by using the direction cosines (Eq. (3.36) in the book of Zare [36]) to carry out the transformation between the space- and body-fixed components of the polarizability tensor. For an elliptical field the expression is rather involved (see Eq. (6.3) in Larsen [46]) and will not be reproduced here. The most important feature of the interaction potential for an elliptical field is that the potential now depends on all three Euler angles with the global energy minimum for molecules aligned with the axis of highest polarizability along the major axis of the electrical field and the axis of second highest polarizability along the minor axis of the field. Please note, that for elliptical polarization the space fixed Z axis is conventionally along direction of propagation for the laser. To clarify the transition from linear to elliptical polarization it is more convenient to define a space fixed frame for the latter case where the major axis of the electrical field defines the Z axis and the minor axis defines the X axis. In this frame the presence of the X component of the electrical field breaks cylindrical symmetry and facilitates a mixing of M states. Just as a superposition of J states can lead to a confinement of the θ angle, a superposition of M states can lead to a confinement of the ϕ angle (as noted previously rotations of the χ angle is already restricted in the case of linear polarization).

Several schemes have been suggested for three-dimensional alignment [20, 47, 48]. A more detailed consideration of their individual strengths will be postponed to Chapter 8. For now the straightforward generalizations of the one dimensional alignment schemes will briefly be outlined. In the adiabatic limit the physical picture is clear. Just as for a linearly polarized field, an elliptically polarized field will slowly guide the molecules into the most energetically favorable configuration with the degree of alignment limited by the thermal energy of the molecule. The two important field parameters are the intensity and the eccentricity. The intensity will always be limited by ionization of the molecules whereas the choice of eccentricity is more subtle. Its value must be determined by a trade-off between the confinement of the axis of highest polarizability compared to the confinement of the molecular plane to the plane of polarization. In the other limit where the molecules are exposed to a short pulse of elliptical polarization things become complicated by the fact that we must consider the dynamical aspect along with the properties of the interaction. In this case the choice of eccentricity becomes restrained by the fact all three Euler angles must be confined at the same time. In a simplified picture we can think of the molecules as getting a kick around two perpendicular body fixed axes with different moments of inertia. These kicks must lead to alignment at the same time so the eccentricity must be chosen the match the kick strengths to the moments of inertia. In a classical picture, the kick strength depends on the initial orientation of the molecule and the choice of eccentricity becomes non-trivial.

CHAPTER 3

Experimental setup

Molecular alignment can be measured in a number of different ways. Many methods rely on the fact that the interaction between polarized light and molecules depend on their relative orientation. Amongst these angle-dependent effects are linear dichroism [49, 50], the optical Kerr effect [51–54] and recently high-order harmonic generation in molecules has been shown to be very sensitive to alignment [55–59]. Measuring the change of the rotational contour of a Raman transition has also been used to track the transition from field-free states to pendular states [17]. Finally, adiabatic alignment has been observed in an electron diffraction experiment [60]. In our lab we have chosen a different approach that directly visualizes the orientation of the molecule: photo-fragment imaging, a technique also used by several other groups [21, 40, 61, 62]. The idea of using photo-fragment imaging for studying molecular orientation is elaborated below. The equipment used for inducing and measuring molecular alignment is then introduced.

3.1 Photo-fragment imaging

At the core of all our experiments lies the idea of using photo-fragment imaging to reveal the spatial orientation of a molecule. Conceptually this approach is very straightforward and consist of two steps. The first step is to make the molecule break up into

charged fragments. This can, for instance, be accomplished through dissociation into neutral fragments by a UV pulse followed by ionization at a later instant or through multiple ionization by a very intense laser pulse. In the latter case the multiply charged molecular ion is often not stable and rapidly breaks into charged fragments, a process called Coulomb explosion since it is the Coulomb repulsion between the nuclei that drives the fragments away from each other. In both cases it is crucial that fragments separate according to the axial recoil approximation, that is, that their recoil velocity is along the bond axis.[a] If this condition is fulfilled, the recoil velocities of the fragments carry direct information about the spatial orientation of the molecule. For rapid dissociation of the fragments, this statement remains true even if the molecule is rotating: as soon as the fragments start to separate the moment of inertia increases and by conservation of angular momentum the angular velocity must decrease, thus freezing the rotational motion. The second step is to measure the recoil velocity of the fragments. This can be carried out by using moderate electrostatic fields to project the ions onto a position sensitive detector. When using an appropriate configuration of electrodes and fields, the position of impact on the detector depends only on the initial ion velocity. Further, the fragments arrive at times determined by their mass to charge ratio so ion-specific detection can be accomplished by time-gating the gain of the detector. The experimentally measured quantity is thus the recoil velocity of one specific fragment ion.

As an example, consider *tert*-butyliodide. For this molecule the absorbtion of 266 nm light drives a $n \rightarrow \sigma^*$ transition that leads to a fast and direct breakage of the C$-$I bond. The neutral iodine atom can subsequently be ionized and the recoil direction be detected. If, instead, an intense 800 nm pulse is used one may, for instance, rip off three electrons leading to an unstable triply-charged molecular ion that can fragment into a singly-charged iodine ion and some carbohydride fragments. In both cases the recoil velocity of the iodine ion contains information about the orientation of the molecule or more precisely the direction of the C$-$I bond at the instant of fragmentation. Repeating this measurement many times yields an ensemble-averaged distribution of orientations.

3.2 The setup

To carry out an experiment as described above a number of ingredients are needed. First of all, we need some laser pulses to induce and detect the alignment of the molecules. Secondly, charged particle imaging requires that the experiments be carried out under high-vacuum conditions. Finally, in order to obtain a high degree of alignment

[a] For polyatomic molecules it is easy to envisage scenarios where the axial recoil approximation is not valid. For dissociation into neutral fragments a slow, indirect process will give the molecule time to rotate before dissociating and in Coulomb explosion a charge-asymmetric ion maybe created (having a relative excess charge in one side of the molecule) [63].

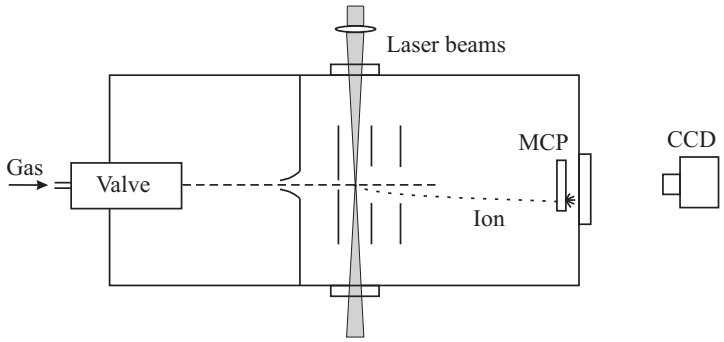

FIGURE 3.1: Schematic drawing off both vacuum systems — see text for details.

we must be able to prepare a sample of cold molecules.

3.2.1 Vacuum and detection system

For the experiments described in this Dissertation, two different vacuum systems have been used. The basic principle of operation is the same, but the more recently build chamber offers some advantages. Figure 3.1 shows a sketch of the basic principle of the vacuum systems.

At first the molecules are mixed with a carrier gas and leaked into the vacuum system through a pulsed valve with a small nozzle. During this expansion the seeded molecules undergo a large number of collisions with carrier gas atoms. Eventually, all carrier gas atoms and seed molecules fly at almost the same speed — the gas has been cooled. Since the seed gas can reach speeds higher than the local speed of sound this process is called a supersonic expansion [64]. The cooling thus obtained can be dramatic — sub-Kelvin temperatures have been reported by Even and co-workers [30, 31]. In the old chamber the molecular sample is sent into the pulsed valve using a gas flow system. In this system a continuous flow of He or Ar at a pressure of a few bar is bubbled through a liquid sample, dragging some molecules along. The pulsed valve (R. M. Jordan, PSV C–211) is a Gentry-Giese type valve that produces gas pulses with a duration of 60 µs at a repetition rate of 20 Hz; translational and rotational temperatures down to a few Kelvin can be obtained. Better cooling is obtained using Ar as carrier gas but the signal level is in general low compared to that obtained with He. The superior cooling in Ar is due to the large momentum transfer in each collision during the expansion, while the higher signal level in He is due to narrower angular distribution for the heavy seed molecule caused by the large difference in Mach numbers [64]. The superior cooling in Ar can partly be compensated by the fact that higher backing pressures of He can used, typically 3–4 bars of He is used

while only 1 bar Ar can be used, since the signal typically becomes too small at higher backing pressures. In the new vacuum system we use an Even-Lavie valve. This valve is a miniaturized, solenoid-actuated valve that can operate at repetition rates of up to 40 Hz. One major advantage of the valve is that the sample holder is placed inside the valve body which can be heated to 250° C, thus facilitating the use of both liquid and solid samples. Gaseous samples can be used by feeding an appropriate gas mixture to the valve. Another advantage of this valve is that very high backing pressures can be used — up to 100 bar of He[b] — whereby sub-Kelvin cooling can be achieved. In order to maintain high-vacuum conditions with low pumping requirements the valve delivers very short gas pulses with durations down to about 10 μs. Finally the valve uses a conical nozzle which reduces the divergence of the molecular beam and thus increase the sample density in the interaction region. All in all the Even-Lavie valve shows superior performance on all parameters compared to the Jordan valve: a higher density of colder molecules with lower pumping requirements is obtained. As an extra feature it possible to access much larger range of temperatures in the molecular beam, see Chapter 5. Most of the experiments presented using this Dissertation were carried out on the old system; only the experiments on adiabatic alignment and on photoelectron spectroscopy were carried out in the new vacuum chamber.

In the vacuum chamber the molecules are sent towards the region where they interact with the laser beams. To reach the best possible vacuum conditions (thus minimizing the background signal from the residual gas) the vacuum system is divided into two (new system) or three (old system) independent sections. In the new system the intermediate chamber was left out to minimize the distance between the pulsed valve and the interaction region; this maximizes the sample density in the laser focus. Between each of the sections a small skimmer (Beam Dynamics) with an opening of 1 mm in diameter is placed. First of all, this skimmer controls the width of the molecular beam that reaches the interaction region. Second, it enables differential pumping whereby a pressure difference of three orders of magnitude can be maintained. In the old vacuum system the typical operating pressure (that is with the pulsed valve running) in the target chamber is in the range of $5 \cdot 10^{-8}$ – $2 \cdot 10^{-7}$ mbar whereas in the new system the typical pressure is $3 \cdot 10^{-9}$ mbar.

In the interaction region the molecular beam is crossed at right angles by a number of focused laser beams (between two and four). As discussed above the measurement is carried out using one or more laser pulses to disintegrate the molecule into charged fragments and measuring their recoil direction. For a point source of ions it is not difficult to measure the recoil direction of the fragments — a homogeneous electric field can be used to accelerate the ions towards a position sensitive detector [65]. Under realistic experimental conditions we must however consider the spatial profile of the laser beam. In our experiments we typically use modest focusing ($f\# \sim 30$) and

[b] Ar cannot be used since the high polarizability compared to He causes these atoms to form neat clusters at a backing pressure of about 30 bar [31].

obtain typical beam waists of about 30 μm and Rayleigh ranges of a few millimeters. Our ions thus come from a line source (with a length determined by the width of the molecular beam, 1 and 3 mm for the old and new vacuum system respectively) which would lead to a significant blurring of the image. This problem was solved by the introduction of velocity map imaging by Eppink and Parker [66]. The technique exploits the fringing fields of electrostatic plates with circular apertures to project the ions onto a position sensitive detector in such a way that the position on the detector only depends on the initial velocity of the ion, not on the spatial position (within some finite volume). Further, since all ions of the same charge state experience the same force their acceleration and thus their velocity during the field flight is only dependent on their mass. The arrival time of a specific ion on the detector is thus determined by its charge to mass ratio. In cases where the original distribution of ion velocities possesses cylindrical symmetry about an axis parallel to the plane of the detector this distribution can be retrieved from the two-dimensional projection by using the inverse Abel transform [66–68].

The detector used in our setup is a chevron-stacked micro-channel plate (MCP) backed by a phosphor screen (El-Mul Technologies). When an energetic particle (kinetic energy above 1 keV) hits the detector a number of electrons are released from the surface layer. When a sufficiently high voltage difference (1500 V or so) is applied between the front and back side of the MCP these electrons cause an avalanche in the material, creating a pulse of thousands of electrons. As the electron pulse propagates through the material it remains confined in the transverse direction by the capillary channels in the detector. If the phosphor screen is kept at a high potential compared to the back side of the MCP these electrons are extracted from the MCP to the screen where their impact causes localized phosphorescence. This flash of light is a direct measure of the position of the ion's impact on the detector and can be recorded by a camera out-side the vacuum system. The detector can be gated by applying a short high-voltage pulse to the front side of the detector and fragment-specific images can thus be recorded. In our data acquisition program these images are analyzed on a shot-to-shot basis to extract the position of each ion hit (typically about 10 ions are detected per laser shot). In a normal experiment each data point is obtained by building a distribution of ion hits from 2,000 laser shots or more whereas the accumulation of 10,000 shots is necessary for images that are intended to be Abel-inverted. Time-of-flight measurements, where the ion yield as function of flight time is recorded, can also be carried out by using the MCP as a fast, high-gain amplifier. Using capacitative read out to a fast oscilloscope it is possible to measure the small but rapid voltage changes induced by the ions. Under typical conditions an extraction voltage of a few kV is used to project the ions onto the detector. For our setup the time-of-flight is then between slightly less than 1 μs for protons and roughly 10 μs for iodine. Since we can apply fast high-voltage pulses with an adjustable width down to 90 ns and no common fragments have masses close to that of iodine, we can easily carry out selective detection of iodine ions. Other ions can, of course, be used as well.

In the new vacuum system we have also initiated work on the detection of electrons. In principle, electrons can be imaged by simply reversing the voltages on the extraction plates, but due to their very low mass they need special attention. The thing to worry about is stray magnetic fields, including the magnetic field of the Earth. For a charged particle accelerated by a voltage difference, V, moving in a homogenous magnetic field, $\mathbf{B}$, the radius for the circular trajectory around direction of $\mathbf{B}$ is $R = \sqrt{2mV/qB^2}$. At a magnetic field strength of 1 Gauss and a voltage of 2 kV this radius becomes about 1.5 m for electrons, not much larger than the distance from the interaction region to the detector (20–60 cm) and a deflection of many centimeters (i.e. the electrons not hitting the detector) would be the consequence. Heavy ions are much simpler; they have radii of hundreds of meters and therefore remain unaffected. Stray magnetic fields perpendicular to the TOF-axis can be removed by shielding the time-of-flight region with a cylindrical sheet of μ-metal (metal of high magnetic permeability) [69]. Stray magnetic fields parallel to the TOF axis are less critical: they only lead to a uniform rotation of the electron distribution around the TOF axis. Taking the value of the Earth's magnetic field (which has a large inclination angle in Århus) the angle of rotation can be estimated to about 5° for electrons accelerated at 1.5 kV. Further, in experiments using UV light care must be taken to avoid scattered light; if the photon energy is larger than the work function of steel, scattered light hitting the repeller plate will have a very high probability for liberating an electron from the material and thus creating a very large background signal. A large fraction of the stray light can be removed by coating the electrostatic plates and the μ-metal with graphite.

3.2.2 Laser pulses

In Figure 3.2 an overview of the laser setup is given. The workhorses of our laboratory are two laser systems: a femtosecond laser and a nanosecond laser. The femtosecond laser consist of an Ti:sapphire oscillator and two independent chirped pulse amplifiers. The output of the oscillator (Spectra Physics, Tsunami), a 88 MHz train of $\sim$100 fs pulses, is used to seed the two amplifiers (Clark MXR, CPA 1000 and Spectra Physics, Spitfire-HPR), both operating at 1 kHz delivering 800 μJ and 2.3 mJ per pulse respectively. The nanosecond laser is an injection-seeded, Q-switched Nd:YAG laser (Spectra Physics, Quanta Ray Pro 270-20) operating at 20 Hz and delivering 9 ns pulses with energies up to 1.5 J per pulse at 1064 nm. The nanosecond laser is locked electronically to the femtosecond laser with sub-nanosecond jitter. This combination of lasers yields a very flexible setup where we are able to carry out experiments on both adiabatic and nonadiabatic alignment. Further, we can probe the molecular alignment using two different processes with complementary advantages and disadvantages: resonant dissociation and Coulomb explosion. The basic philosophy behind these two detection techniques is discussed below, along with an overview of how the necessary pulses are generated. At first, however, the generation of the pulses used to induce molecular alignment is discussed.

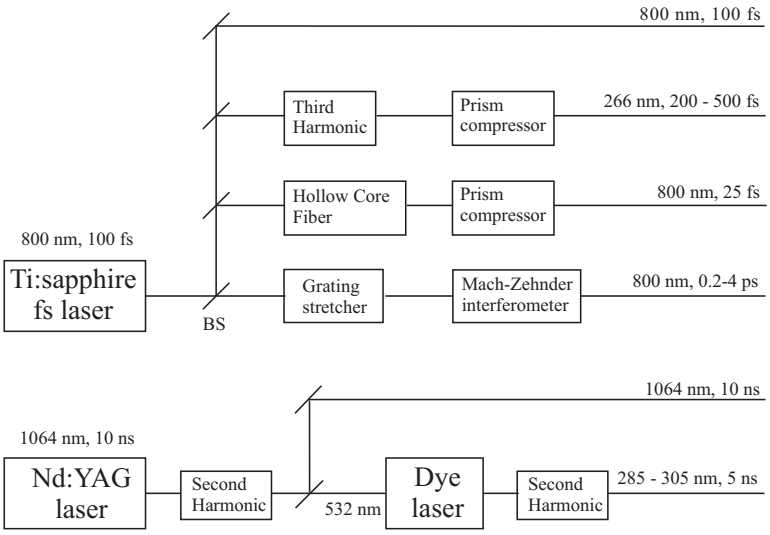

FIGURE 3.2: Overview of the laser setup.

Pump pulses

Two different time regimes must be addressed here: the long pulses needed for adiabatic alignment and the short ones for nonadiabatic alignment. Let us start by considering the simple case of adiabatic alignment. As described in the previous Chapter, the requirement for adiabatic behavior is that the pulse duration is longer than the classical rotational period. For the molecules studied in this work the maximal rotational periods are a few nanoseconds; the 9 ns pulses at 1064 nm are therefore perfectly suited for this purpose. At 1064 nm the photon energy is 1.17 eV which is significantly higher than vibrational energy spacing and still much lower than the energy gap to electronically excited states for the neutral molecules studied. The use of an injection seeder ensures a smooth temporal envelope as needed for the adiabatic behavior and reduces the timing jitter to about 1 ns. The timing of the pump pulse with respect to the femtosecond probe pulse is also straightforward — triggering of the Q-switch is controlled electronically with sub-nanosecond precision using a digital delay generator (Stanford Research Systems, DG535).

The pulses used for nonadiabatic alignment are derived from the femtosecond pulses. For the molecules studied in this work a pulse duration of about 100 fs is too short to obtain a high degree of alignment; the kick strength given by Eq. (2.14) is too small at non-ionizing intensities. Instead the pulses much be stretched to a duration of a few picoseconds. In our first experiments on nonadiabatic alignment of iodobenzene we used a prism-stretcher for this purpose. This approach had some

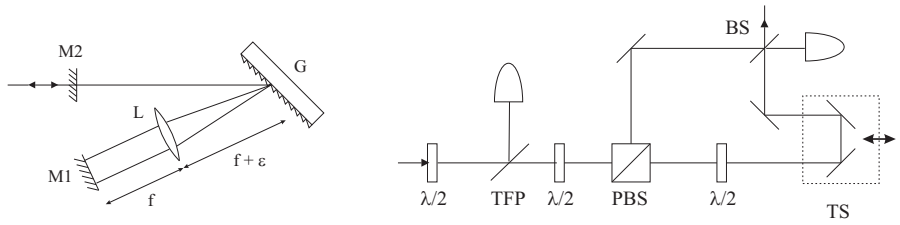

(a) Grating stretcher (b) Modified Mach-Zehnder interferometer

FIGURE 3.3: Details from the optical setup.

major disadvantages: the apex to apex distance between the prisms had to be about 2 meters and the temporal profile of the pulses was unsatisfactory, most likely due to self-phase modulation in the SF11 prisms. Therefore we built a grating stretcher (Fig. 3.3(a)) allowing for easy tuning of the pulse duration. The input is a collimated beam of transform limited pulses. From the grating different frequency components of the beam are reflected at different angles so a cylindrical lens and a folding mirror are used to image the beam back onto the grating. The beam reflected from the grating is now both temporally and spatially chirped. To remove the spatial chirp the beam is reflected back towards the grating and makes another passage through the stretcher. The total group velocity dispersion (GVD) added to the pulse is [70]

$$\frac{\mathrm{d}^2\phi(\omega)}{\mathrm{d}\omega^2} = -\frac{2\,\varepsilon\,\lambda^3}{\pi c^2 d^2}\left[1-\left(\frac{\lambda}{d}-\sin\gamma\right)^2\right]^{-3/2}, \tag{3.1}$$

where λ is the wavelength, $\gamma = 28.7^\circ$ is the Littrow angle of the grating, d is the groove spacing ($d^{-1} = 1200\ \mathrm{mm}^{-1}$) and ε is the displacement of the grating from the focal point. With an input pulse duration of 100 fs we can obtain an output pulse duration of 2 ps with a displacement of about 1 cm. With careful alignment good spatial and temporal profiles can be obtained.

In some experiments we used two alignment pulses to optimize the degree of alignment. For maximum flexibility we wanted to be able to control both the relative intensity and timing of the two pulses. This was obtained by building a modified Mach-Zehnder interferometer (Fig. 3.3(b)). At the entrance of the interferometer we used a half-wave plate in front of a polarizing beamsplitter to adjust the relative energy in the two pulses. A half-wave plate placed in one of the arms was used to rotate the polarization by 90° and a translation stage enabled us to delay one of the pulses by 0–1000 ps with respect to the other pulse. The two arms of the interferometer were recombined on a 50/50 beamsplitter. The total pulse energy was controlled by a half-wave plate and a thin film polarizer placed before the interferometer.

Probe pulses

As already mentioned, we use two different probe techniques: resonant dissociation and Coulomb explosion. These probe processes each have their own strengths — for the resonant dissociation we can, under some circumstances, extract the full angular distribution of the molecule, whereas the use of Coulomb explosion is much more generally applicable since it does not rely on any specific transitions.

Several of our studies concern simple carbohydrides with a singly-bonded iodine atom: iodobenzene (C_6H_5I), methyliodide (CH_3I) and *tert*-butyliodide (C_4H_9I). Common to these molecules is the fact that they all absorb light at 266 nm via a n $\rightarrow \sigma^*$ transition localized on the C−I bond. The promotion of an electron from a non-bonding orbital to an anti-bonding one leads to prompt dissociation into two neutral fragments with the iodine atom either in the ground state or in the spin-orbit excited state 0.943 eV above the ground state [71–76]. For iodobenzene there is a competing $\pi \rightarrow \pi^*$ transition that also leads to the formation of ground state iodine atoms. In that case the molecule is excited to a predissociative state that couples to the dissociative state via vibrational relaxation. The dissociation then occurs to a vibrationally hot phenyl radical and thus an iodine atom with significantly lower translational energy [71, 73]. Hence the iodine atoms from this competing channel are easily separated from those stemming from the direct dissociation channel by using the fact that the latter ones occupy the outermost radial region on the detector. State selective ionization of the iodine atom can be obtained using 2+1 photon resonance-enhanced multiphoton ionization (REMPI) using UV light at either 304.59 nm (ground state) or 303.96 nm (excited state). For methyliodide Eppink and Parker [72] report a nearly parallel transition for the I^* channel in the n$\rightarrow \sigma^*$ transition and a small perpendicular component in the ground state I channel; we observe similar behavior for iodobenzene, in good agreement with the results from Unny *et al.* [76]. An advantage of using the I^* channel for detection is the fact that dissociation induced by (weak) absorption at 304 nm leads almost solely to the formation of ground state iodine. If both alignment and probe laser pulses are linearly polarized (parallel to the detector) we can reconstruct the three-dimensional distribution of recoil velocities, $f_{\text{ion}}(\theta)$, from its two dimensional projection via the inverse Abel transform. Since we know the angular selectivity of the probe, $P_{\text{diss}}(\theta)$, we can thus find the angular distribution of the C−I bond axis, $f(\theta)$, by using the relation

$$f_{\text{ion}}(\theta) = f(\theta) \cdot P_{\text{diss}}(\theta). \tag{3.2}$$

It is in this step that the assumption of axial recoil is crucial: if the dissociation is non-axial the ion velocity distribution, $f_{\text{ion}}(\theta)$, will become a convolution of $f(\theta) \cdot P_{\text{diss}}(\theta)$ with the recoil distribution in the molecular frame. With the angular distribution for the C−I bond in hand, we have all the information we can possibly obtain with this probe technique. For comparison with theoretical results we can, for instance, calculate the

expectation value of $\cos^2\theta$ as

$$\langle\cos^2\theta\rangle = \int \cos^2\theta f(\theta)\sin\theta\,\mathrm{d}\theta. \tag{3.3}$$

The major drawback of using UV dissociation as a probe is that the detection efficiency for molecules with the C−I axis perpendicular to the polarization of the UV pulse is close to zero; planar delocalization is thus hard to detect. In many of our experiments we have only been interested in seing whether the molecules are aligned or not; not to extract the exact degree of alignment. This can be accomplished by analyzing the two-dimensional distribution of ion hits that we obtain from the images. As long as the molecule fragments via well-defined dissociation or Coulomb explosion channels it is often possible to identify radial regions in the image that primarily contain contributions from a given channel. In our data analysis we can therefore extract the angular distribution from a specific radial region and from this calculate the expectation value $\langle\cos^2\theta_{2D}\rangle$ for the two-dimensional distribution on the detector. Numerical simulations of adiabatic alignment show that there is a one-to-one correspondence between $\langle\cos^2\theta_{2D}\rangle$ and $\langle\cos^2\theta\rangle$ [46, Chap. 4.1]; it is our experience that $\langle\cos^2\theta_{2D}\rangle$ in general provides a good qualitative measure for the degree of alignment. It is important to bear in mind that the value of $\langle\cos^2\theta_{2D}\rangle$ is a convolution of the angular distribution of the molecule with the angular selectivity of the probe and can thus only be used as a relative measure for one specific molecule at a time.

The 266 nm light needed to dissociate the molecules is readily obtained as the third harmonic of the 800 nm output from the femtosecond laser. A prism compressor consisting of two Brewster-angle fused silica prisms is used to tune the pulse duration of the UV light; often pulse durations of about 500 fs are used to suppress multiphoton ionization. To generate the UV light for REMPI we use the nanosecond laser. The second harmonic of the output from the Nd:YAG laser (532 nm) is used to pump a dye laser (Lambda Physik, ScanMate 2) using Rhodamine 640 dissolved in methanol. The output at ∼609 nm is then doubled in a thick KDP crystal and tunable UV light is generated with a narrow bandwidth (∼1 cm^{-1}) determined by the dye laser.

For molecules that do not contain iodine and in cases where we do not need to extract the full angular distribution we use Coulomb explosion to probe the orientation of the molecule. The basic idea is to rip off several electrons from the molecule in order to create a very unstable molecular ion that rapidly dissociates due to the Coulomb repulsion between the nuclei. This requires a very intense laser pulse. Such a laser pulse could exert a large torque on the molecules and thus on its own change the orientation of the molecules before they dissociate. The most clear-cut Coulomb explosion is thus obtained by using very short pulses since the molecule will then dissociate before dynamical alignment sets in. In our setup we use pulses with a duration of ∼25 fs and focused intensities on the order of $2\cdot10^{14}$ W/cm^2 [77]. These short pulses are generated from the 100 fs output of the laser by first broadening the spectrum using self-phase-modulation in an argon-filled hollow core-fiber and then recompressing the

pulses in a prism compressor. When Coulomb explosion is used to probe molecular orientation we cannot extract the angular distribution of the molecules prior to ionization since several explosion channels with different angle and intensity dependence are in general open. The distribution of ion recoil velocities can, however, still be used to track changes in the degree of alignment on a qualitative level.

Combining the beams

In all of our experiments the different laser beams are overlapped collinearly. To obtain this we use combinations of dichroic mirrors or beamsplitters. The beams are then focused onto the molecular beam using a $f = 30$ cm lens. In order to probe only those molecules that have been exposed to the aligning laser field, we always ensure that the beam waist of the probe laser pulse at the intersection with the molecular beam is smaller than that of the aligning laser beam. This can be ensured by slightly de-focusing telescopes placed in the alignment laser beam. For the experiments involving the 1064 nm output from the nanosecond laser we use a standard BK7 anti-reflection coated lens, whereas for the experiments with the 266 nm beam as probe we use a custom-made achromatic lens (Eksma). The spatial overlap is obtained by first overlapping the beams in a 10 or 20 μm pinhole outsize the vacuum chamber and then optimizing an ion signal from the target molecule, for instance the C^+ or I^+ yield. For the short pulses we find the temporal overlap by carrying out a cross-correlation measurement in a BBO crystal, while the temporal overlap with the nanosecond pulses can be found using a fast photodiode and an oscilloscope.

CHAPTER 4

Nonadiabatic alignment

In this Chapter experimental results on nonadiabatic alignment induced by a short non-resonant laser pulse are presented. Results are presented for both symmetric and asymmetric tops. The first Section focuses on the evolution immediately after the laser pulse; the first 10 ps interval is the relevant time window for the iodine-containing molecules considered in this work. In the second Section long-time the evolution is considered, focusing on the observation of revivals for both symmetric and asymmetric tops.

4.1 Post-pulse evolution

In this first Section the dynamics of the rotational wave packet is considered in the temporal region immediately after the pulse. In this region it turns out that if we only probe the direction of the axis of highest polarizability the dynamics is on a qualitative level very similar for symmetric and asymmetric tops. Since we have carried out an extensive study on the alignment properties of the asymmetric top iodobenzene this Section will focus on the asymmetric top case.

As stated in the previous Chapter the best quantitative measurement of linear alignment we can carry out with the present setup is the measurement of the probability distribution for the C−I bond axis. The detailed study of the alignment dynamics of

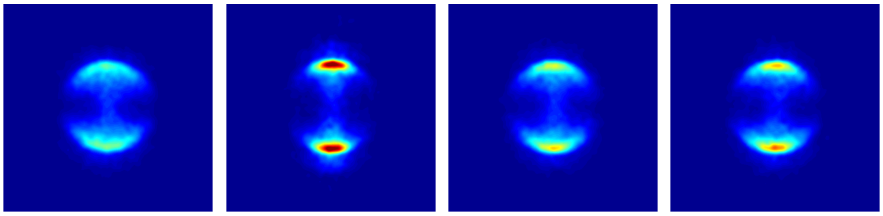

(a) No alignment (b) t = 2.5 ps (c) t = 6 ps (d) t = 8 ps

FIGURE 4.1: Alignment of iodobenzene detected by ion imaging of I^+ ions created from UV photo-dissociation followed by 2+1 REMPI of I^*. The images show the dynamical evolution of the alignment induced by a 1.9 ps, 800 nm laser pulse with a peak intensity of $3 \cdot 10^{12}$ W/cm^2. t is the delay between the alignment pulse and the UV pulse.

iodobenzene was thus carried out using UV dissociation followed by REMPI of iodine for the probe step. The polarizations of both of the UV beams and of the alignment beam are linear and parallel to the plane of the detector. For the results shown below the wavelength of the REMPI laser was tuned to ionization of I^*, but we note that identical behavior is observed when ground state iodine is detected. Figure 4.1(a) shows an ion image of I^+ ions obtained when a randomly oriented sample of iodobenzene is dissociated by 266 nm light and the spin-orbit excited iodine atoms subsequently are selectively ionized. To obtain this image a background image, recorded with only the 266 nm pulse present, has been subtracted; multi-photon absorbtion at 266 nm leads, through dissociative ionization, to the creation of I^+ ions with kinetic energies overlapping with those of iodine atoms from the neutral dissociation channel. The background image typically accounts for about 10% of the total number of iodine ions — there is a tradeoff between getting enough signal and inducing dissociative ionization (and saturating the transition to the dissociative state in the neutral molecule). The anisotropy in the image is a direct fingerprint of the parallel transition dipole for the neutral dissociation channel. Via Abel inversion of this image we can directly extract the angular selectivity for our probe. Next, we include a 1.9 ps, 800 nm laser pulse with a peak intensity of $3 \cdot 10^{12}$ W/cm^2. Fig. 4.1(b)–(d) show snapshots of the subsequent evolution. On the first image, at delay of 2.5 ps, a reduction in the angular width of the ion distribution is seen. This is a direct observation of macroscopic alignment induced in the sample by the non-resonant laser pulse. The following images reveal a non-monotonous behavior for the angular width. Comparing the image taken at 6 ps with the one at 2.5 ps shows the rapid de-phasing of the components of the wave packet while the image at 8 ps shows a small, partial rephasing analogous to the damped, oscillatory behavior in Fig. 2.5.

For a more quantitative discussion we can carry out the analysis described in the previous Chapter and extract the angular probability distribution for each delay of the

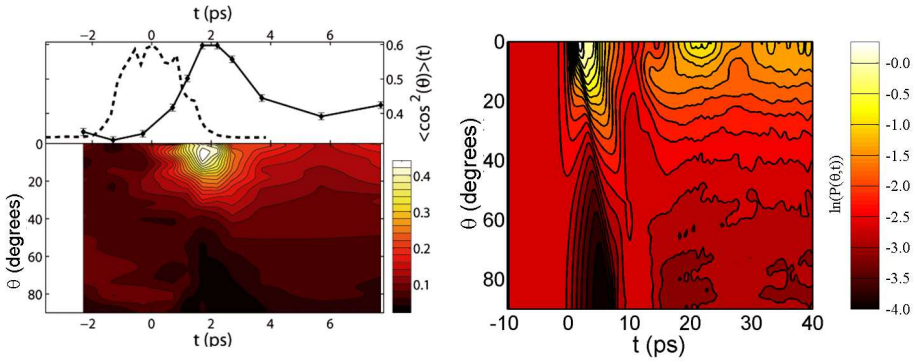

FIGURE 4.2: Probability density plot for the polar angle θ showing the dynamical alignment of iodobenzene. Left: Experimental measurement with a 2.2 ps pulse having a peak intensity of $3.4 \cdot 10^{12}$ W/m^2. Also shown is the expectation value of $\cos^2\theta$ at each delay (triangles) and a cross-correlation of the alignment pulse (dashed line). Right: Numerical calculation using a 3.8 ps pulse with a peak intensity of $6 \cdot 10^{11}$ W/m^2 at a temperature of 400 mK.

probe pulse with respect to the pump pulse. The result is shown in the left panel of Figure 4.2 along with the evolution of $\langle\cos^2\theta\rangle$ calculated from this distribution and with the measured cross-correlation for the alignment pulse. Before the alignment pulse the probability distribution is flat corresponding to a randomly oriented sample. The measurements during the alignment pulse should only be considered to be indicative of the evolving dynamics since the temporal overlap of the 800 nm and 266 nm pulses causes the opening of competing dissociative ionization channels leading to iodine ions of higher kinetic energy[a] as well as depletion to higher charge states. Since the higher (total) charge state channels typically have higher angular selectivity, it is very likely that the most well aligned molecules are removed and we thus underestimate the degree of alignment. This explains the dip in the degree of alignment at the second data-point. At the end of the alignment pulse (around $t = 2$ ps) we see a peak in the degree of alignment reaching a value of $\langle\cos^2\theta\rangle = 0.60$: the molecules are aligned under (nearly) field-free conditions! Following the maximum in the degree of alignment comes a rapid (~ 4 ps) decrease corresponding to the de-phasing of the wave packet. In the angular distribution we see that within our time-resolution the peak in the degree of alignment corresponds to the simultaneous build-up of density close to $\theta = 0°$ and decrease close to $\theta = 90°$. The apparent maximum in the probability density at $\theta \approx 5°$ is caused by centerline noise from the Abel inversion routine and thus an artifact resulting from our analysis; there is nothing in the raw images to support

[a]The angular distribution is extracted by integrating over a small range of kinetic energies corresponding to the specific dissociation channel of interest.

such a shift in the maximum. After the peak in the degree of alignment the density quickly decreases close to the polar axis and with a slight shift starts to build up in the equatorial plane. At the end of time range shown, a small increase in the degree of alignment is seen corresponding to the rephasing in Fig. 4.1(d).

The right panel of Fig. 4.2 shows the angular probability density resulting from a numerical calculation using slightly different pulse parameters. On a qualitative level there is very good agreement between our measurements and the calculated results. All major features are well reproduced: the build-up at small angles, the depletion at large angles and the partial rephasing during the initial field-free evolution. One interesting feature in the numerical results that we were not able to fully resolve experimentally is shear angle of the ridge and crest in the interval 0–10 ps. What this shows is that the maximum probability density close to the polar axis is reached before the minimum in the probability in the equatorial plane. This is in good, qualitative agreement with the δ-kick model: it has the simple classical interpretation that a molecule starting at large angles will lag behind a molecule initially oriented at a small angle with respect to the alignment laser polarization, see Eq. (2.15).

Now that we have established that the rotational kick induced by a short, nonresonant laser pulse does indeed lead to alignment of iodobenzene molecules the obvious next step is to study how the induced dynamics depends on the parameters that we can control experimentally, for instance the intensity of the alignment pulse and the temperature of the molecular sample.

Figure 4.3(a) shows how the induced alignment dynamics changes when the intensity is changed. For both curves the pulse duration is 2.7 ps and the molecules are seeded in helium at a pressure of 3 bar. The circles (connected by a full line that serves to guide the eye) show the data points measured when the alignment pulse had a peak intensity of $1.0 \cdot 10^{12}$ W/cm^2 while the triangles were obtained with a peak intensity nearly three times higher, $2.7 \cdot 10^{12}$ W/cm^2. Two overall changes are readily observed: the dynamics is significantly faster with the more intense pulse and the maximum degree of alignment is higher. These two observations have the same origin, that the more intense pulse produces greater rotational excitation. With a broader wave packet we can obtain better confinement but the different components also get out of phase faster — the rate of dephasing is proportional to square of the width of the wave packet in angular momentum space, ΔJ [78]. This is a good example of a fundamental property of nonadiabatic alignment: there is always a compromise between how high a degree of alignment one can obtain and for how long it can be sustained.

The second parameter we can change is the rotational temperature. Experimentally this can be carried out by changing the backing pressure in the supersonic expansion [64]. Fig. 4.3(b) shows measurements of the alignment dynamics with constant laser parameters but using 1 and 3 bar helium in the supersonic expansion. We see that for the first four picoseconds or so the change between the curves looks like a constant shift. The reason that the rate of dephasing does not change significantly is that the J states populated in the wave packet are much higher than the one populated thermally

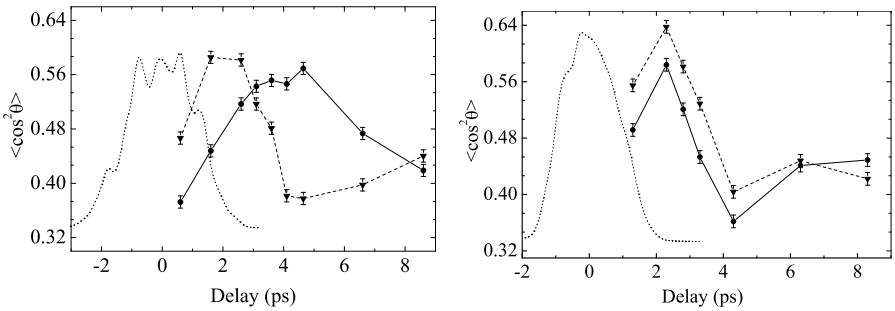

(a) Intensity dependence.

(b) Temperature dependence.

FIGURE 4.3: Measurement of the dependence of the degree of alignment, $\langle \cos^2 \theta \rangle$, on the rotational temperature and on the intensity of the alignment pulse for iodobenzene seeded in He and exposed to a short 800 nm laser pulse. In both graphs the dotted curve shows a cross-correlation of the alignment pulse with a duration of (a) 2.7 ps and (b) 1.7 ps respectively. In (a) the full curve (circles) is with a peak intensity of $I = 1.0 \cdot 10^{12}$ W/cm^2 and the dashed curve (triangles) is with $I = 2.7 \cdot 10^{12}$ W/cm^2. Both experiments were carried out with 3 bar backing pressure. In (b) the alignment pulse has a peak intensity of $3.4 \cdot 10^{12}$ W/cm^2 and the full curve (circles) shows the degree of alignment obtained with 1 bar backing pressure while the dashed curve (triangles) is for 3 bar backing pressure.

under both conditions (previous work suggests that the temperature in both cases is less than 10 K [18]). The reduced Boltzmann averaging at the lower temperature therefore primarily leads to an improved degree of alignment. At significantly higher temperatures we expect qualitative changes in the observed dynamics. However, with the valve used for these experiments it was not possible to run the experiment under such conditions.

The final parameter that can easily be adjusted is the pulse duration and once again its optimal value is determined by two counteracting effects [38, 79]. On the one hand, the peak intensity of the alignment pulse is always limited by the onset of multi-photon ionization and the degree of rotational excitation is (in the impulsive limit) determined by the pulse area, Eq. (2.14) and [32]. This leads us to conclude that we do not want very short pulses. On the other hand, the primary strength of nonadiabatic alignment is the possibility of obtaining alignment under field-free conditions. To obtain this the pulse must not be too long since then the maximum degree of alignment appears during the pulse and eventually rotational de-excitation takes place on the trailing edge of the alignment pulse as we start to approach adiabatic behavior. Recent studies in our group show that the optimal pulse duration for iodobenzene is about 1 ps [79]. For other molecules and temperatures we must expect other pulse durations to be optimal since the dynamics depends on both the rotational constant and the polarizability.

4.2 Long delays — revivals

With post-pulse alignment established, we are now ready to investigate the evolution at larger delays. As discussed in the previous Section, we can, at least on a qualitative level, understand the behavior immediately after the alignment pulse by using classical mechanics. For the wave packet dynamics at larger delays we must turn to quantum mechanics. First, results for symmetric tops are shown; afterwards the more complex case of asymmetric tops is treated.

4.2.1 Symmetric tops

In the context of laser-induced alignment, symmetric top molecules are very similar to the well-studied case of linear molecules: their interaction potentials with the laser have the same mathematical expression and their energy level structure is nearly identical. In fact, since K is conserved, the K-dependent contribution to the field-free energy for symmetric tops only leads to an unimportant overall phase shift for the wave packet during the field-free evolution. The only point where the two classes of molecules do differ is that their selection rules for Raman transitions are different: for linear molecules we have $\Delta J = 0, \pm 2$ only while for symmetric tops $\Delta J = \pm 1$ transitions are also allowed when $K, M \neq 0$. All in all, this leads us so expect that the overall behavior will be much like a linear molecule.

To settle this question and to bridge the gap between linear molecules and asymmetric tops (described below, but those experiments were carried out before the symmetric top ones) we carried out a series of experiments on two symmetric tops: methyliodide (CH_3I) and *tert*-butyliodide ($C(CH_3)_3I$). Unless otherwise noted, the UV dissociation + REMPI probe scheme was used for both molecules. For methyliodide there is a significant contribution to the detected signal from molecules that have been dissociated by the 304 nm light. These ions are easily distinguished by to their lower kinetic energy and the transition does not lead to any depletion effects since the REMPI pulse arrives 10 ns after the alignment and dissociation pulses.

Methyliodide

In the upper panel of Fig. 4.4 an experimental measurement of the alignment dynamics in methyliodide is shown. The alignment was induced by a 0.75 ps pulse with an intensity of $1.3 \cdot 10^{13}$ W/cm^2. The first data point shown is taken at 0.8 ps where the intensity of the alignment pulse is only a few percent of its maximum value. In just 1 ps the wave packet dephases and the alignment drops to its permanent level. This is very similar to the results for iodobenzene show above, but the dynamics is faster due to the lower rotational constant of methyliodide. From the figure it is clearly seen that the permanent level for $\langle \cos^2 \theta_{2D} \rangle = 0.75$ is elevated compare to the value measured without the alignment pulse, 0.71. As discussed in Sec. 2.3, this is a

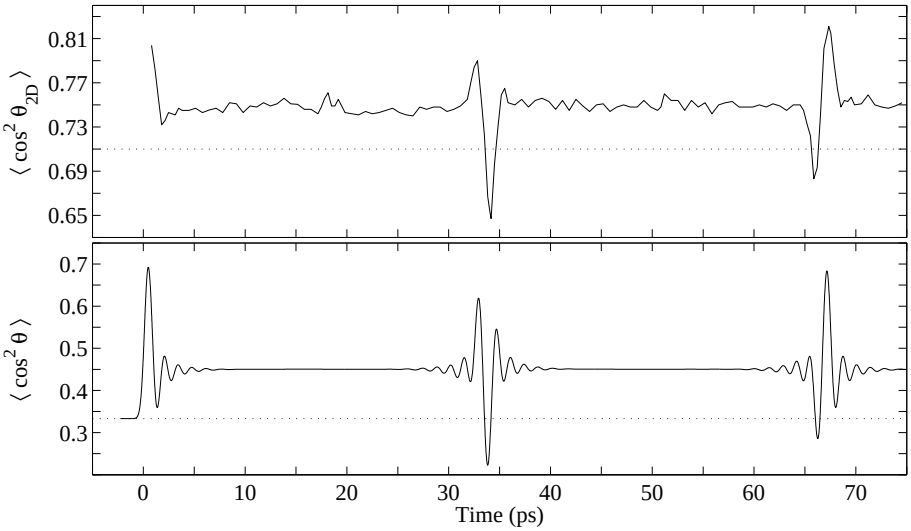

FIGURE 4.4: Dynamical alignment of methyliodide within one rotational period. Upper panel: Experimental measurement using an alignment pulse with a duration of 0.75 ps and an intensity of $1.3 \cdot 10^{13}$ W/cm^2. The dotted line marks the value of $\langle \cos^2 \theta_{2D} \rangle$ in the absence of the alignment pulse. In the supersonic expansion 3 bar helium was used. Lower panel: Numerical calculation using an alignment pulse with the same duration but at an intensity of $1.0 \cdot 10^{13}$ W/cm^2 and assuming a temperature of 10 K. Focal volume averaging is included.

clear signature of the high rotational excitation via M-conserving transitions leading to an ensemble with $\langle \hat{J}^2 \rangle \gg \langle \hat{J}_Z^2 \rangle$. During the course of the first 75 ps we see that the permanent alignment level is interrupted by two short transients located at about 34 ps and 67 ps. These are the half and the full revivals which correspond to brief rephasings of the wave packet — at the full revival the entire initial wave packet is reconstructed while at the half revival the even and odd J states are out of phase by π. From Eq. (2.25) and the known rotational constant [80] we expect the revival time to be $T_{\text{rev}} = 1/2B = 66.655$ ps. The experimentally determined revival time is in excellent agreement. We note that during the transient structure the molecules do not only become aligned: at some delays we see that the value of $\langle \cos^2 \theta_{2D} \rangle$ drops below 0.71, the value for an isotropic distribution. At these delays there is a higher probability for finding the molecules close to the equatorial plane rather than close to the polar axis, a phenomenon often referred to as planar delocalization or anti-alignment. Technically, the term planar delocalization is probably more correct since the molecules are actually confined in a manner similar to the 2D-alignment that can be obtained with a circularly polarized laser pulse (at least in the adiabatic case). The extrema of the tran-

sient revival structures were measured with high statistics such that we could extract the degree of alignment, $\langle\cos^2\theta\rangle$, prior to the probe; at the half revival the maximum and minimum values are 0.46 and 0.29 respectively while the degree of alignment at the full revival changes between 0.31 and 0.49. The permanent degree of alignment was found to be $\langle\cos^2\theta\rangle = 0.39$. These measurements agree with the information extracted from $\langle\cos^2\theta_{2D}\rangle$ and in particular it is worth noting that we do observe planar delocalization in spite of our low probe efficiency close to the equatorial plane.

For comparison, the lower panel of Fig. 4.4 shows the result from a numerical calculation of alignment dynamics for methyliodide exposed to a 0.75 ps pulse with an intensity of $1.0 \cdot 10^{13}$ W/cm^2. The calculation assumes an initial temperature of 10 K (which must be considered an upper limit to the actual temperature) and takes into account the effects of focal volume averaging. Qualitative agreement between experimental and numerical curves is very good, but a quantitative comparison exposes significant differences. At first we note that the calculation is carried out at a reduced intensity. If the calculation is carried out with a peak intensity corresponding to the one quoted for the experiments the shapes of the revivals change dramatically — they become more symmetric such that the half revival consists primarily of one big dip and the full revival is dominated by one peak, both with small and symmetric oscillations on either side of the dip/peak. The experimental intensity is estimated from the duration and the energy of the pulse combined with the measured beam size at the focus. We must therefore ascribe a significant uncertainty to the quoted number. Further an imperfect overlap would lead to an lower effective peak intensity. Therefore, it is reasonable to compare with calculations at a slightly lower peak intensity based on matching the shape of the revival (which, for the full revival, is not very sensitive to minor temperature changes once focal volume averaging is taken into account). This does, however, still leave us with a clear discrepancy in the quantitative comparison. In the calculation the degree of alignment at the half revival takes the extreme values $\langle\cos^2\theta\rangle = 0.62$ and 0.22, while at the full revival we find $\langle\cos^2\theta\rangle = 0.29$ and 0.68. The permanent degree of alignment is found to be $\langle\cos^2\theta\rangle = 0.45$. These values, obviously, do not agree with the experimentally measured degree of alignment — in particular the degree of alignment at instants when the molecules are aligned along the polarization axis is strongly underestimated.

There are several factors that could lead to an underestimation of the degree of alignment. The first is, of course, an imperfect overlap but based on the shape of the revival it is reasonable to assume that the peak intensities in the experiment and in the calculation are fairly close (at lower intensities the maximum degree of alignment at half revival becomes high relative to that at the full revival). A second cause might be found in our data analysis: the images are analyzed on a shot-to-shot basis and the centroid of each ion hit is extracted. If the molecules are well aligned, ion hits on the detector will be highly confined and the individual ion hits may start to overlap. We deal with this by calculating the asymmetry of the intensity pattern on the phosphor screen for each ion hit. For single ion hits the intensity distribution is nearly

circular so a large asymmetry is a strong indicator of two overlapping ion hits. In the acquisition program we keep track of the number of hits with an asymmetry above a certain threshold and do always make sure that this number is kept reasonably low. In the event of a double hit this will only be counted as a single hit. At these modest degrees of alignment we do not believe this to be an important effect. The final issue regarding the measurements is the intensity of the probe pulse. If the intensity is too high the transition to the dissociative state will be saturated. This will lead to a change in the angular selectivity and cause us to find a wrong angular distribution for the neutral molecule. We have checked if saturation could be the reason for the strong underestimate by comparing measured degrees of alignment at different intensities for the probe pulse. The conclusion was that we are close to saturation but not enough to strongly distort our measurements. We find in general that measurements using the photo-dissociation probe underestimate the degree of alignment compared with calculations. This is the case not only for methyliodide, but also for iodobenzene and *tert*-butyliodide.

The discrepancy may instead have much more fundamental cause: iodine containing molecules have large quadrupole hyperfine splittings [81–83]. Using first order perturbation theory the energy shift due to the quadrupole interaction is found to be [36, 84]

$$\Delta E_{\text{HF}} = \tfrac{1}{2}\, eQq_0 \left[\frac{\frac{3}{4}C(C+1) - I(I+1)J(J+1)}{I(2I-1)(2J+3)(2J-1)}\right]\left(1 - \frac{3K^2}{J(J+1)}\right), \qquad (4.1)$$

where $C = F(F+1) - J(J+1) - I(I+1)$ with I being the nuclear spin ($\frac{5}{2}$ for iodine) and F is the total angular momentum. Methyliodide, for instance, has a rotational constant of $B = 7.501$ GHz but the quadrupole coupling is as large as $eQq_0 = -1.934$ GHz [82]. This means that the field-free states are no longer the rigid-rotor states, instead the hyperfine coupled states must be used and we see that the phase shifts induced by the hyperfine coupling are not negligible on the timescale of $T_{\text{rev}} = 1/2B$. Whether this is the cause for the discrepancy between the measured and calculated degrees of alignment remains to be tested by explicit calculations.

Now that we have established the occurrence of revivals of the rotational wave packet, one question that immediately comes to mind is: how long do the revivals persist? For a pure rigid rotor in a perfect vacuum we would expect the wave packet to exhibit perfect rephasing for indefinitely long, but in reality the molecule is not a rigid rotor and will not be in a collision-free environment (although a molecular beam comes very close). Figure Fig. 4.5 shows a measurement of some later revivals in methyliodide: the first, the second, the 16th and the 42nd. The most important conclusion from these measurements is that the revivals can indeed persist for very long times. For these measurements the temporal scan was purely limited by the length of the translation stage we use to delay the probe pulse with respect to the alignment pulse. At each sub-figure a dotted line shows the position of the time $t = n \cdot T_{\text{rev}} + 0.4$ ps. The

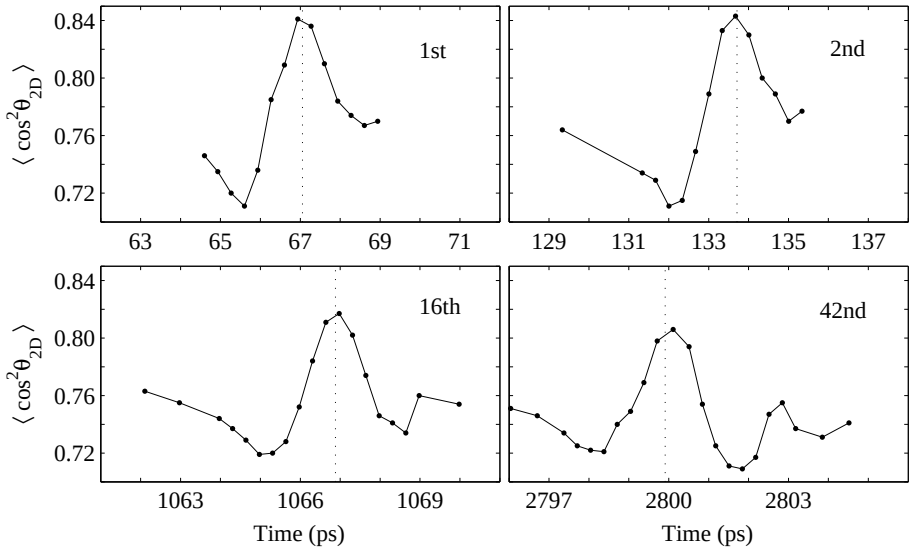

FIGURE 4.5: Measurement of some late revivals for methyliodide seeded in 2 bar argon. Panels show the 1st, the 2nd, the 16th and the 42nd revival respectively. In each panel the dotted line marks the time $t = n \cdot T_{\text{rev}} + 0.4$ ps where n is the order of the revival.

position of each revival conform remarkably well with the expected value. To obtain this good agreement it is necessary to correct for the difference between the speeds of light for 266 nm and 800 nm pulses propagating in air. A closer look at the figure does, however, reveal a small, gradual change in the shape of the revivals. The first and the second revival are almost identical in shape. As we continue to the 16th and further to the 42nd we observe two trends: 1) the maximum degree of alignment decreases and 2) the dip after the peak in the degree of alignment becomes more pronounced. It could be tempting to ascribe observation 1) to an increasingly worse overlap. First of all, we checked the stability of the translation stage by monitoring the focused probe beam in a 10 μm pinhole. Secondly, a poor overlap cannot explain the dip after the peak in the degree of alignment. The origin of the observed change in the shape and magnitude of the revivals lies in the fact that molecules are not rigid rotors: the average angular momentum for the molecules is very high and the molecules therefore become slightly stretched compared to the equilibrium position. To a good approximation this can be accounted for by adding the centrifugal distortion term

$$E_{JK}^{\text{CD}} = -D_J[J(J+1)]^2 - D_{JK}J(J+1)K^2 - D_K K^4, \tag{4.2}$$

to the field-free energies. Calculations of the alignment dynamics at these late revivals have been carried out using values for the D_i constants measured by microwave spec-

troscopy[b] [80]. These calculations (not shown) reveal that the observed changes can all be attributed to centrifugal distortion [85]. Similar effects were also seen in N_2 by Corkum and co-workers [40]. At the very low temperatures and densities in our molecular beam we do not see any effects of inelastic collisions. On top of the low collision rate in the molecular beam, the decoherence due to the inelastic collisions become even further suppressed by the excitation to high J states in the molecule since the rate of inelastic collisions decreases with J [86] . Further, the mere fact that Sussman *et al.* [23] were able to observe revivals persisting for hundreds of ps at room temperature and a pressure of 300 Torr also supports the neglect of collisional effects in our experiments.

tert-butyliodide

Experiments have also been carried out on another symmetric top: *tert*-butyliodide. Fig. 4.6(a) shows a scan of the alignment dynamics for this molecule under conditions much similar to those used for methyliodide; the alignment pulse had a duration of 1.3 ps and an intensity of $8.9 \cdot 10^{12}$ W/cm^2. Apart from the different timescale due to the increased moment of inertia, the trace is similar to that recorded for methyliodide (Fig. 4.4). Within one rotational period the permanent degree of alignment is interrupted by two transients: a half revival at about 162 ps and a full revival at 322 ps. The expected revival time for *tert*-butyliodide based on the rotational constant found from microwave spectroscopy [87] is $T_{\text{rev}} = 319.8$ ps, in perfect agreement with our experimental findings. The time for the half and the full revivals are both slightly off-set because the initial peak in the degree of alignment is off-set from $t = 0$ by about 2 ps. The extremal points at the two revivals were measured with high statistics and the degree of alignment calculated. At the half revival we found $\langle \cos^2 \theta \rangle = 0.50$ and 0.28, at the full revival $\langle \cos^2 \theta \rangle = 0.29$ and 0.49. As for methyliodide these numbers to not agree with numerically calculated ones although the shape of the revivals compare well.

Fig. 4.6(b)+(c) show the half and full revival measured using the Coulomb explosion probe. These revivals are qualitatively very different from the trace shown in Fig. 4.6(a). The reason is found by comparing with Fig. 2.7: in (b) and (c) only molecules from a small portion of the focus of the alignment laser beam are being probed. This can be obtained since the multiple ionization needed for Coulomb explosion has a highly non-linear dependence on the intensity. By keeping the intensity of the probe laser low we effectively restrict the probe volume to a region smaller than the beam waist (and the probe beam already has a smaller beam waist $\omega_{\text{probe}}/\omega_{\text{align}} \sim 2/3$). The effect was discovered by accident on the old system, but was not investigated further since the signal levels were too low at the reduced intensities. Since then two experimental improvements have paved the way for making experiments with strongly

[b] The D_K constant is not measured in the cited work, but just as the K-dependent term in the rigid-rotor energy it only contributes with an overall phase to the wave function.

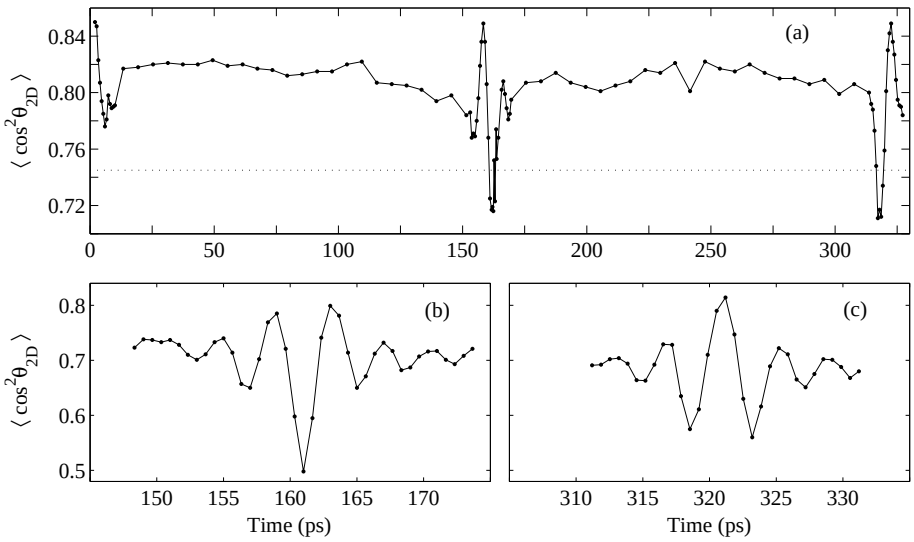

FIGURE 4.6: Revivals for *tert*-butyliodide seeded in 3 bar helium. (a): A full scan of the alignment dynamics using the UV photodissociation probe. The alignment pulse has a duration of 1.3 ps and an intensity of $8.9 \cdot 10^{12}$ W/cm^2. The dotted line shows the value of $\langle \cos^2 \theta_{2D} \rangle$ in the absence of the alignment pulse. (b) and (c): Half and full revival detected using the Coulomb explosion probe scheme. The alignment pulse duration is 1.6 ps and the intensity $4.0 \cdot 10^{12}$ W/cm^2.

reduced focal volume averaging. First of all, a new amplifier was bought for the femtosecond laser, delivering three times higher pulse energies and thus enabling us to increase the beam waist of the alignment pulse without reducing the peak intensity. Secondly, the molecular beam in our new vacuum system has a higher density and thus allows us to use probes with significantly lower ionization probabilities.

Symmetric tops versus linear molecules

In the beginning of this Section the similarities between linear molecules and symmetric tops were briefly outlined and it was mentioned that one would expect these two classes of molecules to behave similarly. The only two differences are the K dependent term in the field-free energy and the allowed $\Delta J = \pm 1$ transitions. As already discussed the K dependent term is of no consequence since K is a conserved quantum number. The changed selection rules do, of course, make the two cases fundamentally different, but using $\langle \cos^2 \theta \rangle$ as observable effectively suppresses the beating between states with $J - J' = \pm 1$ as discussed in connection with Eq. (2.24). Finally, the added degree of freedom for symmetric tops (rotation about the symmetry axis) makes a dif-

ference for the thermal averaging when the temperature is above the energy spacing between the $K = 0$ and $K = 1$ subsets. For the heavy molecules considered here this is not likely to make any major difference since a very large number of initial states are populated already at one Kelvin no matter if the molecule is linear of a symmetric top. Indeed the observed revivals for symmetric tops look very similar to those observed for linear molecules when differences due to nuclear spin statistics are taken into account [21, 40, 51].

Oscillations beyond the up-down structure (as in Fig. 2.7(a) and Fig. 4.6(b)+(c)) have only in one case been seen for linear molecules [21, 38, 39]. This is, however, just a matter of interaction strength. The most popular linear molecules, N_2, O_2 and CO_2, all have small polarizability anisotropies combined with small moments of inertia. The small polarizability anisotropy keeps the coupling between adjacent levels small and the small moment of inertia means that the pulse must be kept very short to remain nonadiabatic. All in all the degree of rotational excitation was too low in those experiments to observe such effects.

4.2.2 Asymmetric tops

The prediction of the field-free alignment dynamics for symmetric top molecules, in particular the occurrence of revivals for the wave packet, was straight forward. From just a few lines of algebra it was directly evident that in the rigid rotor approximation the dynamics is periodic with the period $T_{\text{rev}} = 1/2B$. But what do we then do in the case of asymmetric tops? For these molecules there are no analytical expressions for the energy level structure. Further the wave packet induced by a sequence of Raman transitions is much more complicated in structure since M is the only conserved quantum number — in the basis of symmetric top eigenstates the wave packet is a superposition of states with both J and K different. On the other hand partial rephasings of rotational wave packets in asymmetric top molecules form the foundation of rotational coherence spectroscopy (RCS) [12, 13]. The wave packets formed in those experiments, however, consist only of the superposition of a few eigenstates, dictated by the selection rules for a single transition. For the extremely broad wave packets needed to induce a high degree of alignment, the content of the wave packet cannot be obtained from the selection rules for a single transition since typically many tens of transitions are used to excite the wave packet as is revealed by the very high mean angular momentum (see Fig. 2.3). All in all, where does this leave us? For an experimentalist the best way to find the answer is to carry out the experiment. Experimental results on two molecules, iodobenzene (Fig. 4.7) and iodopentafluorobenzene, are presented and discussed below. The observed results are compared to non-perturbative quantum mechanical calculations and then reconsidered in the framework of classical mechanics.

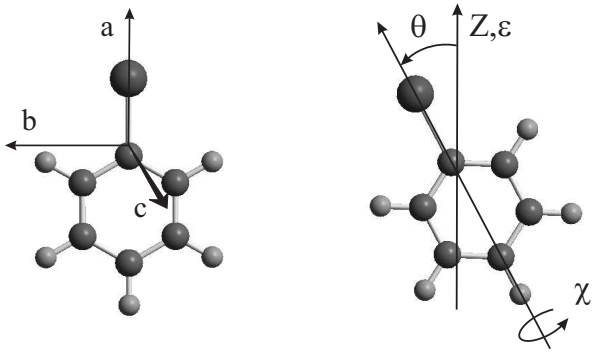

FIGURE 4.7: Left: The principal axes of iodobenzene. Right: Definition of the Euler χ and θ angles. The ϕ angle corresponds to a precession of the symmetry axis around the polarization vector.

Experimental results

Our first experiments concentrated on studying iodobenzene. From the rotational constants, $A = 5671.89$ MHz, $B = 750.416$ MHz and $C = 662.627$ MHz [81], it is readily seen that the molecule is a near-prolate top, as is also revealed by the asymmetry parameter $\kappa = (2B - A - C)/(A - C) = -0.965$. In the limit of a prolate symmetric top κ takes the value -1. A good approximation for the energy level structure is therefore

$$E(J, K_{-1}) = \bar{B}J(J+1) + (A - \bar{B})K_{-1}^2, \tag{4.3}$$

where $\bar{B} = (B+C)/2$ is the average rotational constant perpendicular to the symmetry axis. From our treatment of symmetric tops we would therefore expect revivals at $T_J = 1/2\bar{B} = 1/(B+C) = 707.7$ ps where the revival time has been labelled T_J for reasons that will become clear below.

Figure Fig. 4.8(a) shows a scan in steps of 2 ps of the alignment dynamics induced in iodobenzene by a 2.7 ps pulse with a peak intensity of $4 \cdot 10^{12}$ W/cm^2. Once again the alignment was probed using UV dissociation by a 266 nm pulse followed by REMPI of the iodine photo-fragments. After the pulse we see the post-pulse alignment (Fig. 4.2) lasting just a few picoseconds. After the initial transient the value of $\langle \cos^2 \theta_{2D} \rangle$ levels off at a value of 0.79, significantly higher than the 0.69 recorded without the presence of the alignment pulse[c]. This permanent alignment has exactly the same cause as for the symmetric top case: the confinement of the angular momenta close to the equatorial plane. During the first 800 ps we see the permanent level being

[c]These data were recorded over the course of two days. The shift in the permanent level at ∼400 ps is therefore due to slightly different experimental conditions on these two days. Both the post-pulse alignment and the transient at 380 ps were used to check that conditions were comparable.

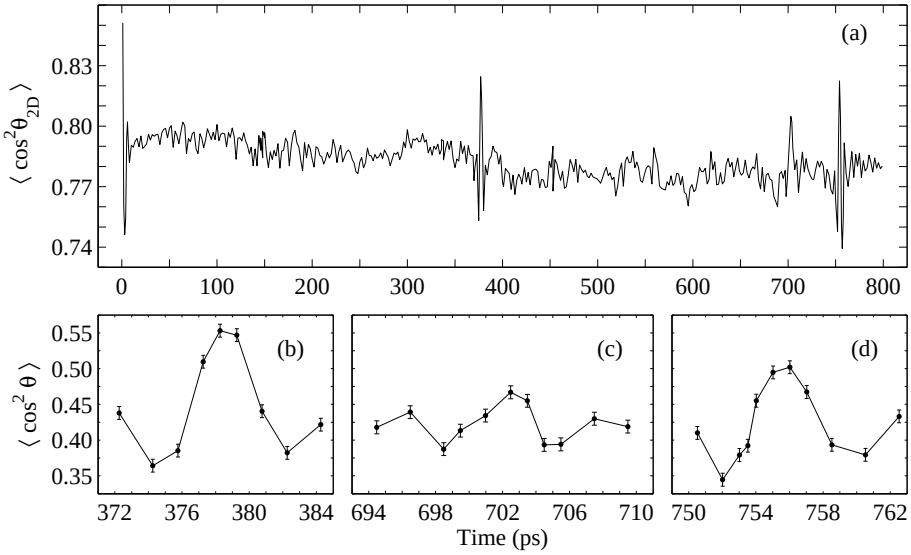

FIGURE 4.8: Alignment revivals for iodobenzene seeded in 3 bar helium. The alignment pulse has a duration of 2.7 ps and a peak intensity of $4 \cdot 10^{12}$ W/cm^2. (a): A complete scan of the revival dynamics. In the absence of the alignment pulse we find $\langle \cos^2 \theta_{2D} \rangle = 0.69$. (b)–(d): Expanded view of the three transients based on high statistics images. Please note the different vertical scales.

interrupted by three short transients, centered at $t = 378.8$ ps, 702.7 ps and 755.9 ps. These measurements were, to our knowledge, the fist demonstration of revivals of the wave packet induced in an asymmetric top by an intense laser pulse. Two things should be noted. First, the timings of the revivals are not explained by the symmetric top approximation in spite of the fact that iodobenzene comes very close to being a symmetric top. Second, the degree of alignment at the revivals is much lower than the degree of alignment immediately after the pulse.

Fig. 4.8(b)–(d) show expanded views of detailed, high statistics measurements of each of the three transients. At first we focus on the transient in (c), centered at 702.7 ps. This delay is close to the expected revival time in the symmetric top approximation. The deviation from the expected revival time of 707.7 ps is due to the fact that the symmetric top approximation tends to underestimate the energies for the high J states that become populated in our experiments. The transient is thus due to a rephasing of components with the same value of K_{-1} but different values of J. Following the convention from RCS this transient is termed a J-type revival. One striking feature in the long scan is the absence of the corresponding half-revival. We shall return to this point below. The figures (b)–(d) also reveal what is hinted

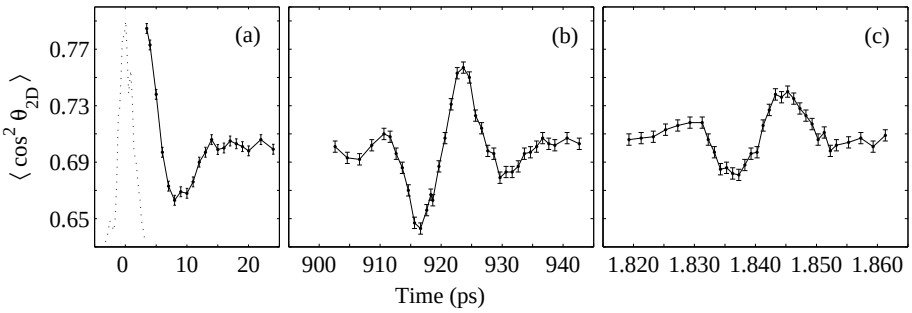

FIGURE 4.9: Revivals for iodopentafluorobenzene in 3 bar helium. The alignment pulse has a duration of 2.5 ps and an intensity of $5.0 \cdot 10^{12}$ W/cm^2. Without the alignment pulse the value of $\langle \cos^2 \theta_{2D} \rangle$ is 0.65.

from the long scan in (a): the two transients at 378.8 ps and 755.9 ps are very similar in shape and have a higher amplitude than the J-type revival. Taking a closer look at the numbers we see that the difference in timing of the former two transients is 377.1 ps so taking into account the off-set of the initial alignment peak with respect to $t = 0$ these transients form a periodic pattern. To find the origin for the transients one must compare these numbers to the rotational constants of the molecule; although the molecule does not have a regular energy level structure the field-free dynamics is still solely determined by the moments of inertia, see Eq. (2.2). Using the rotational constants for iodobenzene we find that $1/4C = 377.29$ ps revealing a very simple relation to the structure of the molecule. In RCS this kind of transients is known as a C-type rephasing and it has been shown that these are due to beatings between components with $\Delta J = \Delta K_1 = 2$ [13]. The transients at 379 ps and 756 ps are thus the first and second C-type revival. They appear because although the inertial tensor is close to that of a symmetric top, the polarizability tensor is highly asymmetric[d], $\alpha_a = 21.5$ Å^3, $\alpha_b = 15.3$ Å^3 and $\alpha_c = 10.2$ Å^3. An intuitive, classical model that explains the occurrence of these two types of transients will be presented below.

To test the influence of the asymmetry molecular structure we measured the alignment dynamics for a more asymmetric molecule: iodopentafluorobenzene. The rotational constants for this molecule have to our knowledge not been measured, but a very simple estimate yields: $A = 1026.6$ MHz, $B = 368.6$ MHz and $C = 271.2$ MHz. The asymmetry parameter is readily found to be $\kappa = -0.742$. While the structure is considerably more asymmetric than iodobenzene the polarizabilties are remarkably similar: $\alpha_a = 23.8$ Å^3, $\alpha_b = 17.9$ Å^3 and $\alpha_c = 10.5$ Å^3. Fig. 4.9 shows parts of a scan of the alignment dynamics of iodopentafluorobenzene exposed to a pulse similar to that used in the iodobenzene experiments. After the pulse the molecules become

[d] Linear response theory calculation at 800 nm by M. D. Poulsen.

well-aligned, at the maximum reaching $\langle\cos^2\theta\rangle = 0.57$. In about 10 ps the wave packet dephases and as for the other molecules studied here, the degree of alignment levels off to a permanent level. Within the first 2 ns, the permanent level is interrupted by the two transients shown Fig. 4.9 in (b) and (c). Their timing, $t = 924$ ps and $t = 1845$ ps, reveals that together with the initial alignment peak at ∼4 ps they form an almost periodic pattern (with a decreasing amplitude). The spacing between the revivals, 921 ps, fit well with $T_C = 1/4C = 921.8$ ps based on the estimated rotational constants. What we have observed are therefore the first two C-type revivals. At the first revival the degree of alignment takes the extreme values $\langle\cos^2\theta\rangle = 0.32$ and 0.44, while at the second revival we find $\langle\cos^2\theta\rangle = 0.33$ and 0.42. Post-pulse alignment is once again superior to the degree of alignment at the revivals. A J-type revival would be expected to appear close to $T_J = 1/(B + C) = 1563$ ps. Experimentally we find no structures in a region of ± 15 ps around this delay. The absence of a J-type revival is ascribed to the larger asymmetry of this molecule, as confirmed by the numerical results below.

Numerical calculations and classical considerations

To gain more insight to the appearance of revivals of asymmetric tops, in particular studying how the relative strength of the J- and C-type revivals depend on various parameters, a series of numerical calculations were performed by our collaborators, Edward Hamilton and Tamar Seideman. The results are included here because they complement the experimental results well.

All of results shown here were obtained assuming a rotational temperature of 400 mK. This temperature is probably about an order of magnitude below the temperature of the molecules in our experiments. Nevertheless, it is reasonable to compare these calculations directly with our experiments because the primary effect of thermal averaging is to remove the oscillatory structures away from the transients [88]. The intensity of the alignment pulse is a parameter that can easily be changed experimentally and it is therefore worth considering how this affects the revivals. Further, the observed experimental results have, as previously discussed, contributions from a large region of the focal volume. Understanding the intensity dependence helps us in predicting the consequences of this averaging. Figure 4.10 shows a calculation of the alignment dynamics in iodobenzene at four different intensities for the alignment pulse. The figure reveals that both the relative strengths and the shapes of the revivals are dependent on intensity. At the lowest intensity we see that J-type revivals are clearly dominant while at the higher intensities C-type revivals dominate. This is in very good agreement with our experiments since they were carried out at a higher intensity than any of the calculations. The calculations also justify the absence of the J-type half-revival. The revival structure overlaps with the oscillations from the first C-type revival and it therefore seems reasonable to assume that it disappears due to the spatial averaging.

To confirm the changes seen when we changed the molecule from iodobenzene to iodopentafluorobenzene another set calculations was carried out where the C-constant was varied for an artificial molecule with all other properties identical to those of iodobenzene. Fig. 4.11 shows the results. In (a) the symmetric top limit is recovered by letting $C = B$ and strong periodic revivals are observed. Fig. 4.11(b) shows the result for iodobenzene (identical to Fig. 4.10(c)), while Fig. 4.11(c) and (d) show the changes as we increase the asymmetry by lowering the C-constant. As we increase the asymmetry away from that of iodobenzene, we see that the J-type revivals completely disappear while the C-type revivals become broader and consist of increasingly more oscillations. The absence of J-type revivals agrees well with our experimental observations. We did not observe an increased number of oscillations, but this is most likely due to the spatial averaging.

Although the calculations presented above show good agreement with our experimental results and allow us to draw general conclusions from our limited number of experiments, it would be helpful to find a simple explanation for the appearance of the observed revivals. It is, therefore, tempting to consider how we would expect the molecules to behave classically. Let us take iodobenzene as an example. Due to the high asymmetry in the polarizability and inertial tensors we need to consider the rotation around all three major axes. The first step is to decompose the torque into its components along the three major axes. Take as an example a molecule with $\theta, \chi \neq n \cdot \frac{\pi}{2}$, that is the electrical field vector is not coincident with any of the three planes spanned by the three principal axes. The component of the electrical field in the plane spanned by the b- and c-axes will induce a torque along the a-axis (see Fig. 4.7). This torque rotates the molecular plane about the a-axis such that the angle between this plane (spanned by the a- and b-axes) and the electric field is reduced. Similar torques apply along the two other axes in order to minimize the energy of the molecule in the presence of the field. If the pulse is truly short the torque is applied impulsively and the molecule starts to rotate after the pulse. The angular frequency is obtained as the transferred angular momentum (the time-integral of the torque) divided by the moment of inertia (see Eq. (2.15)). Since the polarizability anisotropies are of similar magnitude for all three axes, the angular momentum components along each axis are similar. The moments of inertia are, however, very different: the A-constant is nearly an order of magnitude larger than the B- and C-constants and the frequency of rotation around the a-axis (rotations in the χ-angle) is thus much higher than the frequency of rotation around the other two axes. For the slower motion perpendicular to the a-axis (rotations in the θ-angle), the b- and c-axis effectively become indistinguishable — the molecule behaves as a symmetric top with an effective rotational constant $\bar{B} = (B + C)/2$.

The separation of time-scales that underpinned the preceding discussion also means that, if the pulse duration is not truly short compared to the time-scale for re-orientation of the molecule in the field, there exist a range of pulse durations were the symmetry axis becomes aligned after the pulse, but the molecular plane will be confined to the plane spanned by the symmetry axis and the polarization of the laser

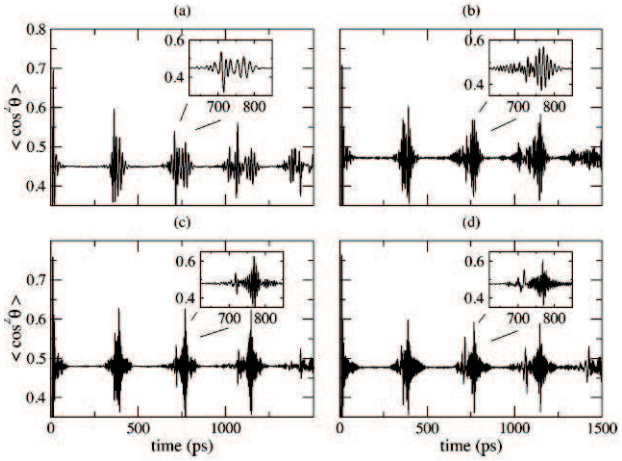

FIGURE 4.10: Numerical calculation of the intensity dependence of the revivals in iodobenzene at 400 mK. The pulse duration is 2.6 ps and the peak intensity is (a) $6.0 \cdot 10^{11}$ W/cm^2, (b) $1.0 \cdot 10^{12}$ W/cm^2, (c) $2.0 \cdot 10^{12}$ W/cm^2 and (d) $3.0 \cdot 10^{12}$ W/cm^2.

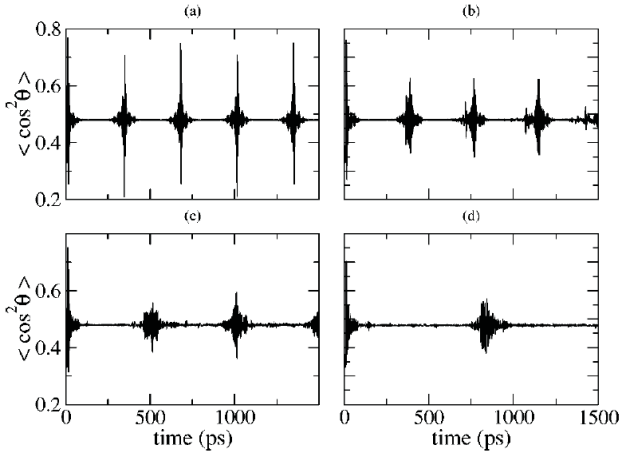

FIGURE 4.11: Numerical calculations showing how the revivals change at fixed laser parameters but with changed values of the C-constant. The pulse duration is 2.6 ps, the intensity $2.0 \cdot 10^{12}$ W/cm^2 and the temperature 400 mK. While all other parameters are fixed the C-constant takes the values (a) 787.44 MHz (prolate symmetric top), (b) 660.87 MHz (iodobenzene, *ab-initio*) (c) 500 MHz and (d) 300 MHz.

(i.e. $\chi \sim 0$) during the interaction with (the last part of) the pulse . In other words, the molecules are forced to rotate around the c-axis. For a molecule rotating with $|\mathbf{J}| \approx J_c$, that is with the angular momentum vector nearly parallel to the c-axis, the classical frequency of rotation is $2CJ$ and our observable, which has no up-down selectivity will thus be modulated at $4CJ$. These are all multiples of the fundamental frequency $4C$ and the molecules will thus rephase at $T_C = 1/4C$ [13]. The semi-classical model thus explains both the timing of J- and C-type revivals and why these are only ones observed. To the latter point it should be noted that rotations around the a-axis are not observable in $\langle \cos^2 \theta \rangle$ and rotations around the b-axis are classically unstable.

If these semi-classical arguments hold true, the pulse parameters in the experiment on iodobenzene must have been in a regime between the two limiting cases presented here. Very recent results from our lab seem to confirm this simple interpretation. In those experiments revivals of iodobenzene were recorded for a range of pulse durations under conditions where focal volume averaging could be neglected. For very short pulses strong J-type revivals were seen (including the previously missing J-type half-revival) while the C-type revivals were completely absent. For longer pulses the J-type revivals completely vanished but clear C-type revivals appeared with many oscillations visible. At intermediate pulse durations both revival types were seen. The absence of focal volume averaging is crucial since the peak intensity of the alignment pulse was shown to produce a similar modulation of the revivals (see also Fig. 4.10).

In the framework of RCS the appearance of partial rephasings for asymmetric tops has been know for many year. Besides using simple, semi-classical arguments as outlined above, a thorough quantum mechanical analysis of the beat structures that form the basis of the observed transients has been carried out. The somewhat surprising result that significant transients were seen even for highly asymmetric tops was summarized by Felker and Zewail [13] 'The reason for this is that significant patches of rotational-level structure in asymmetric tops retain symmetric-top regularities'. With this encouraging remark I will conclude this Chapter in the hope that future work will shed more light on revivals for asymmetric tops in the framework of quantum mechanics.

CHAPTER 5

Adiabatic alignment

Many experiments have unambiguously established and characterized adiabatic alignment of linear, symmetric and asymmetric top molecules [17–19, 60]. In spite of this, there have been a multitude of motivations for studying this technique again. First of all, adiabatic alignment served as a good testing ground for our new valve. Because adiabatic alignment is both simple and well studied it allowed us to examine the properties of the valve. Second, the new valve has opened some new opportunities for us regarding both controlling the rotational temperature and the size of the molecules we can study. These points have become important with the proposals for using alignment as a tool in gas phase diffraction experiments on small molecules and even proteins [89, 90]. Third, our newly proposed scheme for obtaining three-dimensional alignment (see Sec. 8.1) relies on the use of adiabatic alignment for fixing one axis of the molecule. Finally, independent of the previous points, alignment of negative ions was attempted.

This Chapter starts with some considerations about the choice of an optimal probe of adiabatic alignment. The problem to worry about is whether the presence of a moderately intense infrared field disturbs the measurement. Next, results on adiabatic alignment on large molecules are presented, demonstrating wide control over the temperature of the molecular beam. Finally the attempts to align negative ions are briefly reviewed.

5.1 Choosing the probe

For the study of adiabatic alignment it is of particular importance to pay attention to the choice of probe. The primary effect to worry about is the presence of the aligning laser field — to obtain a high degree of alignment it often necessary to work at intensities close to the onset of ionization. The alignment pulse may therefore change the probe process in an unpredictable manner. This has been the case in previous experiments in our lab where UV photodissociation was used to probe adiabatic alignment of iodobenzene [91]. In that case the presence of the alignment laser opened a new dissociation channel into I^* fragments with higher kinetic energy. It was shown that this new channel corresponded to the absorbtion of one photon from the alignment laser during the dissociation, a process that may be expected to be quite general for polyatomic molecules where the density of excited states often becomes high.

Therefore, in our recent studies of adiabatic alignment we turned to Coulomb explosion for probing the alignment. Some caveats do however also pertain to this process, in particular if the ionization pulse is not ultra-short. For the experiments presented below ionization pulses with a duration of $\sim$ 130 fs and intensities of $1 - 3 \cdot 10^{14}$ W/cm^2 were used. The red curve in the lower panel of Fig. 5.1 shows a mass spectrum that was obtained by ionizing iodobenzene with a pulse polarized perpendicular the flight direction and with a peak intensity of $3.4 \cdot 10^{14}$ W/cm^2. Only a small amount (a few mV) of the molecular ion was seen, but is not shown in the figure. In the spectrum the most important peaks have been assigned. A profound disintegration of the molecule is revealed: iodine ions are found in charge states up to $4+$ and carbon is primarily found as single carbon ions (the peaks to the left of iodine $2+$, $3+$ and $4+$ respectively are $C_nH_m^+$ fragments with $n = 4, 3, 2$). The black curve shows the spectrum obtained when we include a 1064 nm pulse with a duration of 9 ns and a peak intensity of $8.0 \cdot 10^{11}$ W/cm^2 to align the molecules parallel to the polarization of the ionization laser (and thus perpendicular to the flight direction). The peak intensity is about a factor of four below the onset of ionization. In spite of the low intensity the nanosecond pulse has a profound effect on the spectrum. All carbon fragments larger than C_2^+ almost completely disappear while the yield of I^{3+} ions is nearly doubled. Further we observe a narrowing of the I^+ and I^{2+} peaks, caused by alignment of molecules prior to ionization. To get an indication of what causes the very different yields we recorded another mass spectrum where the only change is that the nanosecond pulse is now polarized perpendicular to the ionization laser. The red curve in the upper panel of Fig. 5.1 shows the result together with the spectrum obtained for parallel polarizations (same as in the lower panel). The changes in the spectrum are astonishing: iodine in high charge states ($3+$ and $4+$) has completely disappeared from the spectrum. The yield of the doubly charged iodine ion is also strongly suppressed and the peak has become split, just as the peak for singly charged ions. This splitting is a manifestation of alignment: for the perpendicular polarizations the alignment laser is polarized along the flight direction, so if the molecules are well

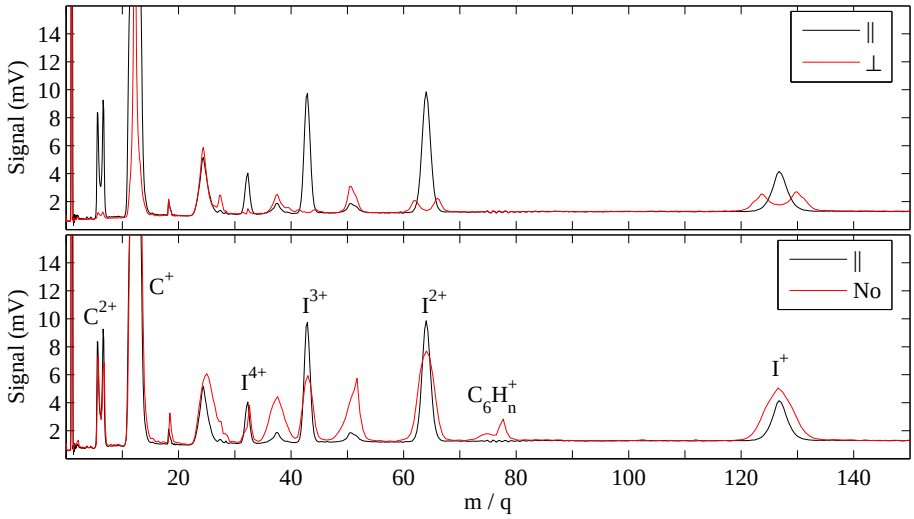

FIGURE 5.1: Mass spectra for iodobenzene. For all curves ionization is caused by a 130 fs, 800 nm pulse polarized perpendicular to the flight direction and with a peak intensity of $\sim 3.4 \cdot 10^{14}$ W/cm^2. In the lower panel the red curve show the spectrum with only the 800 nm pulse present. The other graphs show the spectra obtained by including a 9 ns, 1064 nm pulse ($I \sim 8.0 \cdot 10^{11}$ W/cm^2, polarization parallel to the 800 nm). The polarization of the 1064 nm pulse relative to 800 nm pulse is shown in the legends.

aligned along this direction some ions are ejected directly towards the detector while others go off away from the detector and have to be turned around in the extraction field before they fly towards the detector. The flight time for the latter ones is thus longer and they appear as larger masses. The minimum in center is due to the absence of molecules aligned perpendicular to the flight direction. For the carbon ions only the C^{2+} yield is strongly influenced.

So, what can we learn about the ionization process from these observations and, in particular, what influence does it have on our choice of probe for detecting alignment? An important question to settle is which effects are due to further ionization of the fragments caused by the presence of the alignment laser and which are due to alignment of the neutral molecule prior to ionization by the short pulse. The results strongly indicate that the large carbon fragments, $C_nH_m^+$ ($n = 3, 4, 6$), are ionized by the 1064 nm laser pulse: a strong modulation of their yields are observed when the alignment laser is included independently of how the molecules are aligned. In contrast to this behavior, the highly-charged iodine ions bear evidence of preferential ionization when the C$-$I bond is aligned along the polarization of the short laser pulse. The dramatic change in their yields, observed when comparing the parallel and per-

pendicular polarizations of the two laser, does not on its own tell anything about the cause for the changes. The fact that an almost similar modulation is observed when going from no alignment to perpendicular alignment, is what indicates a strongly preferential ionization of molecules aligned parallel to the polarization of the ionization pulse. The changes from no alignment to parallel alignment conform well with this picture: the yield of singly charged iodine ions is reduced by depletion into higher charge state channels, whose yield are then enhanced. By changing the rotational temperature of the sample it would be possible to check if this interpretation is correct. Even better, a similar experiment should be carried out on field-free aligned molecules. Although the limited experiments shown here cannot unravel the mechanism behind the strongly preferential ionization for channels leading to high charge states of iodine, we speculate that enhanced ionization is at play [8, 9]. To try to settle this point studies should be carried out on field-free aligned molecules with a range of durations and intensities for the ionization pulse.

For the present, the purpose of these studies was to clarify which probe geometry we should use. It is immediately clear that the parallel geometry is ill-suited. The higher charge states of iodine cannot be used since the recoil direction of these fragments is highly directional even when the molecules are not aligned so their angular distributions cannot be used. Tracking the changes in the yield of these ions as function of the intensity of aligning laser field does not give an unambiguous measure of alignment. Singly charged iodine cannot be used either — as evidenced by the lower panel in Fig. 5.1 there is a pronounced depletion from this channel when the molecules become aligned so the ions would primarily stem from the low intensity regions of the focal volume. The perpendicular channel is contrarily well suited for the detecting alignment. First of all, it is unbiased in the plane of the detector meaning that for an unaligned sample the detected distribution is circularly symmetric. Second, since the high charge states are so strongly suppressed, the only depletion effects to worry about are for weakly aligned molecules. In that case there may be a relatively larger fraction of the signal stemming from the outer regions of the focal volume due to depletion of the high intensity regions. This effect was minimized by reducing the peak intensity of the short pulse to $\sim 1.0 \cdot 10^{14}$ W/cm^2. At this intensity the channels leading to singly and double charged iodine ions become dominant.

For the other molecules studied in this Chapter the modulation of the mass spectrum for parallel versus perpendicular polarizations of the alignment and ionization pulses was far less dramatic than what we observed for iodobenzene. Maybe the use of different intensities and pulse durations for the ionization pulse could lead to similar effects. For now we shall stay pleased with the absence of these effects as it gives us a probe method that we can have high confidence in.

5.2 Large, cold molecules

We have just seen that strong evidence for the alignment induced by a nanosecond pulse can be found in the mass spectrum. A more direct measure for the alignment induced in the molecules can be obtained from the angular distribution of selected fragments, just as it was done in the previous Chapter. In this Section results are presented on adiabatic alignment of four molecules: iodobenzene, *p*-diiodobenzene, 3,4-dibromothiophene (DBT) and 4,4′-dibromobiphenyl (DBBP). The structure of these molecules is shown in top row of Fig. 5.2. For all of the molecules we used the perpendicular pump-probe geometry with the short, intense ($1 \cdot 10^{14}$ W/cm^2) probe pulse polarized perpendicular to the plane of the detector while the alignment pulse was polarized parallel to the plane of the detector. Images were recorded for a range of intensities of the alignment pulse (to the onset of ionization) and for a range of backing pressures. The fragments chosen were I^+ for iodobenzene and *p*-diiodobenzene, S^+ for DBT and Br^+ for DBBP.

In the middle row of Fig. 5.2 false color-scale ion images obtained with only the probe pulse present are shown. All four images are as expected circularly symmetric (for the iodobenzene image a small detector inhomogeneity is revealed). In the DBT image the center has been cut out. The reason is that S^+ has the same m/q as O_2^+, so a small amount of O_2 from the molecular beam gives rise to a big, concentrated peak in the center (these ions nearly have zero recoil velocity). The lower row of images were obtained by including the alignment pulse with an intensity just below the onset of ionization and with the coldest possible molecular beam conditions. The contrast is striking. For all four molecules we observe a very strong confinement of the recoil direction for the detected fragments. Since the probe pulse is unbiased in the plane of the detector this is direct evidence of alignment of the neutrals prior to Coulomb explosion. In the cases of iodobenzene and *p*-diiodobenzene two channels with distinct kinetic energies are seen in the outer regions of the images. These correspond the creation of I^+ with a singly and doubly charged counter-ion respectively. As a measure for the degree of alignment we chose $\langle \cos^2 \theta_{2D} \rangle$ (Sec. 3.2.2). The angular distribution used to calculate this number is extracted from the region dominated by the channel corresponding to a singly charged counter-ion. For DBT and DBBP a less well defined radial structure is seen and the radial distribution was thus extracted from broad radial range covering most of the peak. The ion hits just outside the cut-out region in the DBT image are most likely O_2^+ from thermal oxygen in residual background gas in the interaction region.

After establishing that the molecules do indeed become strongly aligned by the 9 ns pulse and having defined the radial region of interest for extracting $\langle \cos^2 \theta_{2D} \rangle$, we are now ready to conduct a systematic study of adiabatic alignment of these molecules. For a given molecule two parameters determine the degree of alignment: the intensity of the alignment laser and the rotational temperature of the molecules (see Fig. 2.2). As already discussed the rotational temperature can be controlled by chang-

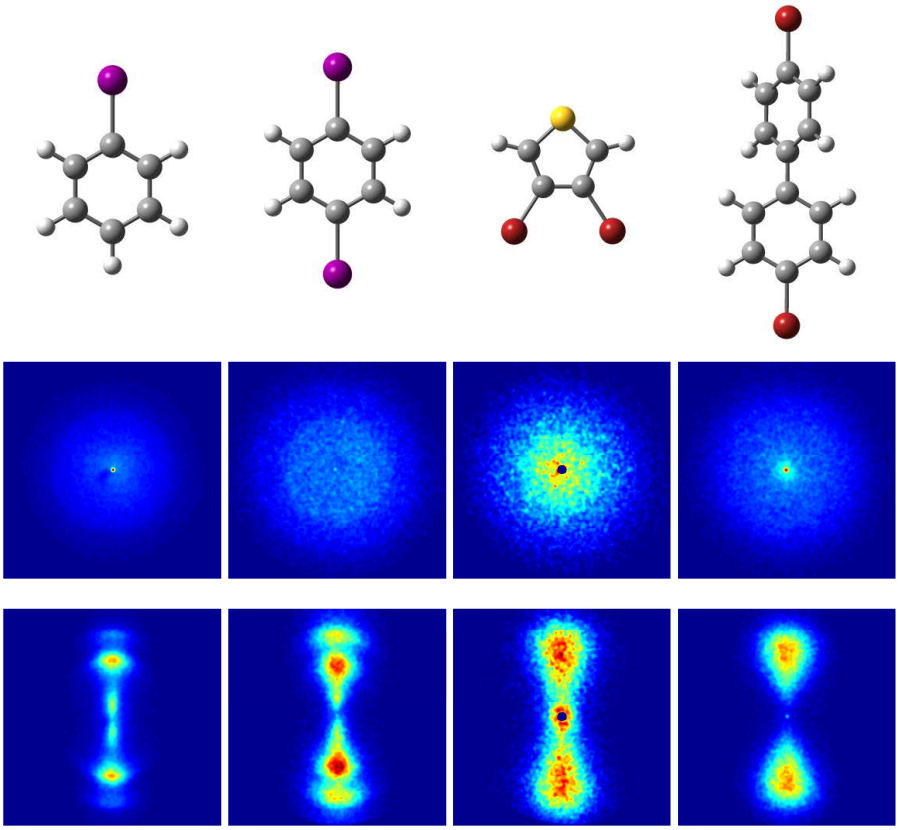

(a) Iodobenzene (I^+) (b) *p*-diiodobenzene (I^+) (c) DBT (S^+) (d) DBBP (Br^+)

FIGURE 5.2: Ion images for the four molecules studied: (a) iodobenzene, (b) *p*-diiodobenzene, (c) 3,4-dibromothiophene and (d) 4,4′-dibromobiphenyl. In the each caption the detected ion shown. In the top row the structure of each molecule is shown. The upper ion images show the distributions recorded when only the probe (polarized perpendicular to the plane of the detector) is included, while the lower images are recorded when a 9 ns, 1064 nm laser pulse (vertical polarization) is included with an intensity just below the ionization threshold. The images show direct evidence of the high degree of alignment in the neutral molecules prior to the Coulomb explosion.

ing the backing pressure in the supersonic expansion. Figure 5.3 summarizes the results obtained for the four molecules. Shown is $\langle \cos^2 \theta_{2D} \rangle$ as function of intensity of the alignment laser for different backing pressures. The data points stop at roughly the highest intensity that could be used without causing ionization. A quick look at the four graphs reveal a very similar behavior: when high backing pressures are used the molecules become very well aligned at modest intensities, whereas for low backing pressures only a small degree of alignment can be obtained at non-ionizing intensities. Comparing the graphs in Fig. 5.3 with Fig. 2.2 immediately reveals that we have a very high degree of control over the temperature in the molecular beam (the x-axis should be re-scaled according to the polarizability anisotropy). Below, the results for iodobenzene are used to set an upper limit of 1.5 K on the rotational temperature and very likely the molecules are colder. From the low pressure results in Fig. 5.3(b)–(d) we roughly estimate the rotational temperature to be $\sim$ 50 K. This large dynamical range has not been accessible before, but may turn out to be very helpful for studies using adiabatic alignment.

Two comments on the pressures used should be given. First, for iodobenzene and *p*-diiodobenzene the maximum pressures shown are quite low. Higher pressures (up to 100 bar) were also used, but lead to curves identical to the curve for the highest pressure shown. Second, the absolute pressures should not be directly compared between the different molecules since another parameter was also changed: the magnitude of the driving current for the solenoid. The amplitude of this current determines amplitude of the excursion for the plunger. We have observed that the temperature of the molecular beam (the width of the gas pulse) is sensitive to this amplitude, so we have changed two parameters that both influence the temperature in the molecular beam. We believe that the reason that the amplitude of the current pulse influences the temperature in the beam is that the expansion does not have time to settle during the very short opening time. Larger excursions for the plunger will therefore lead to larger effective backing pressures in the expansion. This is a point we became aware of while carrying out these experiments. That said, we believe that the temperature of the molecular beam is similar for the highest pressures shown. This is based on measurements of the duration of the gas pulse in the interaction region — unless the translational temperature is very low the gas pulse will disperse significantly during the $\sim$ 45 cm flight from the nozzle to the interaction region.

For a more detailed analysis of the results shown in Fig. 5.3, let us start by comparing the results for iodobenzene and DBT. If we only look at the shape of the curves these two molecules behave very similarly, in particular the bend in the high pressure curve occurs at exactly the same intensity. This is indeed what we should expect — the polarizability tensor of DBT is remarkably similar to that of iodobenzene: $\alpha_b = 20.6$ Å^3, $\alpha_a = 16.0$ Å^3 and $\alpha_c = 10.1$ Å^3 for DBT[a] [20] versus

[a] b is the symmetry axis, a is the axis in the molecular plane being perpendicular to the b axis and c is out of the plane

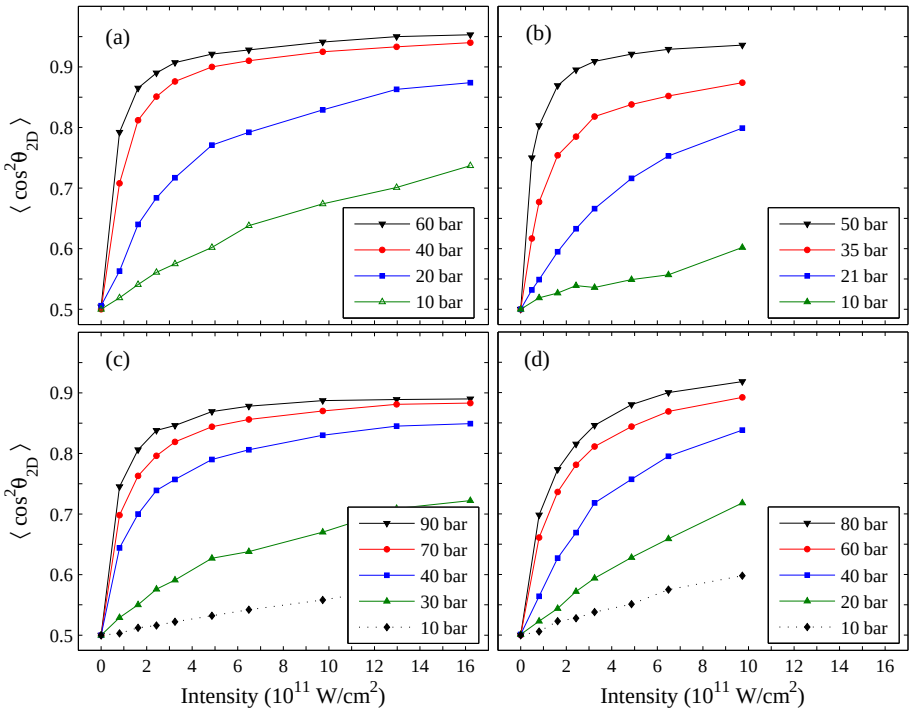

FIGURE 5.3: Adiabatic alignment of (a) Iodobenzene, (b) *p*-diiodobenzene, (c) 3,4-dibromothiophene and (d) 4,4′-dibromobiphenyl. The curves show $\langle \cos^2 \theta_{2D} \rangle$ as function of the intensity of the alignment laser for a range of pressures (see legend).

$\alpha_a = 21.5$ Å^3, $\alpha_b = 15.3$ Å^3 and $\alpha_c = 10.2$ Å^3 for iodobenzene. In the heavy molecule limit the degree of alignment is solely determined by the the ratio of the thermal energy to the interaction energy (Eq. (2.13) and [32]), that is the competition between the confining action from the interaction with the laser field and the random, thermal motion. If we now take a closer look at sub-figures (a) and (c), it is seen that the maximum degree of alignment is different for the two molecules. For iodobenzene the maximum degree of alignment is $\langle \cos^2 \theta_{2D} \rangle = 0.95$, while for DBT a value of $\langle \cos^2 \theta_{2D} \rangle = 0.89$ is reached. Assuming that the rotational temperature is very similar in the two cases (which is very reasonable based on the position where the curve bends), the most likely explanation for this difference is a break down of the axial recoil approximation for DBT. It does not seem unreasonable to imagine that the sulphur atom, being confined inside an aromatic ring, does not with unity probability recoil along the symmetry axis of the molecule. If for instance, a charge-asymmetric molecular ion is created, the force on the sulphur atom will be at an angle to the sym-

metry axis. As discussed previously, the blurring caused by such effects will reduce the observed degree of alignment.

Moving to *p*-diiodobenzene (sub-figure (b)) we are now faced with a molecule for which we do not know the polarizability tensor. If a direct comparison is carried out between the 60 bar data for iodobenzene and the 50 bar data for *p*-diiodobenzene it turns out that they are indistinguishable. Although it is expected that *p*-diiodobenzene has a larger polarizability than iodobenzene the data at least indicate that the polarizability anisotropy is not very much different (assuming once again that the temperature is the same). The final molecule is DBBP and again we do not know the polarizabilities. Comparing the 80 bar data to the best iodobenzene data there is a slower onset of the saturation like behavior. This may be due to a factor of $\sim$2 lower effective polarizability anisotropy, but this larger molecule may not reach the same rotational temperature in the supersonic expansion. Further, the molecule is not rigid since the two aromatic rings can perform torsional motion. How this influences the cooling in the supersonic expansion and the response to the laser field is not known.

Finally, we use the iodobenzene data to try to estimate the rotational temperature of the molecules. To do this we compare with numerically calculated values of $\langle \cos^2 \theta_{2D} \rangle$ as function of intensity for different temperatures. The numerical model is based on treating iodobenzene as a symmetric top (for numerical simplicity). As discussed previously this is a good approximation for the inertia tensor but not for the polarizability. For the polarizability anisotropy we use the average polarizability perpendicular to the symmetry axis. To calculate the value of $\langle \cos^2 \theta_{2D} \rangle$ we first calculate the thermally averaged angular distribution for the θ-angle. Next, we find the two-dimensional projection of this distribution by taking a large number of points in (θ, ϕ) and find their two dimensional projections $(x_{\mathrm{2D}}, y_{\mathrm{2D}})$. From the intensity distribution in $(x_{\mathrm{2D}}, y_{\mathrm{2D}})$ we can build radial and angular distributions for the two-dimensional distribution and calculate $\langle \cos^2 \theta_{2D} \rangle$ for a specific radial region. This model does not take into account the angular selectivity of the probe, but for well aligned molecules this is not a problem since all molecules are confined along an axis perpendicular to the polarization of the probe.

The left panel of Figure 5.4 shows the 60 bar data for iodobenzene plotted together with results obtained with this model by assuming rotational temperatures of 0.5, 1.0 and 2.0 K respectively. At the low intensities the measured points lie in between the 1.0 and 2.0 K curves, while at higher intensities the measured points seem to follow the 2.0 K curve. The strong similarities between the measured and calculated curves is encouraging: it simultaneously shows that the molecules are very cold and that the simplified model is most likely not too far off. It turns out that if the intensities of the numerical data are allowed to be re-scaled, a very good agreement can be found (Fig. 5.4, right panel). There is a good physical explanation for allowing such re-scaling. Part of the problem is the use of the average polarizability perpendicular to the symmetry axis — we know that the χ-angle is confined (see Eq. (2.5) and [20]). In the limit of perfect confinement of the χ-angle we overestimate the polarizability

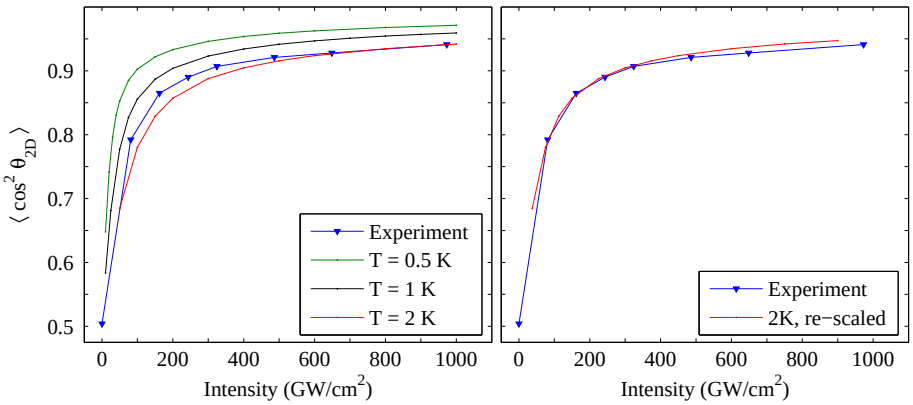

FIGURE 5.4: Comparison between experimental and calculated data for iodobenzene. Left: Calculations at three different temperatures using the average polarizability perpendicular to the symmetry axis. Right: the calculation at 2 K with the intensities re-scaled to 75%.

anisotropy by $\sim 40\%$. Since the polarizability only enters the Hamiltonian via the product with the intensity we can correct for a wrong polarizability by re-scaling the intensity axis. This is, however, only half the story. In Sec. 2.2 we found that at the intensities used in the experiments the degree of alignment only depends on the ratio $k_{\mathrm{B}}T/\Delta\alpha I$. This means that from the intensity dependence of the degree of alignment we can only determine the ratio $T/\Delta\alpha$. Numerically it was found that this scaling also holds for $\langle\cos^2\theta_{2D}\rangle$ for a symmetric top (using the results shown in Fig. 5.4). If we assume that the use of the average polarizability is correct, then the estimated temperature is 1.5 K, whereas if the anisotropy in the plane of the molecule is used the estimated temperature is $\sim$1 K. In order to settle this point, full asymmetric top calculations would be needed.

No matter which of the estimates we rely on we are about an order of magnitude higher than the temperatures measured by Hillenkamp *et al.* [31]. The origin of this discrepancy is at the moment unresolved, but focal volume averaging and non-axial recoils are likely to limit our observations. Hillenkamp *et al.* measured the rotational contour for the $S_0 \rightarrow S_1\, 0_0^0$ transition in aniline and estimated the rotational temperature by comparing with simulated contours. Since the rotational spectrum of aniline has been measured with high precision this is a very direct measurement of the rotational temperature, unlike the modelling presented here.

5.3 Negative ions

In the group of Daniel M. Neumark, adiabatic alignment of negative ions detected by photoelectron angular distributions (PADs) was attempted. Previous experiments have shown that PADs are sensitive to the mild alignment induced by a single photon transition to an excited state [92, 93], so guided by theory [94, 95] we expect that PADs should also be sensitive to the potentially high degrees of alignment that can be obtained using adiabatic alignment. When adiabatic alignment is used in combination with PADs one has to be particularly careful about the intensity in the alignment laser: if the intensity becomes too high the angular distributions become distorted by ponderomotive acceleration of the electrons out of the focus of the nanosecond laser [96]. In our experiments the intensity of the alignment laser was kept below 10^{11} W/cm^2 so the ponderomotive potential was $U_\mathrm{p} = e^2E^2/4m\omega < 10$ meV. With typical electron kinetic energies of 1 eV or more, the relative energy shift would be less than 1%. In the images we observed no signs of distortion.

The experiments were carried out on the anionic carbon clusters C_n^- (n = 2 – 8) and C_nH^- (n = 2, 4, 6, 7), which are all linear chains. A detailed description of the experimental setup can be found in [97]. Briefly, the carbon clusters were created in the supersonic expansion of a mixture of a few percent C_2H_2 and CO_2 in Ne passing through a pulsed discharge. A 1200 eV electron beam was used as a stabilizing charge source for the anion formation. The ions were injected orthogonally into a time-of-flight mass spectrometer, where a pulsed, high-voltage reflector was used to discriminate ions with unit mass selectivity. The selected ion bunch was then crossed by the focused laser beams: 8 ns pulses at 1064 nm were used for alignment and 100 fs, 265 nm pulses synchronized to the peak of the nanosecond pulse were used for electron detachment. A velocity map imaging spectrometer was used to project the electrons onto a MCP backed by a phosphor screen and images were recorded with a CCD-camera.

One of the main reasons for choosing the carbon clusters for these experiments is that they are known to have very large polarizabilities (and polarizability anisotropies). For the neutral C_6 clusters, for instance, *ab initio* calculations have predicted a polarizability anisotropy of about 22 Å^3 [98]. The polarizability of the anion clusters are not known. Closely related to the large polarizabilities is the fact that the anion carbon clusters all have excited states below the detachment threshold. For the even, bare clusters C_4^-, C_6^- and C_8^- this turns out to be a problem. When we sent the 1064 nm pulses onto these clusters we observed a very high number of electrons being detached even without the UV pulse present and at very low intensities for the YAG laser. The photoelectron distributions were peaked at zero energy, had an exponential fall-off and were circularly symmetric. These are the signatures of thermionic emission where a molecule with an internal energy above the detachment threshold emits the electron in a statistical process. The first excited state of these three ions are found slightly more than one eV above the ground state and the $X \rightarrow A$ transitions are dipole allowed [99].

With the energy of a 1064 nm photon being 1.165 eV, the alignment laser is very close to being resonant with the $X \rightarrow A$ transitions. Once the molecules are excited into the A-state, strong vibronic coupling brings the molecule back to the X-state with the excess energy distributed on the vibrational degrees of freedom. The molecules can then go through this cycle several times, each time heating the molecules with 1.165 eV, so after only four cycles the total vibrational energy will be larger than the detachment energy and the electron can then be 'boiled off'.

For the clusters C_2^-, C_2H^-, C_6H^-, C_7^- and C_7H^- there was little or no sign of detachment induced by the 1064 nm laser at intensities up to 10^{11} W/cm^2. Unfortunately there were no changes in the angular distributions either. This leaves us with C_3^- and C_4H^-. For both of these ions the presence of the YAG laser clearly changed the photoelectron kinetic energy distribution at low energies. In the case of C_3^- the presence of the YAG laser gave rise to a broad, featureless distribution a low energies and a very significant depletion of the high energy peaks. The angular distribution for some of the high energy peaks did change with the intensity of the nanosecond laser, but the amount of signal were at the noise level. For the C_4H^- ions some complex features appeared at low electron energies in the presence of the YAG laser; the photoelectron spectrum seemed broad and featureless but the in the images complex angular distributions were observed. The high energy region of the spectrum, corresponding to direct detachment by the absorbtion of a UV photon, consist of three peaks: one big slightly broad peak which actually consist of several unresolved peaks and two smaller peaks. When the YAG laser was included we observed some changes in one of the small peaks, but none in the dominant peak.

All in all we did not observe any conclusive signs of alignment in the photoelectron angular distributions. There are two comments attached to this. First of all, it might be worth trying nonadiabatic alignment of the clusters although the intensity of the alignment pulse will be severely restricted by the low detachment threshold (3–4 eV). If the changes in the PADs are small they will be easier to separate from noise when the changes appear periodically as is the case for a rotational wave packet in linear molecules. This was beautifully demonstrated in the work of Bragg *et al.* [93]. An important motivation for trying this is that it gives a direct measurement of the rotational constant, which can be difficult to obtain for anions. Second, it is worth speculating why we did not observe any changes in the PADs. The most likely answer seems to be the rotational temperature; if the rotational temperature is high then the induced degree of alignment will be low (see Fig. 2.2). Since the anions are created in a quite harsh environment (a high voltage discharge stabilized by 1200 eV electrons) during the stagnation of the supersonic expansion we cannot expect the internal degrees of freedom of the ions to relax to the temperature of the carrier gas. Indeed for the carbon clusters the vibrational temperature can be thousands of Kelvin, whereas the rotational temperature can change from day to day. The best way to estimate the rotational temperature is by using the rotational contour of the vibronic transitions. In this way the temperature has been estimated to 50 K under good conditions. If

we make a guess for the polarizability we can estimate the degree of alignment from Fig. 2.2 using the re-scaling discussed above. For neutral C_4 calculations estimate the polarizability anisotropy to be ~ 10 Å^3 [98]. This would correspond to a temperature of 20 K for *tert*-butyliodide, so from Fig. 2.2 it can be concluded that the degree of alignment must have been very low at the modest intensities used in the experiments.

CHAPTER 6

Two-pulse alignment

In this Chapter a systematic study of nonadiabatic alignment by the use of two short pulses is made. It will be shown that for the right choice of pulse durations, intensities and delay, the alignment induced by two pulses is clearly superior to that induced by a single pulse.

6.1 Introduction

For many experiments utilizing aligned molecules it is desirable to have the molecules as well aligned as possible. In the case of adiabatic alignment we saw that two adjustable parameters, the rotational temperature and the intensity of the alignment laser, determined the degree of alignment. To obtain a strong alignment, the molecules must initially be cold and the intensity must be close to the ionization threshold. But that is all we can do. For nonadiabatic alignment we discussed a third parameter, the pulse duration, but we should rather be thinking of an optimal shape for the electric field. One way of shaping the electric field is to create two or more pulses, for instance by the use of an interferometer.

The first proposal for using multiple pulses to optimize the degree of alignment (or orientation) was made by Averbukh and co-workers [34, 35, 100]. The starting point for their work is the δ-kick model. In Sec. 2.3 we saw that according to this model it

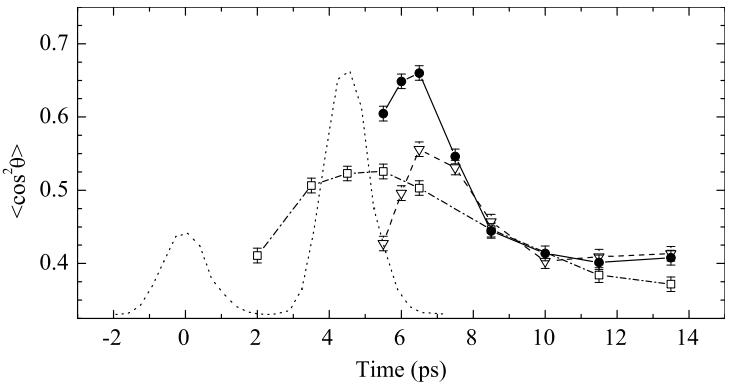

FIGURE 6.1: Two-pulse alignment of iodobenzene. The dotted curves show a cross-correlation of the two alignment pulses ($I_1 = 1.4 \cdot 10^{12}$ W/cm^2, $I_2 = 4.1 \cdot 10^{12}$ W/cm^2). Also shown is the degree of alignment as function of time for the first pulse only (open squares), the second pulse only (open triangles) and both pulses are present (full circles).

is the lag of the molecules initially oriented perpendicular to the laser polarization that causes the saturation of the degree of alignment induced by a single pulse. A more optimal kick is given if the molecules are aligned prior to the kick since a larger number of molecules will then obtain an angular velocity proportional to their initial angle (see Eq. (2.15)). The original proposal by Averbukh and Arvieu [34] was therefore to use a train of identical pulses, each of these synchronized to the maximum degree of alignment from the previous pulses. In practice it is difficult to produce a train of many pulses with different delays between each pair of pulses. Fortunately, it was shown that the degree of alignment can be significantly enhanced by the use of only two pulse with correctly chosen intensities and delays [35].

The dotted curve in Figure 6.1 shows a cross-correlation of the two-pulse combination that was experimentally found to be optimal (in a limited parameter search) for iodobenzene [101]. The two pulses are closely spaced and the peak intensity of the first pulse is about one third of the peak intensity in the second pulse. The figure also shows the degree of alignment due to the first pulse, the second pulse and both pulses. The first thing to notice is that with a single pulse, increasing the intensity by a factor of three only changes the degree of alignment by a small amount ($\langle \cos^2 \theta \rangle = 0.52$ and 0.56 respectively). If all of the pulse energy is collected in a single pulse we obtain $\langle \cos^2 \theta \rangle = 0.57$ — clearly the degree of alignment has become saturated. When the two-pulse combination is used, this saturation is overcome and a degree of alignment of $\langle \cos^2 \theta \rangle = 0.66$ is reached. From the figure we see that the optimal timing is to send the second pulse close to the peak in the degree of alignment due to the first pulse. By pre-aligning the molecules with a relatively weak pulse we push a large fraction of the

molecules into the harmonic region of the interaction potential for the second kick, while keeping their angular velocities low.

In the following Sections a detailed experimental and numerical study of two-pulse alignment of *tert*-butyliodide is presented. The optimal choices of pulse duration, intensity and delay between the two pulses are considered. At the end of this Chapter, other methods for manipulating rotational wave packets are briefly discussed.

6.2 Detailed study: *tert*-butyliodide

In the experiments on two-pulse alignment of iodobenzene that were briefly discussed above, the delay between the two alignment pulses was scanned near the initial peak in the degree of alignment from the first pulse. For asymmetric tops this initial peak is the global maximum in the degree of alignment, but since the peak occurs briefly after the pulse has vanished the choice of delay between the two pulses becomes severely restricted if we want to avoid interference between the two pulses. For symmetric tops this restriction can be overcome by tuning the delay to the first full revival. There, the wave packet is an exact replica of the wave packet immediately after the pulse, but interference effects are no longer a concern. For this reason, and because symmetric tops are simpler to handle numerically, we chose the symmetric top *tert*-butyliodide for a detailed study of two-pulse alignment. The timing sequence used in these studies is shown in Figure 6.2. The upper graph gives an overview and the regions marked in red are shown in detail in the lower graphs. The first alignment pulse is sent at $t = 0$ inducing a modest degree of alignment, peaking at about $t = 5$ ps. At the full revival ($t \sim 323$ ps) the second alignment pulse is sent, forcing the molecules into a high degree of alignment which is then probed at the following full revival ($t \sim 645$ ps). To optimize the degree of alignment we changed the intensity in the first pulse I_1, the (common) duration of the alignment pulses τ and the delay between the alignment pulses Δt. For each setting, the delay of the probe was scanned to identify the highest degree of alignment. The intensity of the second pulse I_2, is fixed, in the experiments at the ionization limit and in the calculations at 6 TW/cm^2 (due to the long computational times at the intensities used in the experiment).

6.2.1 Experimental results

To carry out the desired study of two-pulse alignment of *tert*-butyliodide we must be able to create two pulses with variable duration, delay and intensities. As described in Sec. 3.2.2 the alignment pulses are obtained from the output of the femtosecond laser by first stretching the ∼130 fs pulses in a grating stretcher and then create a pair of pulses with variable delay and intensities using a modified Mach-Zehnder interferometer (see Fig. 3.3(b)). For probing the degree of alignment we used dissociation by a

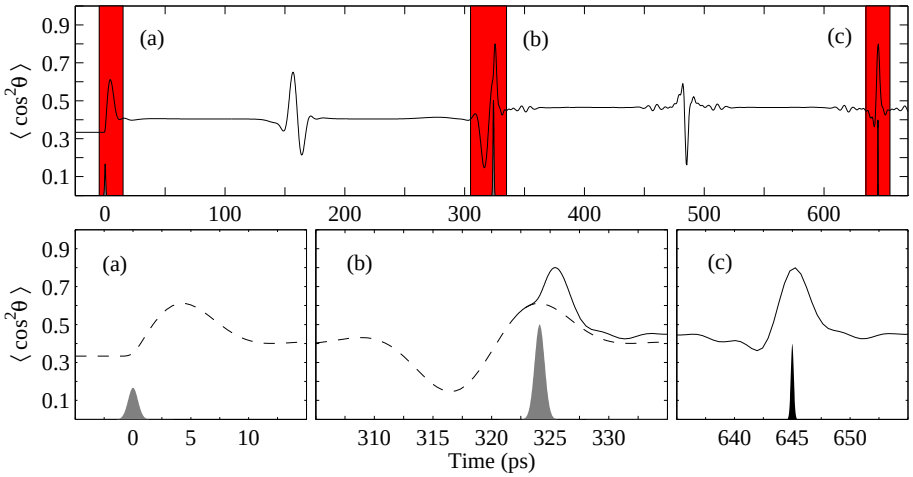

FIGURE 6.2: Optimal timing sequence for two-pulse alignment of *tert*-butyliodide. The gray areas in (a) and (b) show the alignment pulses while the black area in (c) shows the probe pulse. The dashed curve shows the degree of alignment when only the first pulse ($I_1 = 2$ TW/cm^2) is used and the full curve shows the alignment obtained when the second pulse ($I_2 = 6$ TW/cm^2) is included. The calculation assumes a temperature of 1 K, pulse durations of 1 ps and includes focal volume averaging.

266 nm pulse followed by resonant ionization of the iodine fragments, just as in the study of revivals for *tert*-butyliodide (Sec. 4.2).

First, we compare the shapes of the revivals when either one or two pulses are used for alignment. The results, shown in Fig. 6.3, focus on the alignment dynamics around the first half and full revivals following the second pulse. In both cases the pulse duration is 0.5 ps and the intensity of the second pulse, I_2, is 9.4 TW/cm^2, just below the intensity where ionization and fragmentation of *tert*-butyliodide sets in. The relative timing of the two alignment pulses is chosen such that the second pulse is sent at the time where the degree of alignment due to the first pulse reaches the peak value. Starting with the revivals measured with only the second pulse present we observe shapes identical to those presented in Fig. 4.6(a). We note that for the pulse duration considered, an almost identical peak value for the degree of alignment, corresponding to $\langle \cos^2 \theta_{2D} \rangle \sim 0.86$, is observed at the half and the full revival. When the other alignment pulse is included prior to the strong alignment pulse, the revivals change towards a more symmetric shape. Furthermore, we observe that the two-pulse sequence increases the maximum degree of alignment at the full revival to $\langle \cos^2 \theta_{2D} \rangle \sim 0.88$. At the half revival we do not observe the expected corresponding decrease in the minimum degree of alignment (see Fig. 6.2). We ascribe this to the low sensitivity of the parallel transition, used to probe the spatial orientation, to perpendicularly

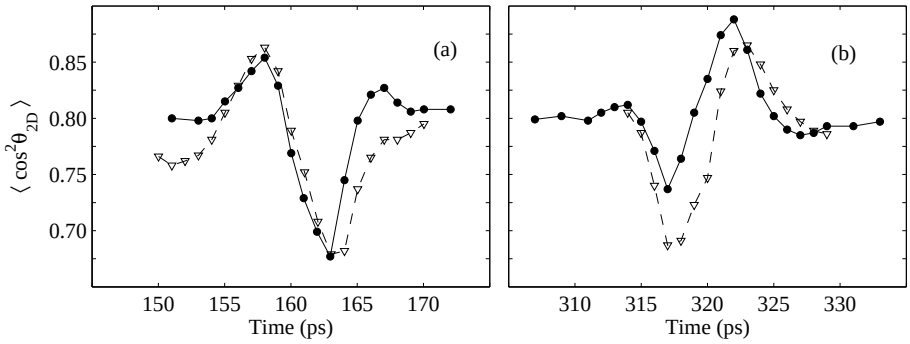

FIGURE 6.3: (a) Half and (b) Full revival for *tert*-butyliodide exposed to one pulse ($I = 9.4$ TW/cm^2, triangles) and two alignment pulses ($I_1 = 4.5$ TW/cm^2, $I_2 = 9.4$ TW/cm^2, circles). The time shown is the delay from the last alignment pulse applied. All pulses have a duration of 0.5 ps.

aligned molecules.

Hereafter, we seek to find the laser parameters leading to the best degree of two-pulse alignment. Guided by the results of Fig. 6.3 we restrict the measurements of the alignment to the first full revival after the second pulse. This approach is justified by the numerical results presented below. We begin by investigating the dependence on the delay, Δt, between the two alignment pulses. To do this, we initially measure the degree of alignment around the first full revival following the first pulse [corresponding to the dashed curve in Fig. 6.2(b)]. Next, we include the second pulse and measure the degree of alignment at the first full revival after the second pulse [corresponding to Fig. 6.2(c)] for different delays between the two pulses. The results are displayed in Fig. 6.4. In this figure the full circles show the degree of alignment due to the first pulse. The open triangles show the highest degree of alignment obtained when the second pulse is sent at the time given on the x-axis. Again referring to Fig. 6.2 this corresponds to plotting the maximum in Fig. 6.2(c) as a function of the delay between the two alignment pulses. The left graph [Fig. 6.4(a)] is obtained with a pulse duration of 1 ps and the first pulse having a peak intensity $\sim 1/4$th of the intensity in the second pulse. There is nearly a one to one correspondence between the curves. The best degree of alignment is, however, obtained when the second pulse is sent slightly after the degree of alignment, due to the first pulse, reaches its peak value. The right graph is obtained with a pulse duration of 0.5 ps and nearly equal intensity in the two pulses. Again, the shape of the degree of alignment obtained with two pulses nearly follows the degree of alignment due to the first pulse at the time when the second pulse is sent.

Next, we investigate the dependence of two-pulse alignment on the intensity in the first pulse, I_1. The intensity of the second pulse, I_2, is fixed just below the value where ionization and fragmentation of the molecules start to occur. For each value of I_1 we

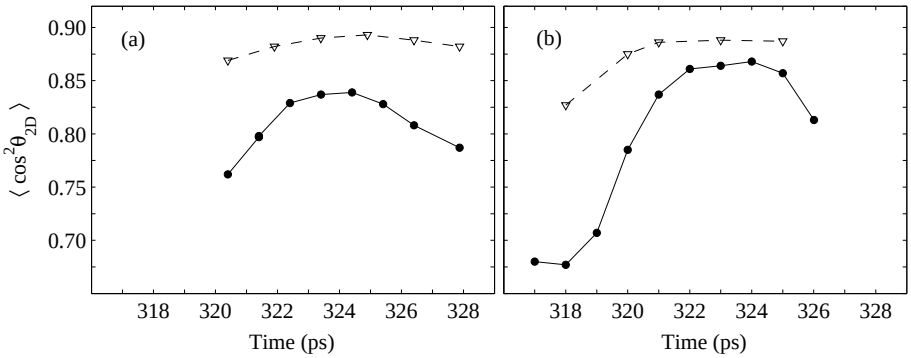

FIGURE 6.4: Dependence of two-pulse alignment on the pulse separation. In (a) the pulse duration is 1 ps, $I_1 = 3.7$ TW/cm^2 and $I_2 = 14$ TW/cm^2. In (b) the pulse duration is 0.5 ps, $I_1 = 8.8$ TW/cm^2 and $I_2 = 9.2$ TW/cm^2. The open triangles show the best degree of alignment obtained with two pulses (see text) as a function of the pulse separation. The full circles show the degree of alignment due to the first pulse at the time when the second pulse arrives.

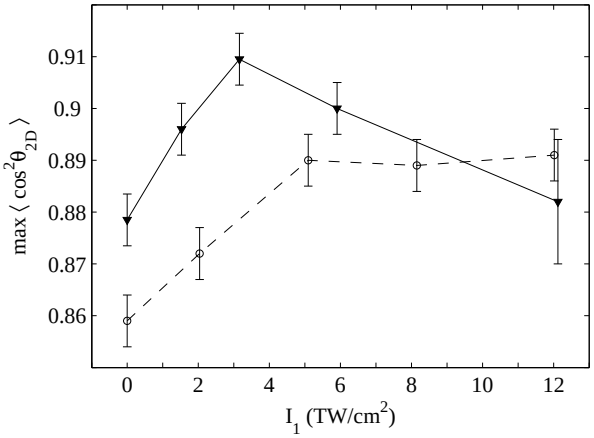

FIGURE 6.5: Dependence of two-pulse alignment on the intensity of the first alignment pulse. At each intensity the data points mark the highest degree of alignment obtained with pulse durations of 0.5 ps (dashed curve, circles) and 1 ps (full curve, triangles). I_2 is fixed at 11 TW/cm^2 and the second pulse is sent when the degree of alignment due to the first pulse peaks.

start by finding the time when the maximum degree of alignment at the revival due to the first pulse occurs. Then we include the second pulse at this time and measure the degree of alignment at the first revival after the second pulse. The results, showing the maximum degree of two-pulse alignment as a function of I_1, are displayed in Fig. 6.5 for pulses with a duration of 0.5 and 1 ps. The full curve, representing the results recorded with 1 ps pulses, exhibits a clear maximum when the intensity of the first pulse is $\sim 1/3$rd the intensity of the second pulse. For the results obtained with 0.5 ps pulses it is seen that the degree of alignment is enhanced with two pulses, but no clear maximum is observed. In general, the results show that almost any ratio $I_1/I_2 \leq 1$ of two optimally timed pulses leads to a significantly higher degree of alignment than that obtained with just one pulse.

6.2.2 Numerical results

We now turn to the numerical exploration of two-pulse alignment of *tert*-butyliodide. In the calculations we used intensities and temperatures lower than those used in the experiments. Our aim is a qualitative rather than a quantitative agreement with the experiments. Unless otherwise noted, all calculations take focal volume averaging into account (see Sec. 2.3.3).

We start by investigating how the degree of alignment at both the half and the full revival after the second pulse depends on the time separation between the two alignment pulses. The calculations are carried out at four different intensities for the first pulse, $I_1 = 0.5, 2, 4$ and 6 TW/cm^2. All other parameters are fixed: $\tau = 1$ ps, $T = 1$ K and $I_2 = 6$ TW/cm^2. The results are shown in Fig. 6.6. For easy comparison with the experimental results, we use the same notation as in Fig. 6.4. Thus, the full curves show the degree of alignment due to the first pulse around the times where the second pulse is sent and the dashed curves in the left (right) column show the best degree of two-pulse alignment at the first half (full) revival after the second laser pulse.

At first we focus on the right column showing the degree of alignment at the full revival after the second laser pulse. These graphs should be compared with the experimental results presented in Fig. 6.4. Several similarities are seen between the two figures. First of all, Fig. 6.6 shows that the best degree of two pulse alignment at the full revival nearly follows the degree of alignment from the first pulse at the time when the second pulse is sent. A closer inspection of Fig. 6.6 (e)–(h) reveals that as the intensity of the first pulse is increased the optimal timing changes from slightly after (~ 1 ps) [(e),(f)] to approximately at [(g),(h)] the alignment peak due to the first pulse. The strongest two-pulse alignment, $\langle \cos^2 \theta \rangle = 0.84$, is obtained for $I_1 = 2$ TW/cm^2 $= 1/3\, I_2$. We now turn to the degree of alignment obtained at the half revival after the second pulse, shown in Fig. 6.6 (a)–(d). At low intensities of the first pulse [(a),(b)] the best two-pulse alignment is obtained when the second pulse is synchronized to the time where the minimum in the degree alignment from the pre-

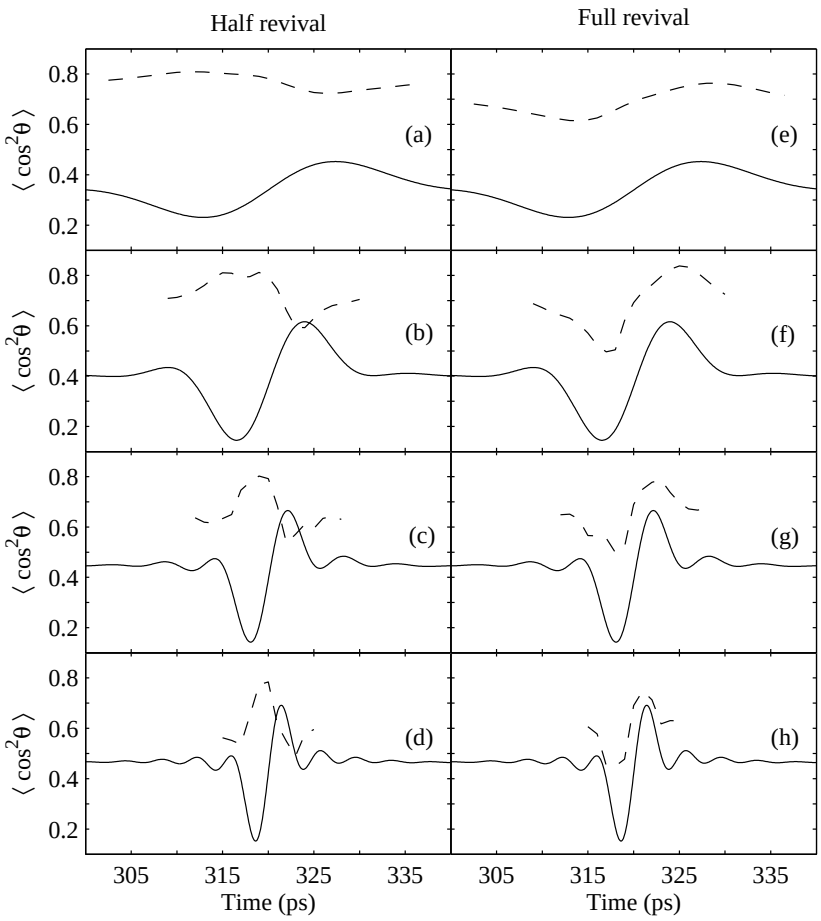

FIGURE 6.6: Theoretically determined dependence on the delay between the two alignment pulses. The full curve is degree of alignment due to first pulse and the dashed curve shows the best degree of alignment obtained with two alignment pulses separated by the given delay. In the left (right) column the dashed curves show the best degree of alignment at the half (full) revival after the second pulse. For all calculations $\tau = 1$ ps, $I_2 = 6$ TW/cm^2 and $T_{rot} = 1$ K. Through each column the intensity of the first pulse is varied: (a),(e) $I_1 = 0.5$ TW/cm^2; (b),(f) $I_1 = 2$ TW/cm^2; (c),(g) $I_1 = 4$ TW/cm^2; (d),(h) $I_1 = 6$ TW/cm^2.

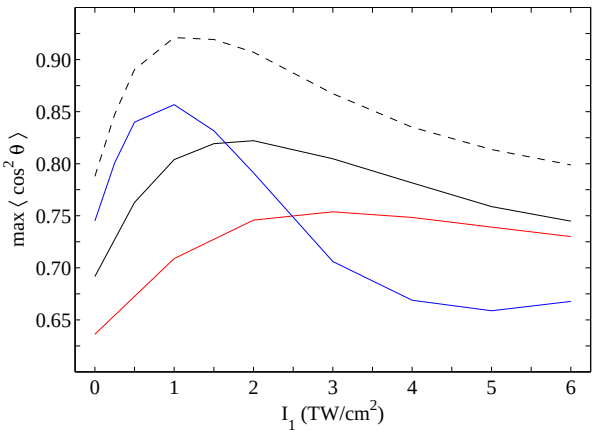

FIGURE 6.7: Calculated intensity dependence of the two-pulse alignment for pulse durations of 0.5 ps (red), 1 ps (black, full) and 2 ps (blue) with focal volume averaging included. The black, dashed curve shows the result for a duration of 1 ps when focal volume averaging is not included.

pulse occurs. At the highest intensity [(d)] the optimal timing occurs when the second pulse is sent slightly after the one-pulse minimum at the point where $\langle \cos^2 \theta \rangle = 0.33$[a]. The strongest two-pulse alignment is $\langle \cos^2 \theta \rangle = 0.81$ and occurs for I_1 in the range 1–2 TW/cm^2. Two important conclusions to be drawn from Fig. 6.6 are: 1) The highest degree of two-pulse alignment is found at the full revival after the second pulse and 2) An optimal intensity exists for the first pulse. The first conclusion re-validates our experimental approach of focusing on the alignment at the full revival. The second conclusion confirms the observations in Fig. 6.5.

Systematically exploring even just the most relevant combinations of pulse intensities, durations and separations for achieving optimal two-pulse alignment is beyond our computational capacity. Instead we use the results from Fig. 6.6 to limit our search. From these results we find that sending the second pulse at the time of maximal alignment due to the first pulse rather than at the optimal delay leads to an error in $\langle \cos^2 \theta \rangle$ of no more the 2% and most often less. The time of maximal alignment at the first full revival after the first pulse is therefore chosen as a (good) approximation for the optimal value of Δt_1.

With the optimal timing in place, we now seek to find the optimal intensity of the first pulse, while keeping the intensity of the second pulse fixed. The procedure is similar to that used in the experiments. First, the optimal value of Δt_1 must be determined. To do this we calculate the degree of alignment due to the first pulse

[a] Although this is also the value for a uniform distribution of molecules this does not mean that the molecules are uniformly distributed [40].

and identify the time at which the maximum (at the first full revival) occurs. Next, the second pulse is included in the calculation. From this calculation we extract the highest degree of alignment at the next full revival. Finally, this peak value is plotted as a function of I_1, just as in Fig. 6.5. Calculations were carried out for pulse durations of 0.5, 1.0 and 2.0 ps, with the peak intensity in the second pulse fixed at 6 TW/cm^2 and a rotational temperature of 1 K. The results, shown in Fig. 6.7, reveal the existence of an optimal I_1 value for each pulse duration. All four curves exhibit a monotonous increase of $\langle\cos^2\theta\rangle$, at low intensities of the prepulse, to the peak value followed by a decrease as I_1 is increased towards the value of I_2. For the 0.5 and 1.0 ps durations the two-pulse alignment is stronger than the alignment obtained with only the second pulse at any value of $I_1 \leq I_2$. For the 2.0 ps duration $\langle\cos^2\theta\rangle$ drops below the one-pulse degree of alignment when I_1 is increased above the optimal value.

Fig. 6.7 shows that the optimal I_1 value is a decreasing function of the pulse duration. In the 0.5, 1.0 and 2.0 ps cases the strongest two-pulse alignment is reached for $I_1 = 3$, 2 and 1 TW/cm^2, respectively. Furthermore, we observe that the maximum $\langle\cos^2\theta\rangle$ value depends critically on the pulse duration. For the 0.5, 1.0 and 2.0 ps durations the maximum value for $\langle\cos^2\theta\rangle$ is 0.75, 0.82 and 0.86 respectively. Calculations were also carried out for a pulse duration of 4 ps (not shown). A maximum degree of alignment of $\langle\cos^2\theta\rangle = 0.82$ was reached at an intensity of 0.3 TW/cm^2. It is therefore concluded that an optimal pulse duration exists for the two-pulse scheme. Based on the four durations studied here, the strongest alignment seems to be obtained for a duration close to 2.0 ps at an intensity of 6 TW/cm^2 for the second pulse.

6.2.3 Discussion

In addition to the parameters discussed in the previous section there is one more important parameter to consider when a high degree of alignment is desired. In an experiment where a large region of the focal volume of the alignment pulse(s) is probed, the measured degree of alignment is severely reduced compared to that obtained just at the peak intensity (see Fig. 2.7). The reason is that the alignment dynamics depends on the intensity of alignment pulse — different regions of the focal volume reach the highest degree of alignment at different delays. The observed maximum is thus only the best compromise. As a consequence, the value of Δt in a two pulse experiment cannot be optimal for all of the focal volume. This leads to a clear reduction in the degree of alignment that can be obtained.

The dashed black curve in Fig. 6.7 shows the intensity dependence of the two-pulse alignment obtained with 1 ps pulses when focal volume averaging is not taken into account. Comparing with the full black curve we immediately see the severe reduction in the degree of alignment caused the focal volume averaging. Starting with the one-pulse results ($I_1 = 0$) it is seen that without focal volume averaging the degree of alignment ($\langle\cos^2\theta\rangle = 0.79$) is significantly higher than with focal volume averaging ($\langle\cos^2\theta\rangle = 0.69$). In fact, the degree of one-pulse alignment without fo-

cal volume averaging is close to the best degree of two-pulse alignment when focal volume averaging is included ($\langle\cos^2\theta\rangle = 0.82$). The I_1-dependence of the non focal averaged results is similar to that for the focal volume averaged results, although the maximum ($\langle\cos^2\theta\rangle = 0.92$) is reached at a lower intensity ($I_1 = 1$ TW/cm^2). All in all, Fig. 6.7 shows that experiments employing nonadiabatic alignment can be significantly improved by minimizing focal volume averaging.

This discussion lead us to consider a comparison with adiabatic alignment. When adiabatic alignment is used the dynamical aspect is absent and for a molecular sample at a given rotational temperature the degree of alignment is solely determined by the intensity. At a low rotational temperature the degree of alignment can be made very high over a large region of the focal volume by saturation of the alignment process (see Fig. 2.2). For instance, at $T_{rot} = 1$ K we find $\langle\cos^2\theta\rangle = 0.87$ and 0.90 for $I = 1.0$ TW/cm^2 and 1.7 TW/cm^2, respectively. The latter is probably the maximum that the molecule can withstand without ionizing. Since the two-pulse calculations were carried out at intensities lower than those employed in the experiment, it seems that two-pulse alignment is superior to adiabatic alignment in the center of the focus. As discussed in the previous Chapter, a potential complication of adiabatic alignment is the presence of the field while the molecules are aligned. This can, however, be avoided by truncating the alignment field rapidly using the switched wave packet approach of Stolow and co-workers [53].

In both experiments and calculations we kept the temperature of our molecules fixed. One interesting, remaining question is how the optimal choice of pulse parameters depends on the temperature. Calculations by Leibscher *et al.* [100] indicate that when the temperature is raised, a higher intensity is needed in the first pulse. This is hardly surprising — at higher temperatures we need higher intensities to induce a significant degree of alignment. Under such conditions one must re-investigate whether the peak of the degree of alignment due to the first pulse is still the optimal time for the second pulse. In the δ-kick model this would not be unexpected — the basic ansatz, that the initial angular velocity is small compared to the angular velocity imparted by the kick from the interaction with the laser pulse, will fail in that case. This leads us to a comparison with work on two-pulse alignment of N_2 by Lee *et al.* [102]. They measured the degree of alignment as function of the delay between the two alignment pulse with the intensity of the alignment pulses fixed, both being close to the onset of multi-photon ionization and the pulse durations were 50 fs (due to the small moment of inertia the rotational dynamics of N_2 is very fast). The temperature in their molecular beam has previously been estimated to be about 100 K [40] and they found that the optimal timing was to send the second alignment pulse between the minimum and maximum in the degree of alignment. By comparing the Boltzmann distribution for N_2 at 100 K with the thermally averaged distribution of J-states for the wave packet induced by a single pulse [40, Fig. 6(a)] it is revealed that the molecules are not truly in the strongly driven regime; although the peak of the population distribution shifts by about 10 J-states the two distributions still have a significant overlap and the thermal

motion cannot be neglected. The conclusion is that both the intensities and the timing need attention when two-pulse alignment is used.

6.3 Other methods for manipulating rotational wave packets

With the advent of nonadiabatic alignment a number of schemes for manipulating rotational wave packets have been presented. Some schemes have been proposed as routes to optimize the degree of alignment, others were meant as general ways of changing the shape of the revivals. Let us start by mentioning another approach for optimizing the degree of alignment, which was recently demonstrated in our group [79]. In that work a combination of a long and a short pulse was used. The idea was to use adiabatic alignment instead of short-pulse alignment pulse to pre-align the molecules before the kick from the second pulse (which was sent at the peak of the long pulse). A wave packet of pendular states was thus created and it was shown that soon after the short pulse the molecules indeed became very strongly aligned. Since adiabatic alignment in our experience is superior to short-pulse alignment (at least for low temperatures), the use of a long pulse to pre-align the molecules is expected to yield a higher degree of alignment. To obtain field-free aligned molecules it would therefore seem ideal to use a long turn on/short turn off pulse [23, 53] to pre-align the molecules. Another approach to optimize the degree of alignment was recently presented by Horn *et al.* [103]. They used a pulse shaper controlled by a genetic algorithm to optimize the degree of alignment and found asymmetric pulse shapes to lead to the highest degree of alignment; the optimal pulses had a slow turn-on and fast turn-off, but were not comparable to the pulses used by Stolow and co-workers [23, 53]; the turn-on time of the pulses were too short to be adiabatic, but maybe this is a matter of the total pulse energy available — as the pulses are chirped the peak intensity drops and the degree of rotational excitation goes down. It would be very interesting to see these experiments repeated at higher pulse energies to see if the adiabatic turn-on/abrupt turn-off pulses turn out to be optimal. One point worth mentioning here is that the combination of a very long and a very short pulse seems unlikely to be found by a genetic algorithm and thus highlight the importance of the physical insight that is often gained by quite simple models such as the δ-kick model.

The studies of two-pulse alignment presented in the previous Section focused on optimizing the degree of alignment, but we observed that in doing so we also changed the shape of the revivals (see Fig. 6.3). Using several short pulses is therefore another way two manipulate the revivals. Renard *et al.* [104] used a pulse shaper to create a pair of equally intense pulses and showed that when the delay between these pulses were exactly $T_{\text{rev}}/2$, no revivals were seen after the second pulse. Lee *et al.* [105] later showed theoretically and experimentally that the pulse pair together form a zero-

effect pulse pair, where the second pulse annihilates the wave packet formed by the first pulse. Even more surprisingly, if a wave packet is excited prior to the zero-effect pulse pair, then the initially excited wave packet survives the two pulses. Another scheme for manipulating revivals was proposed theoretically by Spanner *et al.* [41] and demonstrated experimentally by Lee *et al.* [106]. The scheme relies on adding phase changes to parts of the wave packet at the fractional revivals. It was demonstrated that with the use of relatively weak pulses it was possible to effectively turn revivals off and then on again, or to double the number of revivals observed within a rotational period.

Finally, Spanner *et al.* [41] showed that by using a half-cycle pulse to induce a phase shift at a fractional revival, a high degree of orientation could be induced. The strength of that proposal is that the degree of orientation is solely determined by the degree of alignment in the initial wave packet (but only 50% of the molecules achieve the forward-backward asymmetry). This is in contrast to brute-force orientation, where the degree of orientation is determined by the ratio of the thermal energy kT to the interaction energy μE [3]. The combination of brute force orientation with laser induced alignment has been suggested [107–109], but at least in the parallel field configuration (and $kT/h \gg B$) the laser only confines the angular distribution — it does not change the forward-backward population ratio. The scheme for orientation proposed by Spanner *et al.* also seems superior to schemes relying solely on the use of half-cycle pulses [110] because the angular confinement is induced by the alignment pulse (which can induce a significantly broader wave packet than the half-cycle pulse).

All in all rotational wave packets exhibit very rich dynamics and it will be interesting to see to what extend these control schemes can be transferred to asymmetric tops.

CHAPTER 7

Applications of aligned molecules

Although the study of laser induced alignment and rotational wave packets is interesting on its own, the main motivation for developing these techniques has been to utilize the aligned molecules for other studies. The original inspiration for studying laser induced alignment came from the use of static electric fields in stereochemical studies, with the hope that molecular alignment could be used as a tool in the study of orientational effects in chemical reactions [3, 4]. Over the years many other applications have started to appear. In this Chapter a few of these will be discussed.

Probably the first application of laser-induced alignment of molecules was the demonstration of control over the photodissociation of I_2 and later of iodobenzene [49, 50]. In these experiments the branching ratio between two competing dissociation channels was controlled by utilizing the different orientations of the transition dipoles in the molecular frame. If, for instance, the polarization of the dissociation laser pulse was parallel to that of the alignment laser, then the channel with a parallel (to the internuclear axis) transition dipole was enhanced while the channel with a perpendicular transition dipole was suppressed. These experiments therefore bear strong resemblance to the experiments by Dong and Miller [111] where the direction of vibrational transition dipole moments were measured by orienting bio-molecules

in liquid helium droplets with electrostatic fields. Laser-induced alignment may be a better-suited tool for measuring the orientation of transition dipoles. First of all, the angular confinement obtained with laser induced alignment is much higher than for brute-force orientation due to the much larger electric fields that can be obtained with a pulsed laser. Secondly, the head-versus-tail order given by the orientation is of no use for spectroscopic measurements — since the optical period for visible light is on the order of a femtosecond, the probe (i.e. the laser pulse) has no head-versus-tail preference.

Just as light can be used to change the spatial orientation of molecules, a macroscopic sample of aligned molecules can affect light. For instance, the refractive index for light polarized parallel and perpendicular to the internuclear axis of a linear molecule will in general be different. A gas of aligned molecules is therefore a birefringent medium, in fact such induced birefringence is the cause of the optical Kerr effect [112]. For short-pulse alignment the induced birefringence becomes particularly interesting: since the induced alignment at the revivals changes from planar delocalization to maximum alignment within a few hundred femtoseconds, the medium has an extremely rapidly modulated index of refraction. This rapidly changing index of refraction has been shown theoretically and experimentally to be a valuable and flexible tool for the generation of ultra-short UV pulses [113, 114]. The transient birefringence has also been proposed as a way to obtain very broadband phase-matching for third-harmonic generation in a gas filled hollow-core fiber [115].

Two research fields where the use of aligned molecules have caught special attention are UV photoelectron spectroscopy and strong field physics. These topics will be discussed in the following two Sections.

7.1 Photoelectron spectroscopy

For the study of excited state processes in polyatomic gas-phase molecules, clusters and anions, time-resolved photoelectron spectroscopy (TRPES) has emerged as a valuable tool being sensitive to both electronic and nuclear dynamics [116–119]. In a typical TRPES experiment the molecule is excited by a short visible or UV pulse and then at various delays the photoelectron spectrum resulting from ionization by a UV pulse is measured. Several TRPES experiments have examined the coupling between two electronically excited states. In the most favorable case, the photoelectrons corresponding to ionization of each state have different kinetic energies so the dynamical evolution of the electronic wave packet can be followed by observing the intensity of the corresponding peaks. In this case the accompanying nuclear dynamics, which often promote the coupling between the electronic states via non Born-Oppenheimer couplings, can be seen as changes in the shape of each photoelectron peak due to changes in Franck-Condon overlaps. In less favorable cases the photoelectron peak from different electronic states overlap and the dynamics becomes difficult to observe.

Measuring the angular distribution of the emitted electrons could enhance the amount of information extracted in such experiments [120–122], but it requires some degree of alignment; for a sample of randomly oriented molecules most of the information in the photoelectron angular distribution (PAD) is removed [94, 123–125].

Two approaches can be used to connect the laboratory fixed frame and molecular frame. If the molecule dissociates, coincidence measurements of electron and photofragment recoil velocities allows one to find the electron angular distribution in the recoil frame [126–131]. The other approach is to actively align the sample molecules, for instance by the methods described in the previous Chapters. Several recent calculations indicate that PADs are indeed very sensitive to the alignment that can be induced by a laser pulse [94, 95, 132]. Just as alignment may prove important to measurements of PADs, the PADs may therefore also turn out to be useful probes of alignment. For instance, when moving attention to larger and more complex molecules than previously studied, photofragment imaging may not give an unequivocal measure for the degree of alignment anymore. Suzuki and co-workers have experimentally demonstrated that the PADs resulting from two-photon ionization of the S_1 state in pyrazine were sensitive to the evolution of the rotational wave packet created in the excited state by single photon excitation from the ground state [92, 133]. This experiment is analogous to the rotational coherence spectroscopy experiments mentioned in Sec. 4.2, in particular is the degree of alignment of the excited state not very high. This fact is, however, only encouraging since the anisotropy of the observed PADs may then be expected to become further enhanced if the molecules are strongly aligned.

One concern regarding the use of PADs as a probe was discussed by Reid and co-workers [134, 135]. They found that the PADs from $1 + 1'$ resonance enhanced two-photon ionization of *p*-difluorobenzene via the S_1 state were almost independent of the alignment in the S_1 state. Instead the PADs were primarily determined by the kinetic energy of the electrons. This behavior was ascribed to the presence of a shape resonance (a single-electron excited state at energies above the ionization threshold). In other words, there is a chance that the emitted electron is temporarily trapped in the vicinity of the ion core and this interaction gives rise to large phase shifts for those outgoing partial waves that posses the same symmetry as the resonant state. Bellm *et al.* [135] made a tentative assignment of the shape resonance to a delocalized π^* state on the benzene ring and speculate that such resonances may commonly be found in benzene derivatives. Their work pin-points the importance of taking structures in the continuum into consideration when planning future experiments and calls for input from theory to determine if the presence of a shape resonance, in general, reduces the sensitivity of PADs to alignment prior to ionization.

A part of my work in the laboratory was dedicated to establishing a setup for carrying out time-resolved photoelectron imaging. In the paragraph below it is demonstrated that a working photoelectron imaging spectrometer was indeed build. Unfortunately, there was no time to carry out experiments measuring PADs from aligned molecules. Such experiments are planned for the very near future in the laboratory.

7.1.1 Demonstration of a working spectrometer

To prove that we can detect electrons and to calibrate the spectrometer, a test experiment was carried out on aniline. For this experiment, aniline was ionized with UV pulses created as the frequency-doubled output from the nanosecond dye laser. The low bandwidth of the dye laser (< 1 cm^{-1} or 0.12 meV) combined with the narrow line-width of the vibronic levels (< 2 cm^{-1} or 0.25 meV for the $S_0 \rightarrow S_1\, 0_0^0$ transition) means that electrons are produced with a perfectly well-defined kinetic energy; the measured energy distributions therefore directly reveal the resolution of our detection technique. Aniline was chosen for calibration since its photoelectron spectrum has been measured with high resolution and a full assignment carried out [136, 137]. We chose $1+1$ resonance enhanced two-photon ionization (R2PI) via the $S_0 \rightarrow S_1\, 0_0^0$ transition to ionize the molecule (transition dipole perpendicular to the plane of the molecule). Fig. 7.1(c) shows a schematic energy level diagram for the process. The energy splitting between the ground state and the excited singlet state is larger than half the adiabatic ionization potential I_P. The photon energy needed for the transition between these two states is therefore also high enough to ionize the molecule from the S_1 state. The excess energy from the photon is shared between vibrational motion in the molecular ion and kinetic energy for electrons

$$E_{el} = 2\,h\nu - I_P - E_{vib}, \tag{7.1}$$

where E_{vib} is the vibrational energy (above the zero point energy) in the molecular ion. In the absence of vibronic couplings the relative strength of the photoelectron peaks is given be the Franck-Condon overlap between the S_1 state and the ionic ground state [119]. The reasons for choosing R2PI are that first of all, the required wave length ($\lambda = 293.785$ nm in vacuum) is easily produced with our dye laser. Secondly, we can directly compare our measured electron energies with the results from Meek *et al.* [136].

First, we must produce light at the wavelength for the $S_0 \rightarrow S_1\, 0_0^0$ transition. The dye laser is pumped by the 532 nm output from the nanosecond Nd:YAG laser, so using Rhodamine 610 dissolved in methanol we can produce tunable light in the range ∼570–600 nm with a maximum gain around 580 nm [138]. By doubling the output of the dye laser in a thick KDP-crystal we can then produce tunable UV light at wavelengths around 290 nm. The wavelength (or rather the frequency) of the visible light from the dye laser was calibrated with the Ne lines from a Th/Ne hollow-cathode lamp[a] and checked with the sodium D-lines in another hollow cathode lamb. Care was taken to avoid power broadening during both the calibration and while recording the photoelectron spectra. The next step was to ionize aniline. First, we found the wavelength for the $S_0 \rightarrow S_1\, 0_0^0$ transition by focusing the UV pulses onto our molecular beam and while monitoring the yield of aniline molecular ions in the time-of-flight spectrum we scanned the wavelength of the dye laser (the power of the UV

[a] The lines at 585.249 nm and 588.19 nm were used [75]

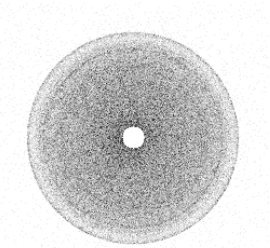

(a) Aniline

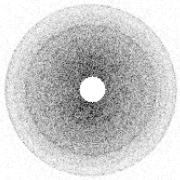

(b) *p*-bromoaniline

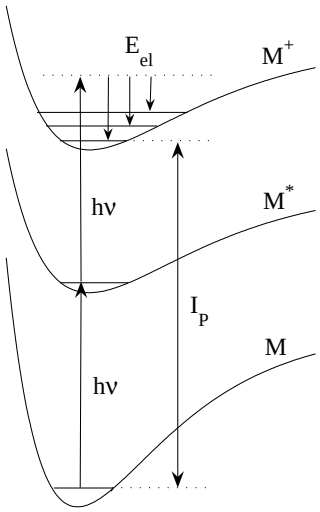

(c) Energy level scheme for R2PI

FIGURE 7.1: Photoelectron images for resonance enhanced two-photon ionization (R2PI) of (a) aniline and (b) *p*-bromoaniline. The relevant energy level scheme is shown in (c).

pulses was constantly monitored with a photodiode). At the intensities used for these experiments we observed no fragmentation of the aniline ions. The observed resonance wavelength $\lambda = 293.785$ nm was 0.09 nm (10 cm^{-1}) lower than the previously reported value [137]. A possible explanation is that these authors may not have corrected for the refractive index for the UV light in air — they calibrated the laser using a grating spectrometer which measures the wavelength rather than the frequency. At slightly larger wavelengths $\lambda = 294.13$ nm we observed a small signal (at high power) from the hot band transition $S_0 \rightarrow S_1\, I_1^0$. This signal was very small compared to the signal at the band origin and only observed at a low backing pressure (10 bar) so the relative population in the vibrationally excited state is very small under the conditions where the experiment was carried out (60 bar helium).

Now that we have identified the resonance frequency for the desired intermediate transition we are ready to look for the electrons produced by the two-photon ionization process. Fig. 7.1(a) shows the raw photoelectron image resulting from R2PI of aniline; the center has been cut out to highlight the features at large radii (high energies). Careful examination of the image reveals several sharp rings, corresponding the cut-off radii for electrons at specific energies. The polarization the UV pulse was parallel to the plane of the detector so the original distribution of electron velocities possessed cylindrical symmetry. From the two-dimensional distribution on the detector we can therefore extract the three-dimensional distribution of electron velocities via the in-

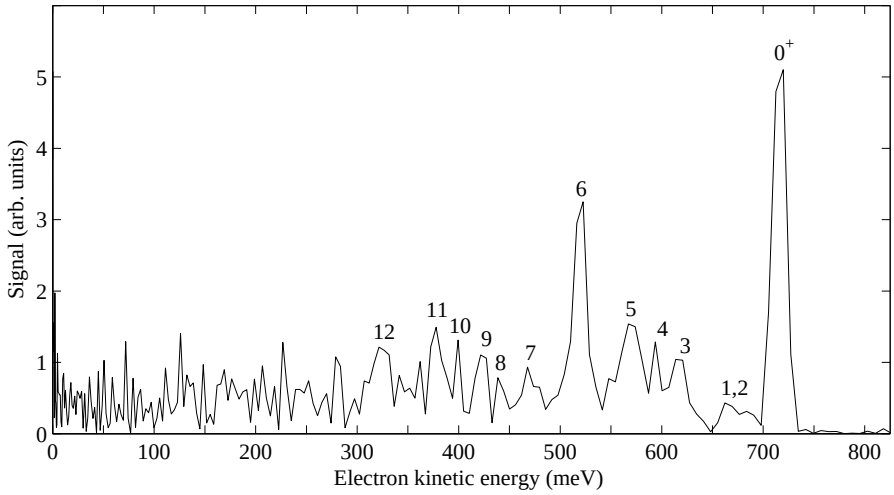

FIGURE 7.2: The photoelectron spectrum for R2PI of aniline via the $S_0 \rightarrow S_1\, 0_0^0$ transition. The dominant peak at 720 meV are electrons coming from ions formed in the vibrational ground state. The assignment of the numbered peaks is given in Table 7.1.

verse Abel transformation (see Sec. 3.2.2), which can then further be converted to a distribution of electron kinetic energies. The obtained photoelectron kinetic energy distribution is shown in Fig. 7.2. The horizontal scale was fixed at one point only: by assigning the dominant, high-energy peak (0^+) to electrons correlated with ions in the vibrational ground state and making use of the well-known photon energy and ionization potential (7.720 eV [139]) we can via Eq. (7.1) find the conversion from radius (in pixels) to electron velocity. The radial distribution from the Abel inversion was then re-scaled according to this conversion factor and thereafter transformed to a kinetic energy distribution (taking into account the Jacobian determinant for the transformation).

The peaks at energies below 720 meV are electrons correlated with ions created in vibrationally excited states. All prominent peaks down to energies of 320 meV have been labelled with numbers on the graph; their assignment is shown in Table 7.1 and the corresponding vibrational energy of the ion is compared with the results reported by Meek *et al.* [136]. Most peaks agree within 10 meV, which at the highest electron energies correspond to a distance of only half a pixel at the camera. It is concluded that the observed energies agree well within the uncertainty in the determination of the position of the electron hit. If needed the resolution could be enhanced by extending the flight distance or reducing the voltage on the extraction plates — the diameter of the outer ring in the image was only about half the size of the detector.

TABLE 7.1: Assignment of peaks in the aniline photoelectron spectrum Fig. 7.2. The reference energies in the last column are from Meek *et al.* [136].

Peak number	E_{kin} (meV)	E_{ion} (meV)	Ion state	E_{ion}^{ref} (meV)
1	684	36	$16a^1$	45
2	664	56	$6a^1$	67
3	617	103	1^1	99
4	594	126	12^1	120
5	570	150	$9a^1$	145
6	520	200	$8a^1$	195
7	468	252	$8a^1 6a^1$ / $9a^1\ 1^1$	— / 246
8	439	281	$9a^1\ 12^1$	263
9	422	298	$8a^1\ 1^1$	297
10	399	321	$8a^1\ 12^1$	313
11	378	342	$8a^1\ 9a^1$	
12	325	395	$8a^2$	

Figure 7.1(b) show a photoelectron image for R2PI of *p*-bromoaniline via the $S_0 \rightarrow S_1\ 1_0^1$ transition. The photoelectron spectrum, shown in Fig. 7.3, is dominated by two peaks, one at 470 meV which is correlated with ions formed in the $9a^1$ vibrational state and one at 275 meV corresponding to the formation of ion the $8a^1 9a^1$ vibrational state [140]. Overall, the spectrum seems more noisy and further assignment of the other peaks has not been attempted.

Apart from the electron energies, the imaging technique also allows us to extract the angular distribution of the photoelectrons. From the images in Fig. 7.1 one may be tempted to conclude that for aniline there is no angular preference, while for *p*-bromoaniline an anisotropy can be observed in the image. To substantiate this we fitted the angular distributions from the Abel inversion to an expansion in Legendre polynomials. For a two-photon transition we must include the two first even-order polynomials [124], that is

$$I(\theta) = I_0[1 + \beta_2 P_2(\cos\theta) + \beta_4 P_4(\cos\theta)]. \tag{7.2}$$

For aniline we indeed find that the asymmetry parameters β_i are very small ($-0.01 < \beta_2 < 0.06(\pm 0.02)$, depending on the electron energy). The angular distributions for *p*-bromoaniline on the contrary are asymmetric at most energies and β_2 changes sign, that is the preferred direction for the electrons changes from parallel to perpendicular to the laser polarization. For the three kinetic energy ranges marked with the shaded area in Fig. 7.3 we found $\beta_2^{(1)} = 0.15 \pm 0.01$, $\beta_2^{(2)} = 0.03 \pm 0.02$ and $\beta_2^{(3)} = -0.16 \pm 0.02$. The β_4-parameters were found to be negligible in all three cases. This is exactly the same behavior as that observed for *p*-difluorobenzene by Bellm *et al.* [135].

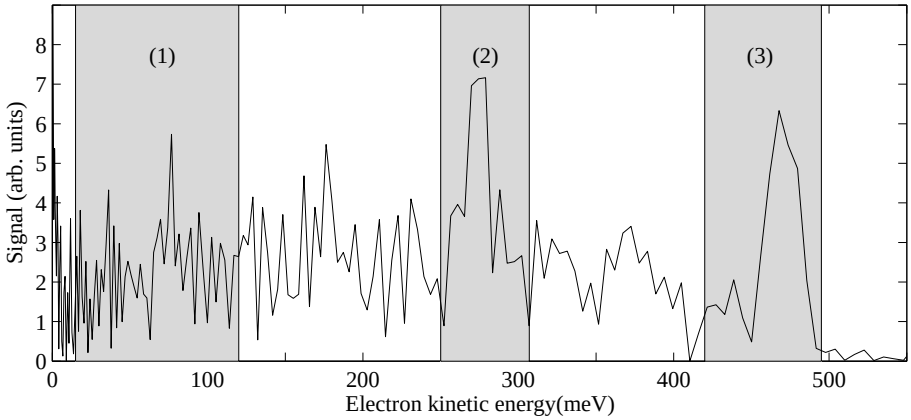

FIGURE 7.3: Photoelectron spectrum for *p*-bromoaniline resulting from R2PI via the $S_0 \rightarrow S_1\, 1_0^1$ transition. The dominant peaks at 470 meV and 275 meV correspond to ions in the $9a^1$ and $8a^1 9a^1$ vibrational states respectively.

It is therefore tempting to ascribe it to the presence of a shape resonance, but such assignment would require a detailed study like that of Bellm *et al.* [135]. It would be interesting to align the molecules adiabatically and measure the photoelectron angular distributions for the aligned molecules to test if the PADs are insensitive to alignment. In that case one must be careful about the intensity for the alignment laser. First of all, the Stark shift induced by the infrared laser will shift the resonance. Secondly, one must be careful to avoid ponderomotive acceleration of the electrons by the intensity gradient of the focused nanosecond laser [96].

In conclusion, a working photoelectron imaging spectrometer has been demonstrated with a resolution of ∼20 meV at 700 meV kinetic energy. This resolution can probably be nearly doubled.

7.2 Strong field physics

Stable, table-top femtosecond lasers delivering milli-Joule pulses with durations below 50 fs have almost become standard in laboratories seeking to study high intensity effects. Modest focusing of such pulses easily produces intensities above 10^{15} W/cm^2. At these intensities most atoms and molecules will become at least singly ionized, but the emitted electron is born in the presence of a strong, oscillating electric field so in the case of linear polarization the electron is steered back and may re-scatter with its parent ion within one or two half-cycles for the optical field. This scattering event can occur in three ways: 1) elastically, 2) inelastically or 3) as a recombination

between the electron and the ion [141]. If the electron scatters elastically, the outcome is an unusually high electron kinetic energy; this process is known as above threshold ionization (ATI) since it corresponds to the absorbtion of a higher number of photons than needed to reach the ionization threshold. In the case that the electron scatters inelastically, it will cause either direct double ionization or excitation in the residual ion which will then subsequently be further ionized by the laser field [142, 143]. This process leads to unusually high double ionization rates at intensities below saturation of single ionization and is known as non-sequential double ionization. For molecules the process can also lead to fragmentation if the doubly-charged molecular ion is not stable. Finally, the electron can recombine with the parent ion with the emission of a singly VUV/XUV photon, a process known as high-order harmonic generation (HHG) [144]. This process is particularly interesting for a number of reasons. First of all, it allows generation of high intensity laser pulses in the VUV/XUV spectral regions by table-top systems [145] and progress has been made towards the generation of X-ray laser pulses. Secondly, the generated XUV pulses are actually trains of attosecond pulses and when special care is taken, single attosecond pulses can be generated [146]. Such pulses are the shortest pulses created to date and open the possibility for direct temporal studies of correlated electron dynamics [147]. Finally, the harmonics emitted from a molecule are sensitive to the structure of the molecule and may therefore be used as probes for molecular dynamics with sub-femtosecond time-resolution [148].

7.2.1 Single ionization

Single ionization is the event that triggers all of these scattering events, so it is of course crucial to understand this step in detail. *Ab inito* models are numerically too demanding for anything more complex than the hydrogen molecule, so approximate single-active electron models must be used. For atoms the models by Kelysh and Reiss can be used to calculate multi-photon ionization rates [149, 150]. The common foundation for these models is the strong field approximation: the assumption that in the final state the interaction of the electron with the laser field dominates over its Coulomb interaction with the residual ion. The final state used in these models is therefore a Volkov state. This assumption leads to ionization rates that are about two orders of magnitude too low. The discrepancy is often resolved by introducing a WKB correction [151, 152]. Keldysh introduced an adiabaticity parameter $\gamma = \sqrt{I_\mathrm{p}/2U_\mathrm{p}}$, where I_p is the ionization potential and $U_\mathrm{p} = E_0^2/4\omega^2$ (in atomic units) is the ponderomotive potential for the quiver motion of the electron in the oscillating electric field $E(t) = E_0 \cos(\omega t)$. In the limit of a large Keldysh parameter the ionization dynamics becomes quasistatic and the ionization rate is determined by the instantaneous amplitude of the electric field. In this limit the ionization event can be described by as tunnelling of an electron through the barrier created by the external field and the field from the ion. The tunnelling model derived by Keldysh underestimates the ionization rate by one or two orders of magnitude, but an improved model by Ammosov, Delone

and Krainov (the ADK-model) [153] that takes into account the Coulomb interaction in the final state describes the ionization rate of atoms well in the quasistatic limit for intensities below barrier suppression [154].

For molecules the situation is more complicated. Measurements of the ionization rates of small molecules compared to atoms of nearly the same ionization potential revealed that ADK theory was insufficient to describe tunnelling ionization of molecules [155–161]. It was realized that the theoretical models had to take into account the structure of the molecular orbitals, in particular, the occurrence of nodal planes is important [159, 162–164]. A simple argument can be made to illustrate why this is the case. During strong field ionization by a linearly polarized laser the electrons are usually emitted close to polarization vector since this is the direction of the external force; in the tunnelling picture this is the direction where the barrier is most narrow. If we now consider ionization of a molecule with a nodal plane in the highest occupied molecular orbital and oriented such that the polarization of the laser field is in the nodal plane, then the electron density is zero in the direction of the laser field. For such orientations the ionization rate is therefore strongly suppressed compared to that of an atom.

These considerations have inspired several theoretical studies of ionization of aligned molecules [165–171]. As the simple argument from above suggests, the calculations show that both the total ionization rate and the angular distribution of the emitted electrons depend on the relative orientation of the molecule and the laser field. Significant discrepancies still persist between measured and calculated (orientation averaged) ionization rates [172], but the recent measurements of strong field ionization of aligned molecules [173, 174] may provide important clues to the discrepancies. For instance, based on the measurement of the ionization rate for aligned N_2 molecules [173], Kjeldsen and Madsen [168] showed that the choice of gauge the strong field approximation plays an important role; while the velocity gauge formulation of the strong field approximation gave the wrong qualitative behavior for the angular dependence of the ionization rate, the length gauge SFA agreed with the experiments.

As an example, lets us consider ionization of the ethylene molecule (Fig. 7.4(a)) by an 800 nm laser pulse. To calculate the ionization rate we use the length gauge SFA. Consistent with the neglect of electron correlations implied by the single-active electron approximation, we use the Hartree-Fock wave function for the initial state. Assuming a Slater determinant with the highest occupied orbital (HOMO) replaced by a Volkov state for the final state(i.e. an un-relaxed ion core), the N-electron problem reduces to a one-electron problem involving only the transition from the HOMO $\psi(\boldsymbol{r})$ to the laser-dressed continuum. The angular differential ionization rate can then be expressed as [171, 175]

$$\frac{\mathrm{d}W}{\mathrm{d}\hat{\boldsymbol{q}}} = \sum_{n=n_0}^{\infty} \left|A_{\boldsymbol{q}n}\right|^2 q_n, \tag{7.3}$$

where $\hat{\boldsymbol{q}}$ is the direction of the outgoing electron and n_0 is smallest number fulfilling

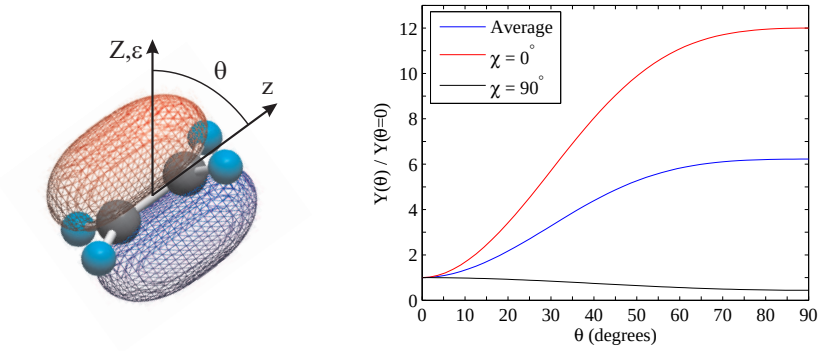

(a) HOMO of ethylene

(b) Ionization rate $W(\theta)$ for ethylene

FIGURE 7.4: Angular dependence for the ionization yield of ethylene exposed to a 20 fs, 800 nm pulse with a peak intensity of $5 \cdot 10^{13}$ W/cm^2. (a) HOMO of ethylene and the definition of the molecule- and space-fixed z (Z) axes. χ is zero for the shown orientation (the body fixed (x, y) component of the polarization is perpendicular to the plane of the molecule). (b) Angular dependence of the ionization rate calculated in the strong-field approximation (length gauge) for three situations: $\chi = 0^\circ, 90^\circ$ and averaged over all values of χ.

energy conservation $n\hbar\omega \geq I_p + U_p$. The transition amplitudes

$$A_{\boldsymbol{q}n} = \frac{1}{T}\int_0^T \mathrm{d}t\, \left(-I_p - \tfrac{1}{2}Q_n^2(t)\right) \tilde{\psi}\left(\boldsymbol{Q}_n(t)\right) \times \exp i\left(n\omega t + \boldsymbol{q}_n \cdot \boldsymbol{\alpha}_0 \sin(\omega t) + \frac{U_p}{2\omega}\sin(2\omega t)\right), \quad (7.4)$$

are evaluated at the average momentum for the electron in the oscillating electric field $q_n = \sqrt{2(n\omega - I_p - U_p)}$. $\boldsymbol{Q}_n(t) = \boldsymbol{q}_n + \boldsymbol{A}(t)$ is the time-dependent momentum for the electron is the laser field with vector potential $\boldsymbol{A}(t) = \boldsymbol{A_0}\cos(\omega t)$, and $\boldsymbol{\alpha}_0 = \boldsymbol{A}_0/\omega$ is the quiver radius for the electron. We see that the initially bound state enters the expression via its momentum space representation $\tilde{\psi}(\boldsymbol{q})$. For the length gauge version of the strong-field approximation, the Coulomb correction factor is not needed [168, 172].

Figure 7.4(b) shows the result of calculations of the total ionization rate

$$W = 2\pi \sum_{n=n_0}^{\infty} \int \left|A_{\boldsymbol{q}n}\right|^2 q_n \mathrm{d}\hat{\boldsymbol{q}}, \quad (7.5)$$

as a function of the relative orientation between the C−C axis and the polarization of the laser field. Three curves are shown, one for $\chi = 0\circ$ where the polarization of

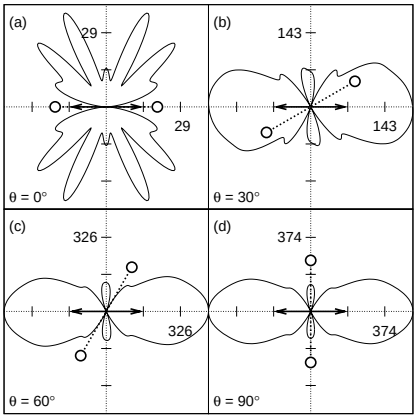

FIGURE 7.5: Angular distribution of the photoelectrons from ethylene for different orientations between the molecule and the polarization axis (shown by the double headed arrow). The orientation of the C−C axis is shown by the circles, the plane of the molecule is fixed perpendicular to the plane of the paper. Laser parameters are as in Fig. 7.4.

the laser is perpendicular to the plane of the molecule, one for $\chi = 90^\circ$ where the polarization is in the plane of the molecule and one where the results are averaged over all values of χ. For the $\chi = 0\circ$ and the χ-averaged curves a pronounced angular dependence of the ionization rate is observed, while the $\chi = 90\circ$ orientation in general leads to a strong reduction of the ionization rate. To explain this behavior we turn to a detailed examination of the angular differential ionization rate. Fig. 7.5 shows polar plots of the angular distribution for the emitted electrons for different orientations between the molecule and the strong laser field. The polarization of the laser is fixed in the horizontal direction while the C−C axis (shown by the circles) is rotated from parallel to perpendicular to the polarization direction. In all four figures the plane of the molecule is perpendicular to the plane of the paper ($\chi = 0\circ$). Qualitatively the distributions in (b)–(d) are very similar — most of the electrons are emitted close to the polarization of laser field as expected. This is not the case when the C−C axis is parallel to the polarization vector (a). For this orientation we observe a dramatic, qualitative change in the angular distribution. Most notably, no electrons are emitted in the direction of the laser field. Simultaneously, we observe that the magnitude of the ionization rate changes dramatically: from (d) to (a) the scale on the axes goes down by more than an order of magnitude.

The reason for these changes must be found in the transition amplitude in Eq. (7.4). As noted above, the structure of the molecule enters this equation via the momentum space representation of the HOMO. The key to understanding the qualitative changes is the fact that there is a one-to-one correspondence between nodal planes in coordinate

space and in momentum space. As seen from Fig. 7.4(a) the plane of the molecule is a nodal plane for the coordinate space representation of the wave function. The molecular plane is therefore also a nodal plane for the momentum space representation of the HOMO. When the polarization vector coincides with the molecular plane the term $\tilde{\psi}\left(\boldsymbol{Q}_n(t)\right)$ (where $\boldsymbol{Q}_n(t) = \boldsymbol{q}_n + \boldsymbol{A}(t)$) in Eq. (7.4) is therefore zero for $\boldsymbol{q}_n$ parallel to $\boldsymbol{A}(t)$. Not only does this explain the angular dependence for the $\chi = 0$ orientation, it also explains why the ionization rate is so much lower for the $\chi = 90\circ$ orientation: for $\chi = 90\circ$ the laser polarization always coincides with the molecular plane independent of θ. We are hereby lead to a general statement: for molecules of symmetry species C_s or higher (containing a plane of reflection) and containing a nodal plane the ionization rate is expected to be reduced for orientation where the laser polarization coincides with the nodal plane.

The dramatic changes in the photoelectron angular distributions imposed by the presence of a nodal plane in the HOMO may be important to take into account when interpreting re-scattering experiments on molecules. Bhardwaj *et al.* [176] were the first to consider this point. They measured the ellipticity dependence of the yield of doubly charged benzene ions and of some fragments ions. From the measurements they concluded that re-scattering the was the dominant mechanism behind the production of these ions, but observed an anomalous behavior at small ellipticities. The effect was ascribed to the presence of nodal planes in the HOMO of benzene; as demonstrated by the calculations above, nodal planes in the HOMO are, for some orientations, transferred to the wave packet in the continuum. For these orientations we may, therefore, expect a a lower re-scattering cross section for linear polarization than for a slightly elliptical polarization. The experiments were carried out on randomly oriented molecules so the observed effect was very small. Repeating the experiment with aligned molecules may help to confirm the interpretation. Alnaser *et al.* [177, 178] carried out experiments where they measured the angular dependence of dissociative ionization induced by re-scattering for a range of small molecules. The observed dependence was ascribed to the angular dependence of the first ionization step by a qualitative comparison with molecular ADK calculations. One may, however, speculate on the importance of a plausible angular dependence of the re-scattering step as just described. The experiments by Alnaser *et al.* cannot disentangle the angular selectivity of the ionization step and of the re-scattering step. Further measurement of the angular dependence of the single ionization rate and of the photoelectron angular distribution may help to elucidate the details of the mechanism.

In ending the discussion of single ionization of molecules we note that the theory discussed above is only valid in the limit where multi-photon excitation to excited states can be neglected. For larger molecules nonadiabatic multi-electron effects become important due to the larger delocalization of the valence electrons and the presence of low lying excited states [179–182]. There is a lack of both theory and experiment on the orientational dependence of these effects, but based on the qualitative arguments behind these models it might be expected that these phenomena are

strongly alignment dependent.

7.2.2 High-order harmonic generation

Due to its many future applications, high-order harmonic generation has attracted a vast amount of attention over the years. Most recently, there has been a rapidly growing interest in HHG from aligned molecules [55–59, 183–186]. In particular experiments on aligned molecules have shown that the intensity of the emitted harmonics are sensitive to the relative orientation between the molecule and the polarization of the driving laser. Lein *et al.* [187] showed that this angular dependence can qualitatively be explained by considering the atoms in the molecule as point emitters whose phase is determined by the phase of the re-colliding wave packet as it returns to each of these sites. Since there is perfect temporal coherence between these point emitters the harmonics emitted from the atomic sites in the molecule will interfere in the far field. For a diatomic molecule with the vector $\mathbf{R}$ pointing from one atom to the other, the phase difference between the harmonics emitted from the two atoms is $\mathbf{k}_{\text{el}} \cdot \mathbf{R} = 2\pi R/\lambda_{\text{el}} \cos(\theta)$ with $\mathbf{k}_{\text{el}}$ being the wave vector for the returning electron and θ the angle between the electric field and the internuclear axis. Harmonics of a given order correspond to electrons returning with a given kinetic energy and thus a given de Broglie wavelength, so the fixed magnitude of R/λ_{el} thereby determines the alignment angle for which there is positive interference (maximum yield) and the modulation depth is largest when the de Broglie wavelength is similar to the internuclear distance. Since λ_{el} is determined by the energy of the emitted harmonics, the interference is directly related to the structure of the molecule [57, 59], and structural changes should be observable as changes in the harmonic spectrum for aligned molecules. Perhaps even more spectacularly Itatani *et al.* [185] showed that by measuring the harmonic spectrum (including all the relative phases) as a function of the alignment angle it was possible to carry out a tomographic reconstruction of the highest occupied orbital of N_2. All in all these findings pave the way for a completely new type of measurements of ultra-fast dynamics [148].

CHAPTER 8

What's next?

The previous chapter dealt with some of the applications of aligned molecules that should emerge in the following years. Before ending this Dissertation it is appropriate to discus some ideas for future directions of laser induced alignment as well — what developments are needed to take laser induced alignment one step further in terms of its usefulness as a tool? This Chapter starts with a discussion of the very important problem of three dimensional alignment where progress is currently made at a high speed. The discussion involves a scheme that has recently been demonstrated in our group. As previously mentioned three-dimensional alignment is important because most molecules are asymmetric tops. Studies of orientational effects in such molecules naturally involves confinement of all three Euler angles — free rotation of the ϕ-angle obscures the observation of anisotropies perpendicular to the axis of highest polarizability. The second section contains a more speculative discussion about alignment of flexible molecules. This necessarily includes considerations of how one can actually probe alignment of such molecules.

8.1 Three-dimensional alignment

The idea of obtaining three-dimensional (3D) alignment was introduced in Section 2.4 and two schemes based on the use of elliptically polarized pulses were discussed. The

use of a long pulse with elliptical polarization is conceptually clear: the molecules will slowly be guided into the orientations of minimum energy, that is with the axis of highest polarizability along the major axis of the field and the axis of second highest polarizability along the minor axis of the field. The scheme inherently involves a trade-off between how well the axis of highest polarizability is aligned and the confinement in the ϕ-angle. With a short pulse the dynamical aspect complicates matters; the molecules get an asymmetric rotational kick which involves motion in all three Euler angles, but the speed of rotation depends on the moments of inertia, the polarizability tensor and on the initial orientation of the molecule. In this scheme the ellipticity of the alignment pulse seems to be fixed by this delicate balance.

To circumvent or at least minimize the trade-off in the choice of ellipticity, Underwood *et al.* [48] suggested the use of two temporally separated pulses with orthogonal polarizations; the idea was to use the first pulse (defining the lab-fixed Z axis) to align the axis of highest polarizability and then, close to the time of best alignment, send the second pulse (defining the lab-fixed X axis) to kick the axis of second highest polarizability into alignment in the plane perpendicular to the Z axis. In a numerical study the authors compared this scheme to the two schemes proposed above (although the long pulse was rapidly truncated to produce field-free alignment) and concluded that the use use of two separate pulses is superior. By sending an orthogonally polarized pulse at the time where the molecules are best aligned, the deteriorating effect of the X-component of the electric field on the alignment of the axis of highest polarizability is minimized and a high degree of three dimensional alignment is obtained.

As a variant of this scheme we have studied 3D-alignment using a combination of a long and a short pulse. The long (adiabatic) pulse is used to align the axis of highest polarizability and the short pulse, synchronized to the peak of the long pulse, makes the molecules spin around this axis. The advantage of using adiabatic alignment to linearly align the axis of highest polarizability is that, as previously discussed, we generally find adiabatic alignment to be superior to one pulse nonadiabatic alignment. The scheme has been tested experimentally on 3,4-dibromothiophene (see Fig. 5.2). The components of the polarizability tensor for this molecule were given in Sec. 5.2; the axis of highest polarizability is along the C_2 symmetry axis (the b axis), while the axis of second highest polarizability is in the plane of the molecule and orthogonal to b axis (the a axis). The long pulse will therefore align the symmetry axis and short pulse will, if the molecules are well aligned, enforce rotation around the b axis.

One remaining concern is if we are able to faithfully probe the degree of alignment of both the symmetry axis and of the plane of the molecule. We chose to use laser-triggered Coulomb explosion, but as discussed in Sec. 5.1, the use of this technique for probing alignment requires special attention to the artifacts that geometrical alignment may induce. To avoid enhanced ionization, which has strong angular selectivity and can lead to depletion of subsets of molecules, we use very short (25 fs) and intense ($2 \cdot 10^{14}$ W/cm^2) pulses to multiply ionize the molecules. By observing the recoil direction of S^+ ions we obtain information about the linear alignment of the symmetry

axis, whereas Br^+ ions are used to reveal alignment of the molecular plane. Since our method of detection can only measure the two-dimensional projection of the ion distribution in a direction perpendicular to the propagation direction of the lasers, we must align the molecules in two different directions compared to the time-of-flight axis to obtain information about the alignment of both the symmetry axis and the molecular plane. To (partially) measure alignment of the symmetry axis the molecules must be aligned with this axis parallel to the plane of the detector, while a measurement of the alignment of the molecular plane is best obtained when the symmetry axis is aligned perpendicular to plane of the detector. In both cases the polarization of the probe laser is linear and parallel to the polarization of the long pulse. On the one hand, this means that the detection of the sulphur ions is directionally biased, but we can still obtain a relative (qualitative) measure for the degree of linear alignment. On the other hand, the detection of Br^+ ions has no angular bias in the plane of the detector. One of the most serious concerns regarding the use of Coulomb explosion to probe alignment is that the sometimes strong directional selectivity may result in only a subset of molecules being probed. Here, strong alignment of the symmetry axis minimizes this effect and we have good reason to believe that the S^+ and Br^+ ions do not stem from different subsets of the ensemble.

We now turn to the experimental results. Figure 8.1 shows a series of false color ion images which directly reveals 3D-alignment. In the lower left corner the polarizations of the three laser pulses relative to the plane of the detector are shown. When S^+ is detected (rows A, C) the long alignment pulse and the probe pulse are vertically polarized, whereas the short alignment pulse is polarized perpendicular to the plane of the detector. The centers of these images have been cut out to remove a large signal from O_2^+ (the experiment was carried out on the old system; oxygen stems from residual gas in the chamber and from the molecular beam). When Br^+ is detected (rows B, D) all polarizations are rotated by $90°$. Column 1 shows images obtained with only the probe pulse present; as expected the Br^+ distribution is circularly symmetric (B1), while the S^+ image (A1) reveals the angular selectivity imposed by the probe. When the long pulse (1064 nm, 9 ns, $1.4 \cdot 10^{12}$ W/cm^2) is included, the symmetry axis is well aligned along the polarization of this pulse as revealed by image A2 but the ϕ-angle remains unrestricted, resulting in a still circularly symmetric Br^+ image in B2. To induce 3D-alignment we now include the short alignment pulse (800 nm, 0.7 ps, $10 \cdot 10^{12}$ W/cm^2 in rows A, B and $2.5 \cdot 10^{12}$ W/cm^2 in rows C,D). Columns 3–6 show ion images obtained for different delays of the probe pulse with respect to the short alignment pulse (time is shown under each pair of images). If we start with the results for the strong kick (rows A and B), we see that immediately after the short alignment pulse the Br^+ distribution has been dramatically changed (B3) — rather than being circularly symmetric it now has an elongated, cigar shape. This image provides compelling evidence for alignment of the molecular plane. Referring to the corresponding S^+ distribution (A3), we see that the symmetry axis is still strongly confined; in fact, the vertical strip is even narrower than in A2. This added confinement is a conse-

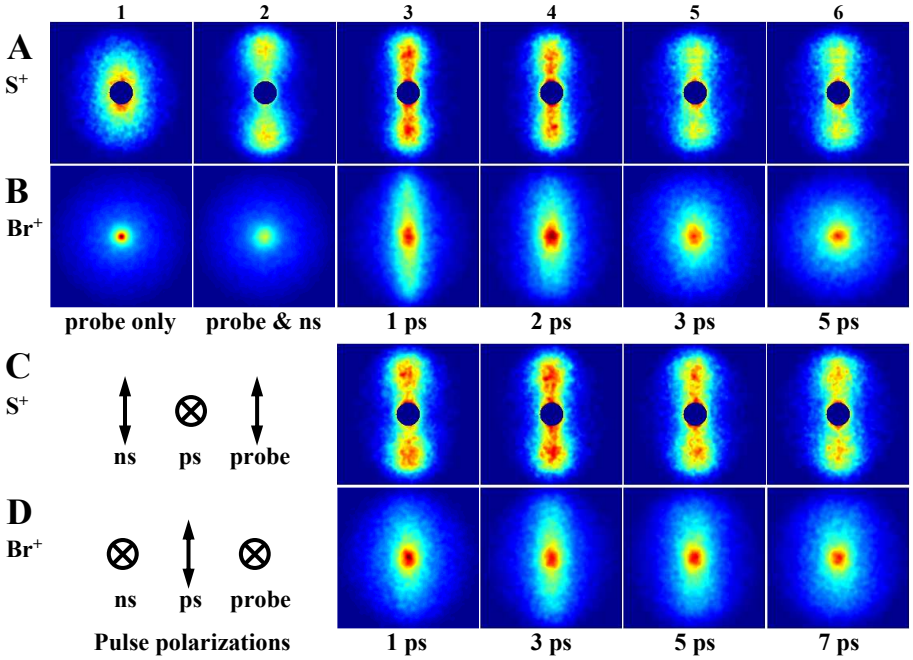

FIGURE 8.1: Ion images showing three-dimensional alignment of 3,4-dibromothiophene by the combination of a short and a long pulse. See text for details.

quence of the confinement of the ϕ-angle to the plane perpendicular to the detector. More worrying is the fact that the radial distributions have also changed. This could indicate that the molecules are aligned to the plane spanned by the polarization of the two alignment lasers, but that the symmetry axis is not aligned along the polarization of the long pulse. A comparison with images taken with circular polarization for the long pulse and no short pulse present reveals that linear alignment is to a large extend preserved (the distribution in A3 still looks like a figure eight, not a pancake). Measurements of the full velocity distribution, for instance using slice imaging techniques [188, 189], are needed to provide more details on this point. The rows C and D show images recorded with the intensity of the short alignment pulse reduced by a factor of four, all other parameters are fixed. The images show that the alignment of the molecular plane, as revealed by the Br^+ images in D3–D6, evolves more slowly and that the maximum degree of alignment is slightly lower. Further, the S^+ distribution is less affected by the weaker pulse. This is exactly the behavior that is expected from the lower kick strength.

Preliminary measurements indicate that this technique is superior to the use of adiabatic alignment alone with an elliptically polarized pulse. A next generation of

experiments, which will benefit from the lower temperatures and thus higher degrees of alignment in the new setup, are planned for the very near future. The question of which method to use for obtaining the optimal 3-D alignment is still not fully settled and will require further contributions from both theory and experiments to be answered. It is, however, clear that the answer will depend on the type of application. Reactive scattering experiments on aligned molecules (or oriented by combining laser induced alignment and electrostatic orientation [107, 108]) will require the molecules to be aligned for long periods of time since typical supersonic valves produce gas-pulses with μs durations and the single-molecule diffraction scheme proposed by Spence and Doak [90] uses cw-sources. Contrarily, for studies of strong-field physics (Sec. 7.2) the molecules will only need to be transiently aligned.

A true challenge, not only for 3D-alignment but also for linear alignment, is to address the possible use of alignment in femtosecond pump-probe spectroscopy. This point is far from trivial. Obviously, if adiabatic alignment is used, one runs the risk of strongly perturbing the process under study. Pump-probe experiments are particularly sensitive since they usually involve dynamics in electronically excited state. First of all, excited states are much more easily ionized than the ground state and secondly, polyatomic molecules often contain a plethora of excited states so accidental resonances with higher lying states may be hard to avoid. If adiabatic alignment cannot be used we must turn to nonadiabatic alignment, but then the molecules only stay aligned for a short time so, unless the process under study is ultra-fast, the degree of alignment will change between the early and late probe stages. One could envision that, rather than aligning the molecules prior to the pump, the alignment pulse could be send briefly before the probe pulse. This approach must also be taken with caution. First of all, the alignment pulse may perturb the system in an unwanted way for the same reason that adiabatic was found to be troublesome. Secondly, the response of the different electronically excited states to the external electric field (the polarizability), and thereby the degree of alignment, may be very different.

8.2 Flexible molecules

Does an intense, non-resonant laser pulse affect the conformation of flexible molecules? This question will be important to answer before laser induced alignment can fully mature to become a reliable tool in the study of large molecules.

Molecules often exist in many different conformations. Some of these conformations are trapped in potential wells that are deep compared to thermal energies at room temperature and therefore exist as distinct chemical species — they are known as isomers of the molecule. Z/E (or cis/trans) configurations of a C=C double bond is a prominent example of this case. Other conformations exist as energy minima in a shallow potential, whose barriers may be crossed at thermal energies. The three staggered conformations that may be formed by rotations around a C−C single bond are

typically separated by barriers of about 130 meV, so at room temperature and on the time-scale of minutes there is essentially free rotation around this bond. This changes under the very cold, collision-free conditions in a supersonic jet: the three conformers then exist as distinct, stable geometries. Since a barrier of 130 meV between them is still larger than the typical interaction energies for the molecules presented in this Dissertation, we do not expect that the presence of a non-resonant laser will change the conformation of small molecules. As one goes to larger molecules the number of local minima increase correspondingly. The energy difference between these minima can be very small, but the barriers are often still on the order of 50–100 meV and the conformers that are found a room temperature can again be identified as isolated species in supersonic expansions [190]. For moderately large molecules one should thus not expect the interaction with the laser to suppress the barrier between the different conformers, but it may provide a coupling between the isolated wells and thus induce conformational changes. A short pulse might, for instance, induce stimulated Raman transitions to other conformations.

Even if the laser cannot change the conformation of a molecule, the different conformers might still have different polarizabilities and moments of inertia and thus align differently. Previous experiments in our lab were aimed at exploring nonadiabatic alignment of a molecule with different conformers [91]. The molecule used in those experiments, 1-iodopropane, comes in one anti and two gauche conformers. The anti and gauche conformers have different moments of inertia and may thus be expected to have different revivals times. The experiments were complicated by the fact that the principal axes of the inertia and the polarizability tensors are not coincident either with each other or with the direction of the C−I bond (which is the recoil direction for the iodine atom upon UV dissociation). The observed distribution of recoil directions for the iodine atoms is therefore a convolution of the probability of dissociating a C−I bond with the lab-frame distribution of these bond directions. This distribution is itself a convolution of the lab-frame distribution of the principal axes (for either the polarizability or inertia tensor) with the distribution of C−I bond directions in the molecular frame. All in all, the observed revival transients were very weak and hard to interpret, but did show small changes in the degree of alignment at times corresponding to the revival time for the two conformers.

Those experiments expose the difficulties in using resonant dissociation as a probe of alignment for molecules where the recoil frame does not coincide with the principal axes frame. Obviously, Coulomb explosion will, to some extent, suffer from the same difficulties and has its own issues regarding geometrical alignment and the accompanying depletion effects. Further, the breakup of larger molecules may be complicated by charge-asymmetric states and fragments carrying away energy in rotational and vibrational modes. As focus is moved to larger molecules new probe techniques are therefore needed. One such probe might be photoelectron angular distributions, but it is difficult to extract quantitative information about the degree of alignment from the PADs. Further theoretical work is needed to provide more insight to the amount

of information that can be extracted from such measurements. The most promising route may be to carry out linear dichroism measurements on electronic and vibrational transitions — this has as a very important application the possibility of assisting the assignment of spectroscopic transitions in samples containing molecules with different conformers [111, 190].

CHAPTER 9

Summary

Molecules in general have asymmetric shapes and many of their properties, for instance bi-molecular reaction rates or their interaction with polarized light, depend on their orientation in space. In a normal gas-phase experiment the sample of molecules will be randomly oriented, so any measured observable will be orientationally averaged and details of the underlying physics may be obscured. In this Dissertation several methods of using intense non-resonant lasers to obtain control over the spatial orientation of molecules have been demonstrated. Laser-induced alignment is a versatile tool since the only requirement for the molecule is that the polarizability is anisotropic, that is have different values along different directions in the molecule, and that the molecule is able to survive the applied field; the interaction with the electric field of the laser will then lead to a torque on the molecule, forcing the most polarizable axis in the molecules towards the polarization of the laser.

The experiments are carried out on a cold molecular beam and we use charged photo-fragment imaging to measure the degree of alignment. Either resonant dissociation induced by an ultraviolet femtosecond pulse followed by resonant multi-photon ionization by a nanosecond pulse or Coulomb explosion induced by a very short and intense femtosecond pulse is used to probe the degree of alignment. When the molecule starts to dissociate (or explode due to the Coulomb repulsion) the moment of inertia increases rapidly, thus freezing out any rotational motion. If the fragments

recoil along a well-defined direction in a coordinate system fixed to the molecule, a measurement of the recoil velocity of such fragments will reveal the orientation of the molecule in a laboratory-fixed coordinate system. We use electrostatic lenses to image the recoil velocity onto a position-sensitive detector and use the distribution of ion hits on the detector to extract information about the average spatial orientation for our sample of molecules.

When the duration of the laser pulse is sufficiently short compared to the rotational timescale for the molecule, the molecule gets a rotational kick towards the polarization axis and becomes aligned after the pulse. The alignment does, however, persist only for a short while — the angular velocity imposed by the kick from the laser causes the molecules to rotate away from the polarization axis. The degree of alignment is observed to depend on the intensity and duration of the alignment laser and on the initial rotational temperature of the molecules. Lowering the rotational temperature always improves the degree of alignment. The choice of laser parameters, especially the pulse duration, is more subtle. The intensity is limited from above by the onset of multi-photon ionization, but the degree of alignment may saturate at lower intensities. Determining the optimal pulse duration involves balancing between maximizing the kick-strength of the laser pulse and keeping the molecules aligned under field-free conditions, i.e. after the pulse.

In classical mechanics only the dynamics immediately after the pulse would be interesting since this is the only time the molecules would be aligned, but the rotational energies are quantized so the wave packet induced by the short pulse can rephase, leading to recurrences in the degree of alignment with a period corresponding to the rotational period. For linear molecules and symmetric tops the wave packet at the revivals is a perfect reconstruction of the wave packet immediately after the pulse so the revivals continue to occur for long periods of time; experimentally we measured the 42nd revival for methyliodide and were limited only by the length of the delay stage. For asymmetric tops the revivals are only partial rephasings of the initially excited wave packet, so the degree of alignment at the revivals is reduced compared to that observed just after the pulse. For the near-symmetric top iodobenzene we observed two different revival times, corresponding to rotational motion around an axis perpendicular to the symmetry axis and with a moment of inertia equal to the average moment of inertia perpendicular to the symmetry axis, and to rotation about the c-axis.

For many applications it is desirable to have the molecules as well aligned as possible. It is therefore interesting to identify schemes that can optimize the degree of alignment. Guided by a theoretical proposal, we showed experimentally and numerically that two properly chosen pulses can significantly enhance the degree of alignment compared to that obtainable with just one pulse. The calculations also highlighted the importance of considering the effects of focal-volume averaging, which may significantly reduce the effective degree of alignment compared to the alignment in the center of the focus.

Some of the applications of aligned molecules that have appeared in the recent years were also discussed. In strong field physics it is, for instance, now recognized that ionization rates for molecules depend on the orientation of the molecule with respect to the polarization of the laser. Measurements of ionization rates for aligned molecules might therefore be important to settle current disputes on which theoretical models to use. Also the emission of high-order harmonics has been shown to depend strongly the alignment of the molecules with respect to the driving field. Another important future application of aligned molecules is in photoelectron spectroscopy. When randomly oriented molecules are ionized, the often richly structured molecular frame photoelectron angular distributions are concealed by orientational averaging. When molecules are aligned, the molecular frame is brought to coincide with the laboratory frame and the observed angular distributions should tend towards the molecular frame distribution.

APPENDIX A

Calculating the degree of alignment

In Sections 2.2 and 2.3 the procedure for calculating adiabatic and nonadiabatic alignment was outlined. In this Appendix the relevant matrix elements are given as well as some details on central points from the numerical implementation used for calculating nonadiabatic alignment for symmetric tops. Further it is shown how angular distributions can be extracted. All the relevant angular momentum algebra can be found in the book of Zare [36].

A.1 Symmetric top matrix elements

For calculating both adiabatic and nonadiabatic alignment the critical point is to calculate the matrix elements of the Hamiltonian

$$\begin{aligned}\hat{H} &= \hat{H}_{\text{rot}} + \hat{V} \\ &= B\hat{J}^2 + (A-B)\hat{J}_z^2 - \frac{E_0^2}{4}\left(\Delta\alpha\cos^2\theta + \alpha_\perp\right). \end{aligned} \tag{A.1}$$

The first two terms in the last equation stem from the field-free symmetric top Hamiltonian and are thus inherently diagonal in the symmetric top basis

$$\langle J'K'M'|\hat{H}_{\text{rot}}|JKM\rangle = \left[BJ(J+1) + (A-B)K^2\right]\delta_{J,J'}\delta_{K,K'}\delta_{M,M'}. \quad \text{(A.2)}$$

In the interaction term the only nontrivial task is to calculate the matrix elements of $\cos^2\theta$. To obtain this we rewrite $\cos^2\theta$ in terms of the Wigner rotation matrix

$$\cos^2\theta = \frac{2}{3}D^2_{0,0}(\Omega) + \frac{1}{3}, \quad \text{(A.3)}$$

with $\Omega = (\phi, \theta, \chi)$ as a collective index for the three Euler angles. Since the spatial representation of the symmetric top wave functions is proportional to a Wigner rotation matrix

$$\langle\hat{R}|JKM\rangle = (-1)^{M-K}\left[\frac{2J+1}{8\pi^2}\right]^{\frac{1}{2}} D^J_{-M-K}(\Omega), \quad \text{(A.4)}$$

the matrix elements of $\cos^2\theta$ are readily calculating using (3.118) in Zare. The result is

$$\begin{aligned}
&\langle JKM|\cos^2\theta|J'K'M'\rangle \\
&\quad = \tfrac{2}{3}\langle JKM|D^2_{00}(\Omega)|J'K'M'\rangle + \tfrac{1}{3}\langle JKM|J'K'M'\rangle \\
&\quad = \Big[\tfrac{2}{3}(2J+1)^{\frac{1}{2}}(2J'+1)^{\frac{1}{2}}(-1)^{M-K}\begin{pmatrix} J & J' & 2 \\ K & -K & 0\end{pmatrix}\begin{pmatrix} J & J' & 2 \\ M & -M & 0\end{pmatrix} \\
&\qquad + \tfrac{1}{3}\delta_{J,J'}\Big]\delta_{M,M'}\delta_{K,K'}.
\end{aligned} \quad \text{(A.5)}$$

This result explicitly shows that states of different K and M quantum numbers are not coupled. The Wigner 3-j symbols are only nonzero when $|J - J'| \leq 2$ and for these analytical expressions can be found in Table 2.5 in Zare. In the case of nonadiabatic alignment this result is also used to calculate the observable $\langle\cos^2\theta\rangle$ for the wave packet.

A.2 Angular distributions

For calculations of both adiabatic and nonadiabatic alignment the wave function found by determining the expansion coefficients in the symmetric top basis, that is finding the $c_{J'}$'s in

$$|\psi\rangle = \sum_{J'} c_{J'}|J'KM\rangle, \quad \text{(A.6)}$$

Using this expansion, an expression for the angular distribution is readily found

$$\begin{aligned} P(\theta) &= \int_0^{2\pi}\int_0^{2\pi} |\langle \hat{R}|\psi\rangle|^2 \,\mathrm{d}\phi\,\mathrm{d}\chi \\ &= \sum_{J'} |c_{J'}|^2 \left(J'+\tfrac{1}{2}\right)\left(d^{J'}_{-M-K}(\theta)\right)^2 \\ &\quad + \sum_{J'<J''} 2\,\mathrm{Re}\left(c_{J'}c^*_{J''}\right)\left(J'+\tfrac{1}{2}\right)^{\frac{1}{2}}\left(J''+\tfrac{1}{2}\right)^{\frac{1}{2}} d^{J'}_{-M-K}(\theta)\, d^{J''}_{-M-K}(\theta), \end{aligned} \tag{A.7}$$

where $d^J_{M',M}(\theta)$ is Wigner's reduced rotation matrix. The angular distribution is normalized such that

$$\int_0^{\pi} P(\theta)\sin\theta\,\mathrm{d}\theta = 1. \tag{A.8}$$

The elements of the reduced rotation matrix can be evaluated using (3.57) in Zare

$$\begin{aligned} d^J_{M'M}(\theta) = \sum_{\nu} (-1)^{\nu} \frac{\left[(J+M)!\,(J-M)!\,(J+M')!\,(J-M')!\right]^{\frac{1}{2}}}{(J-M'-\nu)!\,(J+M-\nu)!\,(\nu+M'-M)!\,\nu!} \\ \times \left[\cos\left(\frac{\theta}{2}\right)\right]^{2J+M-M'-2\nu} \left[-\sin\left(\frac{\theta}{2}\right)\right]^{M'-M+2\nu}, \end{aligned} \tag{A.9}$$

where the index ν runs over all integer values for which the arguments of the factorials are nonnegative.

For small, linear molecules like N_2 and O_2 thermally averaged angular distributions can readily be calculated at experimentally realistic temperatures (50 K) and intensities (50 TW/cm^2) on a standard PC. Calculating angular distributions for larger symmetric tops is on the other hand a computationally *very* demanding task due to the smaller rotational constants and the extra degree of freedom. The reason for the angular distributions being so troublesome lies is the double sum over products of reduced rotations matrices. Even at intensities lower than those employed in our experiments a basis set of 60 J states is needed and the size scaling of the computation time is probably quadratic in J due to the double sum. These high J states also lead to another concern: the numerical stability in the calculation of the reduced rotation matrix elements. The value of the matrix element is in the range $[-1\,;\,1]$ but is obtained by a fine tuned cancellation of large alternating terms in Eq. (A.9). For high J values each of factorials involve *very* large numbers (and small for the reciprocals) and rounding errors of the numbers in the computer therefore become an issue. The numerical stability was checked by monitoring the normalization of the rotation matrices (Eq. (3.113) in Zare). Starting from J in the low fifties (the exact number being dependent on K, M) the normalization abruptly starts to diverge. For the heavy molecules

studied in our group it has therefore only been possible to extract angular distributions at experimentally realistic conditions for adiabatic alignment.

A.3 Numerical implementation for calculating nonadiabatic alignment

Units of polarizability

In quantum chemistry calculations of molecular polarizability most often find what is called the polarizability volume (given in Å^3). The polarizability, α_i, entering in Eq. (2.1) is related to the polarizability volume, α_i', by $\alpha' = \alpha/(4\pi\varepsilon_0)$. The relation between electric field strength, $\mathcal{E}_0$ and the intensity of field is $I = c\varepsilon_0\mathcal{E}_0^2/2$. All in all this yields

$$V_0 = \mathcal{E}_0^2\alpha = \frac{8\pi}{c} I\alpha' \tag{A.10}$$

With $V_0/\hbar$ in ps^{-1} (THz) we therefore find

$$\frac{V_0}{\hbar} = \frac{8\pi}{\hbar c} I\alpha' = 7.9495592825 \cdot I(\text{TW/cm}^2) \cdot \alpha'(\text{Å}^3) \qquad [\text{ps}^{-1}] \tag{A.11}$$

Propagation in the field

While the molecules are interacting with the laser pulse we can only obtain the wave function by direct solution of the coupled differential equations in Eq. (2.18). Many approaches can be used to do so. Since we can expect the solutions to be well behaved, no singularities should occur and their magnitude is limited from above, we can readily make use of Runge-Kutta methods. A well balanced method for carrying out adaptive step-size integration of the equations is the Cash-Karp imbedded method which is based on a clever combination of a fourth and a fifth order Runge-Kutta solution [28]. By using an adaptive step-size routine we only need to be sure that the first couple of steps are sufficiently small and that the routine has enough flexibility for readjusting the step-size during the evolution of the laser pulse. If these conditions are fulfilled the routine will automatically adjust the temporal step size to to follow the evolution of the coefficients faithfully. We can thus expect a gain in computational speed at low intensities and during the rising edge of the pulse as compared to a fixed step-size routine. The numerical stability has been tested by changing the error tolerance. Further, calculations have been carried out on linear molecules using the same code with $K = 0$ and compared to published results from several independent groups [27, 52, 192]. Please note an error in the latter publication: in Eq. (3) the numerical factor in $f(t)$ is a factor of two too low so that intensities quoted are a factor of two too high.

Partition function and the selection of initial states

Thermally averaged calculations are carried out by launching calculations from a range of initial states representing the thermal ensemble. The selection of initial states is done according to their statistical weight. At first the partition function is calculated by summing over all states in the basis (the size of the basis must always be large enough that the contribution from the high J end of the basis is negligible and the sum has converged). The states are then sorted according to their statistical weight. A list of populated initial states is then created by summing the statistical weights in the sorted list until the sum reaches a value of 99.9 % of the partition function. For *tert*-butyliodide at a temperature of 1 K about 300 states are included in the set of initial states (counting only states of non-negative K, M).

By examination of the interaction matrix elements it is readily seen that these only depend on the relative sign of K and M, not on their absolute values. Thus instead of exploring all four combinations $\pm K, \pm M$ we need only the $|K|, |M|$ and $-|K|, |M|$ combinations (for the calculation of $\langle \cos^2 \theta \rangle$); care must of course be taken to handle the $K = 0$ and/or $M = 0$ situations correctly. This small symmetry consideration does however cut down the number of initial states by nearly a factor of two and thus reduces the computational time for thermally averaged calculations by the same factor.

The possible use of Monte Carlo sampling at high (dimensionless) temperatures seems to be worth consideration. This could faithfully sample the thermal ensemble by using a significantly lower number of states.

Intensity dependent size of basis set

To make the most efficient use of the computer time the size of the basis set was chosen to be dependent on the intensity. This is particularly useful for carrying out focal volume averaged calculations. The procedure is aimed at situations where many calculations are to be carried out for the same molecule with only modest changes in the conditions as was the case for the two pulse calculations on *tert*-butyliodide.

To find the minimal basis set size for *tert*-butyliodide calculations were carried out in a large basis set ($J_{\text{max}} = 90$) for a few initial states. For each of these calculations the population distribution was examined to find the highest state, J_{m}, with a population above 10^{-3}. The minimal basis size was then chosen to be $J_{\text{max}} = J_{\text{m}} + 5$ since higher J states may be populated during the interaction with the laser pulse (for longer pulse durations this effect can be quite pronounced). For *tert*-butyliodide the initial states were $|000\rangle$ and $|15, 5, 5\rangle$ (highest J state populated at a temperature of 2 K). In Fig. A.1 J_{max} is plotted versus intensity for a 1 ps alignment pulse. Also shown is a quadratic fit to the points; in the intensity region examined the basis set size is well fit by a second order polynomial. This fit is what the program use to determine the basis. The intensity dependence is quite pronounced; in the intensity regime explored in the two pulse calculations the size varies by a factor of two. The computational

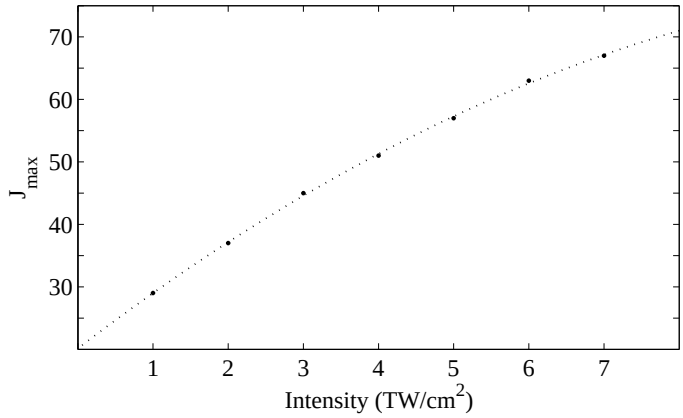

FIGURE A.1: Dots: Estimate of the minimal basis size as function of peak intensity. Dotted line: quadratic fit to the points. See text for details.

time used at the low intensities turns out to faster by roughly the same factor. For the calculations with a pulse duration of 2 ps the size of the basis set was expanded by another 15 J states. Once the intensity dependence was settled calculations were carried out at a fixed intensity for a handful of different initial states to check that the basis was sufficient for these states as well. In general, the states with large initial J required the largest basis but the initial states dependence was modest: about 10 more states was necessary for $J_i = 15$ compared to $J_i = 0$. As a final check, the evolution of $\langle \cos^2 \theta \rangle$ was calculated with intensity dependent choice of basis set and with a large basis set. The results were almost exactly identical.

REFERENCES

[1] H. Stapelfeldt and T. Seidemann, *Colloquium: Aligning molecules with strong laser pulses*, Rev. Mod. Phys. **75**, 543 (2003).

[2] D. H. Parker and R. B. Bernstein, *Oriented Molecule Beams via the Electrostatic Hexapole: Preparation, Characterization, and Reactive Scattering*, Ann. Rev. Phys. Chem. **40**, 561 (1989).

[3] B. Friedrich, D. P. Pullman, and D. R. Herschbach, *Alignment and Orientation of Rotationally Cool Molecules*, J. Phys. Chem. **95**, 8118 (1991).

[4] H. J. Loesch and A. Remscheid, *Brute force in molecular reaction dynamics: A novel technique for measuring steric effects*, J. Chem. Phys. **93**, 4779 (1990).

[5] B. Friedrich and D. Herschbach, *Alignment and Trapping of Molecules in Intense Laser Fields*, Phys. Rev. Lett. **74**, 4623 (1995).

[6] D. Normand, L. A. Lompre, and C. Cornaggia, *Laser-induced molecular alignment probed by a double-pulse experiment*, J. Phys. B **25**, L497 (1992).

[7] D. T. Strickland, Y. Beaudoin, P. Dietrich, and P. B. Corkum, *Optical studies of inertially confined molecular iodine ions*, Phys. Rev. Lett. **68**, 2755 (1992).

[8] E. Constant, H. Stapelfeldt, and P. B. Corkum, *Observation of Enhanced Ionization of Molecular Ions in Intense Laser Fields*, Phys. Rev. Lett. **76**, 4140 (1996).

[9] T. Seideman, M. Y. Ivanov, and P. B. Corkum, *Role of Electron Localization in Intense-Field Molecular Ionization*, Phys. Rev. Lett. **75**, 2819 (1995).

[10] C. H. Lin, J. P. Heritage, and T. K. Gustafson, *Susceptibility Echos in Linear Molecular Gases*, Apl. Phys. Lett. **19**, 397 (1971).

[11] J. P. Heritage, T. K. Gustafson, and C. H. Lin, *Observation of Coherent Transient Birefringence in CS_2 Vapor*, Phys. Rev. Lett. **34**, 1299 (1975).

[12] P. Felker, *Rotational coherence spectroscopy: studies of the geometries of large gas-phase species by picosecond time-domain methods*, J. Phys. Chem. **96**, 7844 (1992).

[13] P. M. Felker and A. H. Zewail, *Molecular Structures from Ultrafast Coherence Spectroscopy*, in *Femtosecond Chemistry*, edited by J. Manz and L. Wöste (VCH (Weinheim) 1995), pp. 193–260.

[14] T. Seideman, *Rotational excitation and molecular alignment in intense laser fields*, J. Chem. Phys. **103**, 7887 (1995).

[15] T. Seideman, *Revival Structure of Aligned Rotational Wave Packets*, Phys. Rev. Lett. **83**, 4971 (1999).

[16] J. Ortigoso, M. Rodriguez, M. Gupta, and B. Friedrich, *Time evolution of pendular states created by the interaction of molecular polarizability with a pulsed nonresonant laser field*, J. Chem. Phys. **110**, 3870 (1999).

[17] W. Kim and P. M. Felker, *Spectroscopy of pendular states in optical-field-aligned species*, J. Chem. Phys. **104**, 1147 (1996).

[18] J. J. Larsen, H. Sakai, C. P. Safvan, I. Wendt-Larsen, and H. Stapelfeldt, *Aligning molecules with intense nonresonan laser fields*, J. Chem. Phys. **111**, 7774 (1999).

[19] H. Sakai, C. P. Safvan, J. J. Larsen, K. M. Hilligsøe, K. Hald, and H. Stapelfeldt, *Controlling the alignment of neutral molecules by a strong laser field*, J. Chem. Phys. **110**, 10235 (1999).

[20] J. J. Larsen, K. Hald, N. Bjerre, H. Stapelfeldt, and T. Seideman, *Three Dimensional Alignment of Molecules Using Elliptically Polarized Laser Fields*, Phys. Rev. Lett. **85**, 2470 (2000).

[21] F. Rosca-Pruna and M. J. J. Vrakking, *Experimental Observation of Revival Structures in Picosecond Laser-Induced Alignment of I_2*, Phys. Rev. Lett. **87**, 153902 (2001).

[22] C. M. Dion, A. Keller, O. Atabek, and A. D. Bandrauk, *Laser-induced alignment dynamics of HCN: Roles of the permanent dipole moment and the polarizability*, Phys. Rev. A **59**, 1382 (1999).

[23] B. J. Sussman, J. G. Underwood, R. Lausten, M. Y. Ivanov, and A. Stolow, *Quantum control via the dynamic Stark effect: Application to switched rotational wave packets and molecular axis alignment*, Phys. Rev. A **73**, 053403 (2006).

[24] B. Friedrich and D. Herschbach, *Polarization of Molecules Induced by Intense Nonresonant Laser Fields*, J. Phys. Chem. **99**, 15686 (1995).

[25] B. A. Zon and B. G. Katsnel'son, *Nonresonant scattering of intense light by a molecule*, Sov. Phys.-JETP **42**, 595 (1976).

[26] L. D. Landau and E. M. Lifshitz, *Quantum Mechanics (Non-relativistic theory)* (Butterworth-Heinemann, Oxford 1991), third edition.

[27] R. Torres, R. de Nalda, and J. P. Marangos, *Dynamics of laser-induced molecular alignment in the impulsive and adiabatic regimes: A direct comparison*, Phys. Rev. A **72**, 023420 (2005).

[28] W. H. Press, S. T. Teukolsky, W. T. Vetterling, and B. P. Flannery, *Numerical Recipes in C++* (Cambridge University Press, Cambridge 2002).

[29] P. Atkins and R. Friedman, *Molecular Quantum Mechanics* (Oxford University Press, Oxford 2005), fourth edition.

[30] U. Even, J. Jortner, D. Noy, N. Lavie, and C. Cossart-Magos, *Cooling of large molecules below 1 K and He clusters formation*, J. Chem. Phys. **112**, 8068 (2000).

[31] M. Hillenkamp, S. Keinan, and U. Even, *Condensation limited cooling in supersonic expansions*, J. Chem. Phys. **118**, 8699 (2003).

[32] T. Seideman, *On the dynamics of rotationally broad, spatially aligned wave packets*, J. Chem. Phys. **115**, 5965 (2001).

[33] B. Friedrich and D. Herschbach, *Statistical mechanics of pendular molecules*, Int. Rev. Phys. Chem. **15**, 325 (1996).

[34] I. S. Averbukh and R. Arvieu, *Angular Focusing, Squeezing, and Rainbow Formation in a Strongly Driven Quantum Rotor*, Phys. Rev. Lett. **87**, 163601 (2001).

[35] M. Leibscher, I. S. Averbukh, and H. Rabitz, *Molecular Alignment by Trains of Short Laser Pulses*, Phys. Rev. Lett. **90**, 213001 (2003).

[36] R. N. Zare, *Angular Momentum* (Wiley-Interscience, New York 1988).

[37] I. S. Averbukh and N. F. Perelman, *Fractional Revivals: Universality in the long-term evolution of quantum wave packets beyond the correspondence principle dynamics*, Phys. Lett. A **139**, 449 (1989).

[38] F. Rosca-Pruna and M. J. J. Vrakking, *Revival structures in picosecond laser-induced alignment of I_2 molecules. II. Numerical modeling*, J. Chem. Phys. **116**, 6579 (2002).

[39] F. Rosca-Pruna and M. J. J. Vrakking, *Revival structures in picosecond laser-induced alignment of I_2 molecules. I. Experimental results*, J. Chem. Phys. **116**, 6567 (2002).

[40] P. W. Dooley, I. V. Litvinyuk, K. F. Lee, D. M. Rayner, M. Spanner, D. M. Villeneuve, and P. B. Corkum, *Direct imaging of rotational wave-packet dynamics of diatomic molecules*, Phys. Rev. A **68**, 023406 (2003).

[41] M. Spanner, E. A. Shapiro, and M. Ivanov, *Coherent Control of Rotational Wave-Packet Dynamics via Fractional Revivals*, Phys. Rev. Lett. **92**, 093001 (2004).

[42] C. Ellert and P. B. Corkum, *Disentangling molecular alignment and enhanced ionization in intense laser fields*, Phys. Rev. A **59**, R3170 (1999).

[43] M. J. Weida and D. J. Nesbitt, *Collisional alignment of CO_2 rotational angular momentum states in a supersonic expansion*, J. Chem. Phys. **100**, 6372 (1994).

[44] V. Aquilanti, D. Ascenzi, D. Cappelletti, and F. Pirani, *Velocity dependence of collisional alignment of oxygen molecules in gaseous expansions*, Nature (London) **371**, 399 (1994).

[45] F. Pirani, D. Cappelletti, M. Bartolomei, V. Aquilanti, M. Scotoni, M. Vescovi, D. Ascenzi, and D. Bassi, *Orientation of Benzene in Supersonic Expansions, Probed by IR-Laser Absorption and by Molecular Beam Scattering*, Phys. Rev. Lett. **86**, 5035 (2001).

[46] J. J. Larsen, *Laser Induced Alignment of Neutral Molecules*, Ph.D. thesis, Institute of Physics and Astronomy, University of Aarhus (2000).

[47] E. Péronne, M. D. Poulsen, C. Z. Bisgaard, H. Stapelfeldt, and T. Seideman, *Nonadiabatic Alignment of Asymmetric Top Molecules: Field-Free Alignment of Iodobenzene*, Phys. Rev. Lett. **91**, 043003 (2003).

[48] J. G. Underwood, B. J. Sussman, and A. Stolow, *Field-Free Three Dimensional Molecular Axis Alignment*, Phys. Rev. Lett. **94**, 143002 (2005).

[49] J. J. Larsen, I. Wendt-Larsen, and H. Stapelfeldt, *Controlling the Branching Ratio of Photodissociation Using Aligned Molecules*, Phys. Rev. Lett. **83**, 1123 (1999).

[50] M. D. Poulsen, E. Skovsen, and H. Stapelfeldt, *Photodissociation of laser aligned iodobenzene: Towards selective photoexcitation*, J. Chem. Phys. **117**, 2097 (2002).

[51] V. Renard, M. Renard, S. Guérin, Y. T. Pashayan, B. Lavorel, O. Fraucher, and H. R. Jauslin, *Postpulse Molecular Alignment Measured by a Weak Field Polarization Technique*, Phys. Rev. Lett. **90**, 153601 (2003).

[52] V. Renard, M. Renard, A. Rouzée, S. Guérin, H. R. Jauslin, B. Lavorel, and O. Faucher, *Nonintrusive monitoring and quantitative analysis of strong laser-field-induced impulsive alignment*, Phys. Rev. A **70**, 33420 (2004).

[53] J. G. Underwood, M. Spanner, M. Y. Ivanov, J. Mottershead, B. J. Sussman, and A. Stolow, *Switched Wave Packets: A Route to Nonperturbative Quantum Control*, Phys. Rev. Lett. **90**, 223001 (2003).

[54] S. Zamith, Z. Ansari, F. Lepine, and M. J. J. Vrakking, *Single-shot measurement of revival structures in femtosecond laser-induced alignment of molecules*, Opt. Lett. **30**, 2326 (2005).

[55] R. Velotta, N. Hay, M. B. Mason, M. Castillejo, and J. P. Marangos, *High-Order Harmonic Generation in Aligned Molecules*, Phys. Rev. Lett. **87**, 183901 (2001).

[56] M. Lein, N. Hay, R. Velotta, J. P. Marangos, and P. L. Knight, *Role of the Intramolecular Phase in High-Harmonic Generation*, Phys. Rev. Lett. **88**, 183903 (2002).

[57] C. Vozzi, F. Calegari, E. Benedetti, J.-P. Caumes, G. Sansone, S. Stagira, M. Nisoli, R. Torres, E. Heesel, N. Kajumba, J. P. Marangos, C. Altucci, and R. Velotta, *Controlling Two-Center Interference in Molecular High Harmonic Generation*, Phys. Rev. Lett. **95**, 153902 (2005).

[58] J. Itatani, D. Zeidler, J. Levesque, M. Spanner, D. M. Villeneuve, and P. B. Corkum, *Controlling High Harmonic Generation with Molecular Wave Packets*, Phys. Rev. Lett. **94**, 123902 (2005).

[59] T. Kanai, S. Minemoto, and H. Sakai, *Quantum interference during high-order harmonic generation from aligned molecules*, Nature (London) **435**, 470 (2005).

[60] K. Hoshina, K. Yamanouchi, T. Ohshima, Y. Ose, and H. Todokoro, *Direct observation of molecular alignment in an intense laser field by pulsed gas electron diffraction I: observation of anisotropic diffraction image*, Chem. Phys. Lett. **353**, 27 (2002).

[61] F. Rosca-Pruna, E. Springate, H. L. Offerhaus, M. Krishnamurthy, N. Farid, C. Nicole, and M. J. J. Vrakking, *Spatial alignment of diatomic molecules in intense laser fields: I. Experimental results*, J. Phys. B **34**, 4919 (2001).

[62] H. Tanji, S. Minemoto, and H. Sakai, *Three-dimensional molecular orientation with combined electrostatic and elliptically polarized laser fields*, Phys. Rev. A **72**, 063401 (2005).

[63] F. Légaré, K. F. Lee, I. V. Litvinyuk, P. W. Dooley, A. D. Bandrauk, D. M. Villeneuve, and P. B. Corkum, *Imaging the time-dependent structure of a molecule as it undergoes dynamics*, Phys. Rev. A **72**, 052717 (2005).

[64] G. Scoles (editor), *Atomic and molecular beam methods*, volume I (Oxford University Press 1988).

[65] D. W. Chandler and P. L. Houston, *Two-dimensional imaging of state-selected photodissociation products detected by multiphoton ionization*, J. Chem. Phys. **87**, 1445 (1987).

[66] A. T. J. B. Eppink and D. H. Parker, *Velocity map imaging of ions and electrons using electrostatic lenses: Application in photoelectron and photofragment ion imaging of molecular oxygen*, Rev. Sci. Instr. **68**, 3477 (1997).

[67] M. J. J. Vrakking, *An iterative procedure for the inversion of two-dimensional ion/photoelectron imaging experiments*, Rev. Sci. Intr. **72**, 4084 (2001).

[68] V. Dribinski, A. Ossadtchi, V. A. Mandelshtam, and H. Reisler, *Reconstruction of Abel-transformable images: The Gaussian basis-set expansion Abel transform method*, Rev. Sci. Instr. **73**, 2634 (2002).

[69] J. D. Jackson, *Classical Electrodynamics* (Wiley (New York) 1999), third edition.

[70] S. Backus, C. G. Durfee III, M. M. Murnane, and H. C. Kapteyn, *High power ultrafast lasers*, Rev. Sci. Instr. **69**, 1207 (1998).

[71] P. Y. Cheng, D. Zhong, and A. H. Zewail, *Kinetic-energy, femtosecond resolved reaction dynamics. Modes of dissociation (in iodobenzene) from time-velocity correlations.*, Chem. Phys. Lett. **237**, 399 (1995).

[72] A. T. J. B. Eppink and D. H. Parker, *Energy partitioning following photodissociation of methyl iodide in the A band: A velocity mapping study*, J. Chem. Phys. **110**, 832 (1999).

[73] J. E. Freitas, H. J. Hwang, and M. A. El-Sayed, *Molecular Rotation Clocking of the Subpicosecond Energy Redistribution in Molecules Falling Apart. 2. Excess Energy Dependence of the Rates of Energy Redistribution in the Two Photodissociation Channels of Iodobenzene*, J. Phys. Chem. **97**, 12481 (1993).

[74] Y. S. Kim, W. K. Kang, D.-C. Kim, and K.-H. Jung, *Photodissociation of tert-Butyl Iodide at 277 and 304 nm: Evidence for Direct and Indirect Dissociation in A-Band Photolysis of Alkyl Iodide*, J. Phys. Chem. A **101**, 7576 (1997).

[75] *NIST Physical Reference Data*, http://physics.nist.gov/PhysRefData/contents.html (2006).

[76] S. Unny, Y. Du, L. Zhu, K. Truhins, R. J. Gordon, A. Sugita, M. Kawasaki, Y. Matsumi, R. Delmdahl, D. H. Parker, and A. Berces, *Above-Threshold Effects in the Photodissociation and Photoionization of Iodobenzene*, J. Phys. Chem. A **105**, 2270 (2001).

[77] J. Olesen, *Generation of sub 20 fs laser pulses and Coulomb explosion studies of D_2*, Master's thesis, Department of Chemistry, University of Århus (1999).

[78] E. Péronne, M. D. Poulsen, H. Stapelfeldt, C. Z. Bisgaard, E. Hamilton, and T. Seideman, *Nonadiabatic laser-induced alignment of iodobenzene molecules*, Phys. Rev. A. **70**, 63410 (2004).

[79] M. D. Poulsen, T. Ejdrup, H. Stapelfeldt, E. Hamilton, and T. Seideman, *Alignment enhancement by the combination of a short and a long laser pulse*, Phys. Rev. A **73**, 033405 (2006).

[80] W. J. O. Thomas, J. T. Cox, and W. Gordy, *Millimeter Wave Spectra and Centrifugal Stretching Constants of the Methyl Halides*, J. Chem. Phys. **22**, 1718 (1954).

[81] A. M. Mirri and W. Caminati, *Quadrupole hyperfine structure in the rotational spectrum of iodobenzene*, Chem. Phys. Lett. **8**, 409 (1971).

[82] S. H. Young and S. G. Kukolich, *Microwave Measurements and Calculations of Quadrupole Coupling Effects in CH_3I and CD_3I*, J. Mol. Spec. **114**, 483 (1985).

[83] W. Winkle and H. Hartmann, *Microwave Spectrum of tert-butyliodide - Analysis of rotation spectra with quadrupole hyperfine structure*, Zeitschrift für Naturforschung A **25**, 840 (1970).

[84] C. H. Townes and A. L. Schawlow, *Microwave spectroscopy* (McGraw-Hill (New York) 1955).

[85] E. Hamilton, T. Seideman, T. Ejdrup, M. D. Poulsen, C. Z. Bisgaard, S. S. Viftrup, and H. Stapelfeldt, *Alignment of symmetric top molecules by short laser pulses*, Phys. Rev. A **72**, 043402 (2005).

[86] S. Ramakrishna and T. Seideman, *Intense Laser Alignment in Dissipative Media as a Route to Solvent Dynamics*, Phys. Rev. Lett. **95**, 113001 (2005).

[87] J. Q. Williams and W. Gordy, *Microwave Spectra and Molecular Constants of Tertiary Butyl Chloride, Bromide, and Iodide*, J. Chem. Phys. **18**, 994 (1950).

[88] M. D. Poulsen, E. Péronne, H. Stapelfeldt, C. Z. Bisgaard, S. S. Viftrup, E. Hamilton, and T. Seideman, *Nonadiabatic alignment of asymmetric top molecules: Rotational revivals*, J. Chem. Phys. **121**, 783 (2004).

[89] S. Ryu, R. M. Stratt, and P. M. Weber, *Diffraction Signals of Aligned Molecules in the Gas Phase: Tetrazine in Intense Laser Fields*, J. Phys. Chem. A **107**, 6622 (2003).

[90] J. C. H. Spence and R. B. Doak, *Single Molecule Diffraction*, Phys. Rev. Lett. **92**, 198102 (2004).

[91] M. D. Poulsen, *Alignment of molecules induced by long and short laser pulses*, Ph.D. thesis, Department of Chemistry, University of Aarhus (2005).

[92] M. Tsubouchi, B. J. Whitaker, L. Wang, H. Kohguchi, and T. Suzuki, *Photoelectron Imaging on Time-Dependent Molecular Alignment Created by a Femtosecond Laser Pulse*, Phys. Rev. Lett. **86**, 4500 (2001).

[93] A. E. Bragg, R. Wester, A. V. Davis, A. Kammrath, and D. M. Neumark, *Excited-state detachment dynamics and rotational coherences of C_2^- via time-resolved photoelectron imaging*, Chem. Phys. Lett. **376**, 767 (2003).

[94] Y. Suzuki and T. Seideman, *Mapping rotational coherences onto time-resolved photoelectron imaging observables*, J. Chem. Phys. **122**, 234302 (2005).

[95] J. G. Underwood and K. L. Reid, *Time-resolved photoelectron angular distributions as a probe of intramolecular dynamics: Connecting the molecular frame and the laboratory frame*, J. Chem. Phys. **113**, 1067 (2000).

[96] R. R. Freeman, T. J. McIlrath, P. H. Bucksbaum, and M. Bashkansky, *Ponderomotive effects on angular distributions of photoelectrons*, Phys. Rev. Lett. **57**, 3156 (1986).

[97] A. E. Bragg, J. R. R. Verlet, A. Kammrath, and D. M. Neumark, *C_6^- electronic relaxation dynamics probed via time-resolved photoelectron imaging*, J. Chem. Phys. **121**, 3515 (2004).

[98] A. Abdurahman, A. Shukla, and G. Seifert, *Ab initio many-body calculations of static dipole polarizabilities of linear carbon chains and chainlike boron clusters*, Phys. Rev. B **66**, 155423 (2002).

[99] A. Van Orden and R. J. Saykally, *Small Carbon Clusters: Spectroscopy, Structure, and Energetics*, Chem. Rev. **98**, 2313 (1998).

[100] M. Leibscher, I. S. Averbukh, and H. Rabitz, *Enhanced molecular alignment by short laser pulses*, Phys. Rev. A **69**, 013402 (2004).

[101] C. Z. Bisgaard, M. D. Poulsen, E. Péronne, S. S. Viftrup, and H. Stapelfeldt, *Observation of Enhanced Field-Free Molecular Alignment by Two Laser Pulses*, Phys. Rev. Lett. **92**, 173004 (2004).

[102] K. F. Lee, I. V. Litvinyuk, P. W. Dooley, M. Spanner, D. M. Villeneuve, and P. B. Corkum, *Two-pulse alignment of molecules*, J. Phys. B **37**, L43 (2004).

[103] C. Horn, M. Wollenhaupt, M. Krug, T. Baumert, R. de Nalda, and L. Bañares, *Adaptive control of molecular alignment*, Phys. Rev. A **73**, 031401 (2006).

[104] M. Renard, E. Hertz, S. Guérin, H. R. Jauslin, B. Lavorel, and O. Faucher, *Control of field-free molecular alignment by phase-shaped laser pulses*, Phys. Rev. A **72**, 025401 (2005).

[105] K. F. Lee, E. A. Shapiro, D. M. Villeneuve, and P. B. Corkum, *Coherent creation and annihilation of rotational wave packets in incoherent ensembles*, Phys. Rev. A **73**, 033403 (2006).

[106] K. F. Lee, D. M. Villeneuve, P. B. Corkum, and E. A. Shapiro, *Phase Control of Rotational Wave Packets and Quantum Information*, Phys. Rev. Lett. **93**, 233601 (2004).

[107] B. Friedrich and D. Herschbach, *Enhanced orientation of polar molecules by combined electrostatic and nonresonant induced dipole forces*, J. Chem. Phys. **111**, 6157 (1999).

[108] B. Friedrich and D. Herschbach, *Manipulating Molecules via Combined Static and Laser Fields*, J. Phys. Chem. A **103**, 10280 (1999).

[109] L. Cai, J. Marango, and B. Friedrich, *Time-Dependent Alignment and Orientation of Molecules in Combined Electrostatic and Pulsed Nonresonant Laser Fields*, Phys. Rev. Lett. **86**, 775 (2001).

[110] M. Machholm and N. E. Henriksen, *Field-Free Orientation of Molecules*, Phys. Rev. Lett. **87**, 193001 (2001).

[111] F. Dong and R. E. Miller, *Vibrational Transition Moment Angles in Isolated Biomolecules: A Structural Tool*, Science **298**, 1227 (2002).

[112] R. Righini, *Ultrafast Optical Kerr Effect in Liquids and Solids*, Science **262**, 1386 (1993).

[113] R. A. Bartels, T. C. Weinacht, N. Wagner, M. Baertschy, C. H. Greene, M. M. Murnane, and H. C. Kapteyn, *Phase Modulation of Ultrashort Light Pulses using Molecular Rotational Wave Packets*, Phys. Rev. Lett. **88**, 013903 (2002).

[114] V. Kalosha, M. Spanner, J. Herrmann, and M. Ivanov, *Generation of Single Dispersion Precompensated 1-fs Pulses by Shaped-Pulse Optimized High-Order Stimulated Raman Scattering*, Phys. Rev. Lett. **88**, 103901 (2002).

[115] R. A. Bartels, N. L. Wagner, M. D. Baertschy, J. Wyss, M. M. Murnane, and H. C. Kapteyn, *Phase-matching conditions for nonlinear frequency conversion by use of aligned molecular gases*, Opt. Lett. **28**, 346 (2003).

[116] V. Blanchet, M. Z. Zgierski, T. Seideman, and A. Stolow, *Discerning vibronic molecular dynamics using time-resolved photoelectron spectroscopy*, Nature (London) **401**, 52 (1999).

[117] A. Stolow, *Femtosecond Time-Resolved Photoelectron Spectroscopy of Polyatomic Molecules*, Annu. Rev. Phys. Chem. **54**, 89 (2003).

[118] A. Stolow, A. E. Bragg, and D. M. Neumark, *Femtosecond Time-Resolved Photoelectron Spectroscopy*, Chem. Rev. **104**, 1719 (2004).

[119] D. M. Neumark, *Time-Resolved Photoelectron Spectroscopy of Molecules and Clusters*, Annu. Rev. Phys. Chem. **52**, 255 (2001).

[120] T. Seideman, *Time-resolved photoelectron angular distributions: A nonperturbative theory*, J. Chem. Phys. **107**, 7859 (1997).

[121] T. Seideman, *Time-resolved photoelectron angular distributions as a probe of coupled polyatomic dynamics*, Phys. Rev. A **64**, 042504 (2001).

[122] T. Seideman, *Time-Resolved Photoelectron Angular Distributions: Concepts, Applications and Directions*, Annu. Rev. Phys. Chem. **53**, 41 (2002).

[123] D. Dill, *Fixed-molecule photoelectron angular distributions*, J. Chem. Phys. **65**, 1130 (1976).

[124] K. L. Reid, *Photoelectron Angular Distributions*, Annu. Rev. Phys. Chem. **54**, 397 (2003).

[125] A. M. Rijs, M. H. M. Janssen, E. t. H. Chrysostom, and C. C. Hayden, *Femtosecond Coincidence Imaging of Multichannel Multiphoton Dynamics*, Phys. Rev. Lett. **92**, 123002 (2004).

[126] J. A. Davies, R. E. Continetti, D. W. Chandler, and C. C. Hayden, *Femtosecond Time-Resolved Photoelectron Angular Distributions Probed during Photodissociation of NO_2*, Phys. Rev. Lett. **84**, 5983 (2000).

[127] R. E. Continetti, *Coincidence Spectroscopy*, Annu. Rev. Phys. Chem. **52**, 165 (2001).

[128] O. Gessner, A. M. D. Lee, J. P. Shaffer, H. Reisler, S. V. Levchenko, A. I. Krylov, J. G. Underwood, H. Shi, A. L. L. East, D. M. Wardlaw, E. t. H. Chrysostom, C. C. Hayden, and A. Stolow, *Femtosecond Multidimensional Imaging of a Molecular Dissociation*, Science **311**, 219 (2006).

[129] P. Downie and I. Powis, *Molecule-Frame Photoelectron Angular Distributions from Oriented CF_3I Molecules*, Phys. Rev. Lett. **82**, 2864 (1999).

[130] A. Landers, T. Weber, I. Ali, A. Cassimi, M. Hattass, O. Jagutzki, A. Nauert, T. Osipov, A. Staudte, M. H. Prior, H. Schmidt-Böcking, C. L. Cocke, and R. Dörner, *Photoelectron Diffraction Mapping: Molecules Illuminated from Within*, Phys. Rev. Lett. **87**, 013002 (2001).

[131] R. R. Lucchese, A. Lafosse, J. C. Brenot, P. M. Guyon, J. C. Houver, M. Lebech, G. Raseev, and D. Dowek, *Polar and azimuthal dependence of the molecular frame photoelectron angular distributions of spatially oriented linear molecules*, Phys. Rev. A **65**, 020702 (2002).

[132] K. L. Reid and J. G. Underwood, *Extracting molecular axis alignment from photoelectron angular distributions*, J. Chem. Phys. **112**, 3643 (2000).

[133] M. Tsubouchi, B. J. Whitaker, and T. Suzuki, *Femtosecond Photoelectron Imaging on Pyrazine: $S_1 \rightarrow T_1$ Intersystem Crossing and Rotational Coherence Transfer*, J. Phys. Chem. A **108**, 6823 (2004).

[134] S. M. Bellm and K. L. Reid, *Reevaluation of the Use of Photoelectron Angular Distributions as a Probe of Dynamical Processes: Strong Dependence of Such Distributions from S_1 Paradifluorobenzene on Photoelectron Kinetic Energy*, Phys. Rev. Lett. **91**, 263002 (2003).

[135] S. M. Bellm, J. A. Davies, P. T. Whiteside, J. Guo, I. Powis, and K. L. Reid, *An unusual π^* shape resonance in the near-threshold photoionization of S_1 para-difluorobenzene*, J. Chem. Phys. **122**, 224306 (2005).

[136] J. T. Meek, E. Sekreta, W. Wilson, K. S. Viswanathan, and J. P. Reilly, *The laser photoelectron spectrum of gas phase aniline*, J. Chem. Phys. **82**, 1741 (1985).

[137] X. Song, M. Yang, E. F. Davidson, and J. P. Reilly, *Zero kinetic energy photoelectron spectra of jet-cooled aniline*, J. Chem. Phys. **99**, 3224 (1993).

[138] *Exciton Laser dye catalog*, http://www.exciton.com/ (2006).

[139] *NIST Chemistry WebBook*, http://webbook.nist.gov/chemistry/ (2006).

[140] J. L. Lin, S. C. Yang, Y. C. Yu, and W. B. Tzeng, *Mass analyzed threshold ionization of p-bromoaniline: heavy atom effects on electronic transition, ionization, and molecular vibration*, Chem. Phys. Lett. **356**, 267 (2002).

[141] P. B. Corkum, *Plasma perspective on Strong Field Multiphoton Ionization*, Phys. Rev. Lett. **71**, 1994 (1993).

[142] D. N. Fittinghoff, P. R. Bolton, B. Chang, and K. C. Kulander, *Observation of Nonsequential Double Ionization of Helium with Optical Tunneling*, Phys. Rev. Lett. **69**, 2642 (1992).

[143] G. L. Yudin and M. Y. Ivanov, *Physics of correlated double ionization of atoms in intense laser fields: Quasistatic tunneling limit*, Phys. Rev. A **63**, 033404 (2001).

[144] M. Lewenstein, P. Balcou, M. Y. Ivanov, A. L'Huillier, and P. B. Corkum, *Theory of high-harmonic generation by low-frequency laser fields*, Phys. Rev. A **49**, 2117 (1994).

[145] P. Zeitoun, G. Faivre, S. Sebban, T. Mocek, A. Hallou, M. Fajardo, D. Aubert, P. Balcou, F. Burgy, D. Douillet, S. Kazamias, G. de Lachéze-Murel, T. Lefrou, S. le Pape, P. Mercére, H. Merdji, A. S. Morlens, J. P. Rousseau, and C. Valentin, *A high-intensity highly coherent soft X-ray femtosecond laser seeded by a high harmonic beam*, Nature **431**, 426 (2004).

[146] M. Hentschel, R. Kienberger, C. Spielmann, G. A. Reider, N. Milosevic, T. Brabec, P. Corkum, U. Heinzmann, M. Drescher, and F. Krausz, *Attosecond metrology*, Nature (London) **414**, 509 (2001).

[147] M. Drescher, M. Hentschel, R. Kienberger, M. Uiberacker, V. Yakovlev, A. Scrinzi, T. Westerwalbesloh, U. Kleineberg, U. Heinzmann, and F. Krausz, *Time-resolved atomic inner-shell spectroscopy*, Nature (London) **419**, 803 (2002).

[148] S. Baker, J. S. Robinson, C. A. Haworth, H. Teng, R. A. Smith, C. C. Chirila, M. Lein, J. W. G. Tisch, and J. P. Marangos, *Probing Proton Dynamics in Molecules on an Attosecond Time Scale*, Science **312**, 424 (2006).

[149] L. V. Keldysh, *Ionization in the field of a strong electromagnetic wave*, Sov. Phys. JETP **20**, 1307 (1965).

[150] H. R. Reiss, *Effect of an intense electromagnetic field on a weakly bound system*, Phys. Rev. A **22**, 1786 (1980).

[151] V. P. Krainov, *Ionization rates and energy and angular distributions at the barrier-suppresion ionization of complex atoms and atomic ions*, J. Opt. Soc. Am. B **14**, 425 (1997).

[152] A. Becker and F. H. M. Faisal, *Interplay of electron correlation and intense field dynamics in the double ionization of helium*, Phys. Rev. A **59**, R1742 (1999).

[153] M. V. Ammosov, N. B. Delone, and V. P. Krainov, *Tunnel ionization of complex atoms and of atomic ions in an alternating electromagnetic field*, Sov. Phys. JETP **64**, 1191 (1986).

[154] T. Brabec and F. Krauz, *Intense few-cycle laser fields: Frontiers of nonlinear optics*, Rev. Mod. Phys. **72**, 545 (2000).

[155] M. J. DeWitt, E. Wells, and R. R. Jones, *Ratiometric Comparison of Intense Field Ionization of Atoms and Diatomic Molecules*, Phys. Rev. Lett. **87**, 153001 (2001).

[156] C. Guo, M. Li, J. P. Nibarger, and G. N. Gibson, *Single and double ionization of diatomic molecules in strong laser fields*, Phys. Rev. A **58**, R4271 (1998).

[157] S. M. Hankin, D. M. Villeneuve, P. B. Corkum, and D. M. Rayner, *Intense-field laser ionization rates in atoms and molecules*, Phys. Rev. A **64**, 013405 (2001).

[158] S. M. Hankin, D. M. Villeneuve, P. B. Corkum, and D. M. Rayner, *Nonlinear Ionization of Organic Molecules in High Intensity Laser Fields*, Phys. Rev. Lett. **84**, 5082 (2000).

[159] A. Talebpour, S. Larochelle, and S. L. Chin, *Multiphoton ionization of unsaturated hydrocarbons*, J. Phys. B **31**, 2769 (1998).

[160] E. Wells, M. J. DeWitt, and R. R. Jones, *Comparison of intense-field ionization of diatomic molecules and rare-gas atoms*, Phys. Rev. A **66**, 013409 (2002).

[161] A. Talebpour, C.-Y. Chien, and S. L. Chin, *The effect of dissociative recombination in mulitiphoton ionization of O_2*, J. Phys. B **29**, L677 (1996).

[162] J. Muth-Böhm, A. Becker, S. L. Chin, and F. H. M. Faisal, *S-matrix theory of ionisation of polyatomic molecules in an intense laser pulse*, Chem. Phys. Lett. **337**, 313 (2001).

[163] J. Muth-Böhm, A. Becker, and F. H. M. Faisal, *Suppressed Molecular Ionization for a Class of Diatomcs in Intense Femtosecond Laser Fields*, Phys. Rev. Lett. **85**, 2280 (2000).

[164] X. M. Tong, Z. X. Zhao, and C. D. Lin, *Theory of molecular tunneling ionization*, Phys. Rev. A **66**, 33402 (2002).

[165] T. K. Kjeldsen, C. Z. Bisgaard, L. B. Madsen, and H. Stapelfeldt, *Role of symmetry in strong-field ionization of molecules*, Phys. Rev. A **68**, 063407 (2003).

[166] A. Jaroń-Becker, A. Becker, and F. H. M. Faisal, *Dependence of strong-field photoelectron angular distributions on molecular orientation*, J. Phys. B **36**, L375 (2003).

[167] Z. X. Zhao, X. M. Tong, and C. D. Lin, *Alignment-dependent ionization probability of molecules in a double-pulse laser field*, Phys. Rev. A **67**, 043404 (2003).

[168] T. K. Kjeldsen and L. B. Madsen, *Strong-field ionization of N_2: length and velocity gauge strong-field approximation and tunneling theory*, J. Phys. B **37**, 2033 (2004).

[169] A. Jaroń-Becker, A. Becker, and F. H. M. Faisal, *Ionization of N_2, O_2, and linear carbon clusters in a strong laser pulse*, Phys. Rev. A **69**, 023410 (2004).

[170] A. Jaroń-Becker, A. Becker, and F. H. M. Faisal, *Erratum: Ionization of N_2, O_2, and linear carbon clusters in a strong laser pulse [Phys. Rev. A 69, 023410 (2004)]*, Phys. Rev. A **72**, 069907 (2005).

[171] T. K. Kjeldsen, C. Z. Bisgaard, L. B. Madsen, and H. Stapelfeldt, *Influence of molecular symmetry on strong-field ionization: Studies on ethylene, benzene, fluorobenzene, and chlorofluorobenzene*, Phys. Rev. A **71**, 013418 (2005).

[172] T. K. Kjeldsen and L. B. Madsen, *Strong-field ionization of diatomic molecules and companion atoms: Strong-field approximation and tunneling theory including nuclear motion*, Phys. Rev. A **71**, 023411 (2005).

[173] I. V. Litvinyuk, K. F. Lee, P. W. Dooley, D. M. Rayner, D. M. Villeneuve, and P. B. Corkum, *Alignment-Dependent Strong Field Ionization of Molecules*, Phys. Rev. Lett. **90**, 233003 (2003).

[174] D. Pinkham and R. R. Jones, *Intense laser ionization of transiently aligned CO*, Phys. Rev. A **72**, 023418 (2005).

[175] G. F. Gribakin and M. Y. Kuchiev, *Multiphoton detachment of electrons from negative ions*, Phys. Rev. A **55**, 3760 (1997).

[176] V. R. Bhardwaj, D. M. Rayner, D. M. Villeneuve, and P. B. Corkum, *Quantum Interference in Double Ionization and Fragmentation of C_6H_6 in Intense Laser Fields*, Phys. Rev. Lett. **87**, 253003 (2001).

[177] A. S. Alnaser, S. Voss, X.-M. Tong, C. M. Maharjan, P. Ranitovic, B. Ulrich, T. Osipov, B. Shan, Z. Chang, and C. L. Cocke, *Effects of molecular structure on ion disintegration patterns in ionization of O_2 and N_2 by short laser pulses*, Phys. Rev. Lett. **93**, 113003 (2004).

[178] A. S. Alnaser, C. M. Maharjan, X. M. Tong, B. Ulrich, P. Ranitovic, B. Shan, Z. Chang, C. D. Lin, C. L. Cocke, and I. V. Litvinyuk, *Effects of orbital symmetries in dissociative ionization of molecules by few-cycle laser pulses*, Phys. Rev. A **71**, 031403(R) (2005).

[179] M. Lezius, V. Blanchet, D. M. Rayner, D. M. Villeneuve, A. Stolow, and M. Y. Ivanov, *Nonadiabatic Multielectron Dynamics in Strong Field Molecular Ionization*, Phys. Rev. Lett. **86**, 51 (2001).

[180] M. Lezius, V. Blanchet, M. Y. Ivanov, and A. Stolow, *Polyatomic molecules in strong laser fields: Nonadiabatic multielectron dynamics*, J. Chem. Phys. **117**, 1575 (2002).

[181] A. N. Markevitch, S. M. Smith, D. A. Romanov, H. B. Schlegel, M. Y. Ivanov, and R. J. Levis, *Nonadiabatic dynamics of polyatomic molecules and ions in strong laser fields*, Phys. Rev. A **68**, 011402(R) (2003).

[182] A. N. Markevitch, D. A. Romanov, S. M. Smith, and R. J. Levis, *Coulomb Explosion of Large Polyatomic Molecules Assisted by Nonadiabatic Charge Localization*, Phys. Rev. Lett. **92**, 063001 (2004).

[183] N. Hay, R. Velotta, M. Lein, R. de Nalda, E. Heesel, M. Castillejo, and J. P. Marangos, *High-order harmonic generation in laser-aligned molecules*, Phys. Rev. A **65**, 053805 (2002).

[184] M. Lein, P. P. Corso, J. P. Marangos, and P. L. Knight, *Orientation dependence of high-order harmonic generation in molecules*, Phys. Rev. A **67**, 023819 (2003).

[185] J. Itatani, J. Levesque, D. Zeidler, H. Niikura, H. Pépin, J. C. Kieffer, P. B. Corkum, and D. M. Villeneuve, *Tomographic imaging of molecular orbitals*, Nature **432**, 867 (2004).

[186] K. Miyazaki, M. Kaku, G. Miyaji, A. Abdurrouf, and F. H. M. Faisal, *Field-Free Alignment of Molecules Observed with High-Order Harmonic Generation*, Phys. Rev. Lett. **95**, 243903 (2005).

[187] M. Lein, N. Hay, R. Velotta, J. P. Marangos, and P. L. Knight, *Interference effects in high-order harmonic generation with molecules*, Phys. Rev. A **66**, 023805 (2002).

[188] C. R. Gebhardt, T. P. Rakitzis, P. C. Samartzis, V. Ladopoulos, and T. N. Kitsopoulos, *Slice imaging: A new approach to ion imaging and velocity mapping*, Rev. Sci. Instr. **72**, 3848 (2001).

[189] D. Townsend, W. Li, S. K. Lee, R. L. Gross, and A. G. Suits, *Universal and State-Resolved Imaging of Chemical Dynamics*, J. Phys. Chem. A **109**, 8661 (2005).

[190] T. S. Zwier, *Laser Probes of Conformational Isomerization in Flexible Molecules and Complexes*, J. Phys. Chem. A **110**, 4133 (2006).

[191] T. Kiljunen, B. Schmidt, and N. Schwentner, *Intense-Field Alignment of Molecules Confined in Octahedral Fields*, Phys. Rev. Lett. **94**, 123003 (2005).

[192] M. Tsubouchi and T. Suzuki, *Photoionization of homonuclear diatomic molecules aligned by an intense femtosecond laser pulse*, Phys. Rev. A **72**, 022512 (2005).